

Marshall University

Marshall Digital Scholar

Theses, Dissertations and Capstones

2022

Current and Novel Neuroregenerative Therapies

Arrin Brooks

arrincarterbrooks@gmail.com

Follow this and additional works at: <https://mds.marshall.edu/etd>



Part of the [Nervous System Commons](#), [Nervous System Diseases Commons](#), [Neurosciences Commons](#), [Surgery Commons](#), [Surgical Procedures](#), [Operative Commons](#), and the [Therapeutics Commons](#)

Recommended Citation

Brooks, Arrin, "Current and Novel Neuroregenerative Therapies" (2022). *Theses, Dissertations and Capstones*. 1438.

<https://mds.marshall.edu/etd/1438>

This Dissertation is brought to you for free and open access by Marshall Digital Scholar. It has been accepted for inclusion in Theses, Dissertations and Capstones by an authorized administrator of Marshall Digital Scholar. For more information, please contact zhangj@marshall.edu, beachgr@marshall.edu.

CURRENT AND NOVEL NEUROREGENERATIVE THERAPIES

A dissertation submitted to the Graduate College of Marshall University
In partial fulfillment of
the requirements for the degree of Doctor of Philosophy
In
Biomedical Research
by
Arrin Brooks
Approved by
Dr. Brandon Henderson, Dr. Maria Serrat, Dr. Richard Egleton,
Dr. Larry Grover & Dr. Sasha Zill

Marshall University

April 2022

APPROVAL OF THESIS

We, the faculty supervising the work of Arrin Brooks, affirm that the dissertation, *Current and Novel Neuroregenerative Therapies*, meets the high academic standards for original scholarship and creative work established by the Biomedical Research and the Joan C Edwards School of Medicine. The work also conforms to the formatting guidelines of Marshall University. With our signatures, we approve the manuscript for publication.

Dr. Brandon Henderson		Committee Chairperson	1/20/2022	Date
Dr. Maria Serrat		Committee Member	1/25/2022	Date
Dr. Richard Egleton		Committee Member	1/20/2022	Date
Dr. Larry Grover		Committee Member	1/25/2022	Date
Dr. Sasha Zill		Committee Member	1/26/2022	Date

© 2022

Arrin Carter Brooks

ALL RIGHTS RESERVED

ACKNOWLEDGMENTS

I want to thank my amazingly supportive family, who may never really listen when I talk about my research but never doubted I could do it. My ever-encouraging husband, who, almost to the point of annoyance, never lets me do anything less than my ultimate best. And my dogs, who were continual company and sounding boards for the whole project.

Lab members: Leah Ching and Skylar Cooper

Funding: Funding for “Single-Stage Deep Brain Stimulator Placement for Movement Disorders: A Case Series” provided by Dr Alastair Hoyt and the Marshall Health Neurosurgical Department (Chapter 1). Funding for “Modulating Biodegradation of a Fibrin-Based Scaffold by Neural Cells via Chemically Immobilized Aprotinin”, “In Vivo Neural Tissue Engineering: Cylindrical Biocompatible Hydrogels that Create New Neural Tracts in the Adult Mammalian Brain”, and “Bioengineering Fibrin Cylinder-In-Cylinder (CinC) Brain Implant for Striatal and Cortical Neural Stem Cell Recruitment” provided by Dr. Elmer Price and the National Science Foundation (GrantAward Number: 1003907) (Chapter 2). Funding for “Systematic Review of Nicotine Exposure’s Effects on Neural Stem and Progenitor Cells” and “Expression of Alpha4 Nicotinic Acetylcholine Receptor Subunits on Dopaminergic and GABAergic Neurons of the Ventral Tegmental Area Following Passive Inhalation Vaporized Nicotine in Mice” provided by Dr. Brandon Henderson and Marshall University Research Corporation Startup Funds (Chapter 3).

TABLE OF CONTENTS

List of Tables.....	vii
List of Figures.....	ix
List of Abbreviations.....	xi
Abstract.....	xviii
General Introduction.....	1
Chapter 1.....	4
Single-Stage Deep Brain Stimulator Placement for Movement Disorders: A Case Series.....	4
Introduction.....	4
Material and Methods.....	5
Results.....	6
Discussion.....	12
Conclusion.....	17
Chapter 2.....	18
Chapter Introduction.....	18
Section 1: Modulating Biodegradation of a Fibrin-Based Scaffold by Neural Cells via Chemically Immobilized Aprotinin.....	21
Introduction.....	21
Material and Methods.....	24
Results.....	32
Discussion.....	42

Conclusion.....	44
Section 2: In Vivo Neural Tissue Engineering: Cylindrical Biocompatible Hydrogels that Create New Neural Tracts in the Adult Mammalian Brain.....	45
Introduction.....	45
Material and Methods.....	48
Results.....	55
Discussion.....	64
Conclusion.....	69
Section 3: Bioengineering Fibrin Cylinder-In-Cylinder (CinC) Brain Implant for Striatal and Cortical Neural Stem Cell Recruitment.....	70
Introduction.....	70
Material and Methods.....	73
Preliminary Results.....	77
Discussion.....	80
Conclusion.....	84
Chapter 3.....	85
Chapter Introduction.....	85
Section 1: Systematic Review of Nicotine Exposure’s Effects on Neural Stem and Progenitor Cells.....	86
Introduction.....	86
Nicotine-Related Decreases in NSC Proliferation.....	87
Nicotine-Related Increases in NSC Proliferation.....	95

Nicotine Attenuates A β -Induced Neurotoxicity in NSCs.....	100
Nicotine Induces Mitochondrial Stress in Neural Stem Cells.....	106
Discussion.....	111
Conclusion.....	113
Section 2: Expression of Alpha4 Nicotinic Acetylcholine Receptor Subunits on Dopaminergic and GABAergic Neurons of the Ventral Tegmental Area Following Passive Inhalation Vaporized Nicotine in Mice.....	
Introduction.....	114
Ventral Tegmental Area and Parkinson's Disease.....	114
Nicotine and Nicotinic Receptors in the Brain.....	115
Material and Methods.....	116
Results.....	120
Discussion.....	122
Conclusion.....	125
General Discussion.....	126
Conclusion.....	129
References.....	130
Appendix A: Approval Letter.....	154
Appendix B: Complications Reported in Other Published Works.....	155

LIST OF TABLES

Table 1	Post-op Complications.....	10
Table 2	Post-op Readmissions.....	10
Table 3	Raw Data In Vivo Experiments.....	41
Table 4	Summary of Nicotine-Related Decreases in Neural Stem Cell (NSC) Prolif- eration.....	88
Table 5	Summary of Nicotine-Related Increases in NSC Proliferation.....	96
Table 6	Nicotine-Related Neuroprotection and Neurotoxicity in NSCs.....	101
Appendix B	Complications Reported in Other Published Works.....	155

LIST OF FIGURES

Figure 1	Unilateral Versus Bilateral Placement in Included Patients.....	7
Figure 2	Conditions Treated and Brain Targets in Included Patients.....	8
Figure 3	Flow Chart of Outcomes.....	11
Figure 4	Cleared Brain Samples.....	30
Figure 5	Photomicrographs of Fibrin Domes in SVZ-NPC Culture.....	33
Figure 6	Degradation Rates of Fibrin Domes.....	34
Figure 7	Aprotinin Mediated <i>In Vitro</i> Stability of Fibrin in a Dose-Dependent Manner Over the Course of Fourteen Days.....	35
Figure 8	Aprotinin Mediated <i>In Vitro</i> Stability of Fibrin in a Dose-Dependent Manner.....	36
Figure 9	Concentration Dependence of Crosslinked Aprotinin on Fibrin Stability in Brain Implants.....	37
Figure 10	Quantitation of Fibrin Stability in Brain Implants.....	38
Figure 11	Two-Dimensional Representative Image of Fibrin Cylinders Used for 3D Reconstruction and Surface Area Analysis.....	39
Figure 12	Aprotinin Concentration Dependence of Fibrin Stability Following Brain Implantation.....	40
Figure 13	Diagram of Coronal Section of Rat Brain Showing Location of Hydrogel Implant.....	50
Figure 14	Recruitment of Neural Precursors by the Fibrin Implant.....	56
Figure 15	Neuroblasts in the Implant Track Exhibit Complex Neural Morphology....	57
Figure 16	Higher Magnification of Neuroblasts and Neurites in the Implant Region.	58

Figure 17	Additional Recruitment of Neuroblasts Between the Lateral Ventricle and Implant Site.....	59
Figure 18	Immunolabeled micrographs of Striatum for Each Treatment.....	61
Figure 19	Fibrin Implants Correct Amphetamine-Induced Ipsilateral Rotations in Unilateral 6-OHDA- Lesioned Rats.....	63
Figure 20	Schematic of Engineered CinC Matrix and Components.....	72
Figure 21	Depiction of Cylinder-in-Cylinder Architecture.....	74
Figure 22	EdU (5-ethynyl-2'-deoxyuridine) Labeled Brain Tissue from Rat Receiving Novel CinC Brain Implant 14 weeks Prior.....	79
Figure 23	Graphical Summary of Nicotine's Effects on NSC Proliferation.....	92
Figure 24	Summary of Described Effects of Nicotine E-Cigarettes (EC) Liquid and Aerosols on NSC Mitochondria.....	104
Figure 25	Dopaminergic and GABAergic α 4nAChR Expression in VTA.....	121

LIST OF ABBREVIATIONS

2D – two dimensional

3D – three dimensional

6-OHDA - 6-hydroxydopamine

µg - microgram

µm – micrometer

µM – micromolar

Aβ – amyloid beta

AD – Alzheimer's disease

ALS – amyotrophic lateral sclerosis

ANOVA – analysis of variance

Apro - aprotinin

BBB - blood-brain barrier

BDNF – brain-derived neurotrophic factor

bFGF – basic fibroblast growth factor

BrdU - Bromodeoxyuridine/5-bromo-2'-deoxyridine

BSA - bovine serum albumin

CEPIA - calcium-measuring organelle-entrapped protein indicator

CHAT - choline acetyltransferase

CHOP - C/EBP homologous protein

CinC – cylinder-in-cylinder

CLARITY – Clear Lipid-exchanged Acrylamide-hybridized Rigid Imaging / Immunostaining / in situ-hybridization-compatible Tissue hYdrogel

CO₂ – carbon dioxide

CNS – central nervous system

COX2 - cyclooxygenase-2

CsA - cyclosporine A

CT – computed tomography

d - day

DA – dopamine

DAPI – 4', 6-diamidino-2-phenylindole

Dcx – doublecortin

dia. - diameter

DMEM/F12 – Dulbecco's Modified Eagle Medium: Nutrient Mixture F-12

DG – dentate gyrus

DBS – deep brain stimulation/stimulator

DMSO – dimethyl sulfoxide

DNA – deoxyribonucleic acid

DSS - disuccinimidyl suberate

Ec - e-cigarette

ECM – extracellular matrix

Edu - 5-ethynyl-2'-deoxyuridine

EGF – epidermal growth factor

EGTA - ethylene glycol-bis(β -aminoethyl ether)- N,N,N',N'-tetraacetic acid

ENDS - electronic nicotine delivery systems

ET – essential tremor

FGF 1 – fibroblast growth factor 1

FGF 2 – fibroblast growth factor 2

FGFR-1 - fibroblast growth factor receptor 1

GABA - gamma-aminobutyric

GDNF – glial-derived neurotrophic factor

GFAP - glial fibrillary acidic protein

gm - gram

Gpi – globus pallidus internus

h – hour

H₂O – dihydrogen oxide (water)

H₂O₂ – hydrogen peroxide

HAT - histone acetyltransferase

HDAC1 - histone deacetylase 1

HDAC2 - histone deacetylase 2

HDN - high dose nicotine

HEPA – high-efficiency particulate absorbing

IACUC – Institutional Animal Care and Use Committee

iCT – intraoperative computed tomography

IGF1 - insulin-like growth factor 1

IL - interleukin

iNOS - inducible nitric oxide synthase

i.p. – intraperitoneal

IPG – implantable pulse generator

iPSC – induced pluripotent stem cell

i.v. - intravenous

IVSA - intravenous self-administration

kg – kilogram

LDN - low dose nicotine

LV – lateral ventricle

MAP2ab - microtubule-associated protein 2a and 2b

MCU - mitochondrial calcium uniporter

MECA - mecamlamine

MER – microelectrode recording

min – minute

mg – milligram

mL – milliliter

mm – millimeter

mM - millimolar

MMP - mitochondrial membrane potential

mPFC - medial prefrontal cortex

mPTP - mitochondrial permeability transition pore

mRNA – messenger ribonucleic acid

ms - millisecond

MS – multiple sclerosis

MS-DRG - Medicare Severity—Diagnosis Related Group

mtDNA - mitochondrial DNA

NaB - sodium butyrate

nACh - nicotinic acetylcholine receptor
NaCl – sodium chloride
NAD - nicotinamide adenine dinucleotide
NaOH – sodium hydroxide
NCAM - neural cell adhesion molecule
NeuN – neuronal nuclear protein
NF160 - neurofilament medium
NGF – nerve growth factor
NH₄Cl – ammonium chloride
NPC – neural progenitor cell
NSC – neural stem cell
OB – olfactory bulb
PACT – passive clarity technique
PBS – phosphate-buffered saline
PCL - poly-ε-caprolactone
PCNA - proliferating cell nuclear antigen
PD – Parkinson’s disease
PERK - protein kinase RNA-like ER kinase
PGVG – propylene glycol vegetable glycerin
PFA – paraformaldehyde
PI3K - phosphatidylinositol-3-kinase
POCD - post-operative cognitive dysfunction
PSA - polysialylated

PVDF - polyvinylidene difluoride

RID - raw integrated density

RIMS – refractive index matching solution

RMS – rostral migratory stream

ROS - reactive oxygen species

RT-PCR – reverse transcription polymerase chain reaction

s.c. – subcutaneous

SC – stem cell

SD – standard deviation

SDS - sodium dodecyl sulfate

SEM – standard error of the mean

SGZ – subgranular zone

SIRT1 – sirtuin 1

SNC - substantia nigra pars compacta

STN – subthalamic nuclei

TBI – traumatic brain injury

TH – tyrosine hydroxylase

TMRM - tetramethylrhodamine methyl ester

TNF- α - tumor necrosis factor alpha

TPE - total-puff-equivalents

TrkB - tropomyosin receptor kinase B

TUNEL – terminal deoxynucleotidyl transferase dUTP nick end labeling

UPR - unfolded protein response

UPDRS - Unified Parkinson's Disease Rating Scale

U.S. – United States

VA - valproic acid

VEGF - vascular endothelial growth factor

VIM – ventromedial thalamus

VTA - ventral tegmental area

ABSTRACT

Underlying the physical and cognitive deficits consequent of many neuropathologies is one common factor, the loss of neurons. While neurodegenerative diseases, stroke, and traumatic brain injury arise from a variety of etiologies, they all ultimately result in injury and/or death of neuronal cells and concomitant functional deficits. In the present work we primarily focus on current and potential treatments for localized lesions, particularly those in the striatum of Parkinson's disease (PD) or the cortex as in stroke. First, we discuss a new surgical technique for deep brain stimulator (DBS) placement, as DBS is a mainstay treatment for movement disorders including PD. We then explore a novel brain implant capable of rerouting endogenous neural stem cells (NSCs) within the brain from their usual route to new areas of the brain. These implants are intended to recruit NSCs and regenerate lost brain tissue in disorders like PD and stroke. Finally, we investigate the varying effects of nicotine in the brain. Nicotine has been shown to be both neuroprotective for certain neuronal populations, yet neurotoxic to others. Therefore, awareness of the influences of nicotine on neural cells is vital for understanding how nicotine may be of help or detriment to current and prospective treatments for neurodegenerative disease.

GENERAL INTRODUCTION OF THE PRESENT WORK

Underlying the physical and cognitive deficits consequent of many neuropathologies is one common factor, the death of neurons. The loss of neurons from either disease or injury leads to a disruption of neural circuitry, improper signal propagation, and subsequently loss of function corresponding to the affected neural network (1-5). While neurodegenerative diseases, stroke, and traumatic brain injury (TBI) arise from a variety of etiologies, they all ultimately result in a loss of neuronal cells and concomitant functional deficits. Disorders resulting from the death of neurons afflict millions of people worldwide, creating an enormous universal burden medically, emotionally, and financially every year.

Neurodegenerative diseases, stroke, and TBI are leading causes of morbidity and mortality in the United States and worldwide. The most prevalent neurodegenerative condition is Alzheimer's disease (AD). There are currently 5.8 million Americans diagnosed with AD and its prevalence is predicted to triple by the year 2050 (6, 7). Further, AD is the most common cause of dementia, accounting for 50–75% of the 44 million people living with dementia worldwide (8). After AD, Parkinson's disease (PD) is the second most common neurodegenerative disorder (9) with more than 10 million people worldwide living with PD (10). Like AD, PD incidence and prevalence dramatically increase with age and are influenced by several environmental, genetic and metabolic risk factors (11). Other neurodegenerative and neuroinflammatory conditions, such as Huntington's disease, amyotrophic lateral sclerosis (ALS, or Lou Gehrig's disease), and multiple sclerosis (MS), constitute thousands more individuals suffering from deficits associated with neuronal death. In addition to degenerative conditions, vascular and

traumatic injury to the brain can result in neural cell death and concomitant loss of function. Stroke has an annual incidence of nearly 800,000 people in the U.S. and is the 5th most common cause and death accounting for 1 out of every 20 deaths in America (12, 13). Stroke is also a leading cause of long-term disability worldwide, hindering the mobility of over half of stroke survivors age 65 or older (13). Lastly, over 5 million people across the globe suffer from serious TBI each year (14). In 2014, there were 2.87 million TBI-associated emergency department visits, hospitalizations, and deaths in the U.S., with 837,000 of these events occurring in children (15, 16). Unfortunately, those who survive TBI can have negative effects, including impairments related to cognition and memory, disordered movement, sensory alterations (touch, vision, hearing), or deviations in emotional functioning (personality changes, depression, etc.), that persist for days post-injury or their entire lifetime (17).

Although each of the therapeutic modalities researched in this work have implications across multiple neurological conditions, the scope of the present work is primarily concerned with PD. As such, first, we sought to ascertain the patient outcomes following the current standard of care for advanced-stage PD, namely deep brain stimulation (DBS). The next aim was to investigate novel therapies for PD and other neuropathologies. Secondly, exploitation of the brain's innate neuroplasticity for neuro-restorative was explored. The use of a modifiable, biodegradable brain implant to create an in vivo migratory pathway for endogenous neural stem cell (NSC) recruitment is discussed. Then, the possible neuroprotective versus neurotoxic properties of nicotine are discussed; how the effect of nicotine exposure varies on cell type and location throughout

the brain and the subsequent implications for neurodegenerative conditions and potential confounding effects on aforementioned therapeutic mechanisms.

CHAPTER 1

SINGLE-STAGE DEEP BRAIN STIMULATOR PLACEMENT FOR MOVEMENT DISORDERS: A CASE SERIES

Introduction

Deep brain stimulation (DBS) therapy has become a mainstay for movement disorders including essential tremor (ET), Parkinson's disease (PD), and dystonia (18). More than 160,000 patients have been implanted worldwide and more than 12,000 new patients receive DBS annually (19). Despite decades of experience, patients are frequently offered implantation via multiple, "staged" surgeries. A 2013 international survey of DBS procedural steps revealed that DBS implantations occurring in the United States were more likely to be staged than those at European centers (20). In America, 65% percent of DBS surgeries were staged in 2 days, 22% staged in 3 days and only 13% were performed in a single stage.

Reasons to separate DBS implantation into multiple surgeries vary, including concerns for increased risk of infection, poor stimulation efficacy, and postoperative confusion leading to increased length of stay, particularly when intraoperative microelectrode (MER) recording and neurophysiological testing are used (21, 22). In an effort to simplify care and reduce the burden of multiple surgeries on patients, a single-stage approach has been used routinely in Dr. Alastair Hoyt's practice since his arrival at our institution. We hypothesize that single-stage DBS placement surgery has a similar risk profile, similar or shorter length of hospital stay, and a similar or reduced rate of reoperations compared to the reported outcomes of surgeries performed in multiple stages.

Materials and Methods

Patient Selection

After institutional review board approval, a retrospective review of clinical data from our institution was undertaken for a cohort of patients who underwent DBS implantation from January 2016 to June 2019. The inclusion criteria included all patients receiving initial placement of DBS system or second unilateral placement (no previous electrode in that hemisphere). Revision surgeries and routine implanted pulse generator (IPG) exchanges were excluded.

Surgical Technique

All patients underwent preoperative neurology evaluation, neuropsychological testing, and on/off testing in the case of Parkinson's disease. A stereotactic protocol imaging study was obtained prior to the day of surgery. On the day of surgery, a Leksell Model G Frame (Elekta, Stockholm, Sweden) was fitted under conscious sedation and a registration CT scan was performed, followed by computer-aided surgical planning. Depending on the stimulation target and patient, either "awake" placement with MER and stimulation testing or "asleep" placement under general anesthesia was performed. Intraoperative IPG's and extension leads were routinely placed before exiting the operating theater. All patients underwent a postoperative CT scan of the head to assess for intracranial complications. As our institution does not allow scheduled nursing assessments more frequently than every four hours in general hospital beds, patients were observed in the intensive care unit for neurological monitoring and blood pressure control. Initial programming of the stimulation system typically occurred two to four weeks after

surgery. Patients who did not obtain adequate symptom control, as determined by the patient and the treating neurologist, were offered DBS revision surgery.

Literature Review

Similar reports were identified by a structured search of the PubMed database and were summarized (see Appendix B).

Results

A total of 73 patients that met inclusion criteria were identified. The average age was 65.7 years (range 41–80). Of these patients, 20 were female, and 53 were male. Mean operative time was 3:50 (range 2:30–5:44) for bilateral placements and 2:58 (range 1:59–4:14) for unilateral placements (Fig 1). The mean length of stay was 1.2 days (range 1–3), with 86.3 percent of patients discharged on the first postoperative day. The average follow-up after surgery was 23.3 months (range 2.3–50.9). Of the 73 total patients: 46 were treated for PD, 26 for essential tremor (ET), and one for dystonia. ET was treated with thalamic stimulation and dystonia with pallidal stimulation, while PD was treated with either pallidal or subthalamic stimulation (Fig 2). There were four patients (5.5%) that underwent “asleep” DBS without MER (Fig 2). The average number of microelectrode recording passes per electrode placed was 1.55.

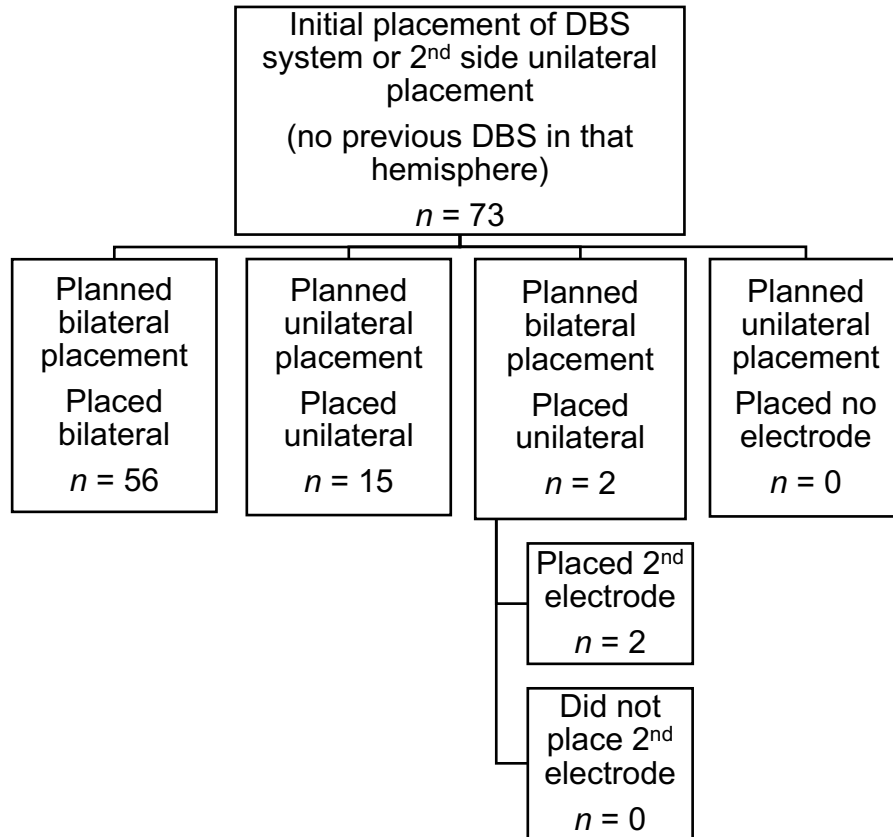


Figure 1. Unilateral Versus Bilateral Placement in Included Patients

This figure describes intended and executed placement of DBS electrodes into unilateral or bilateral hemispheres for all patients.

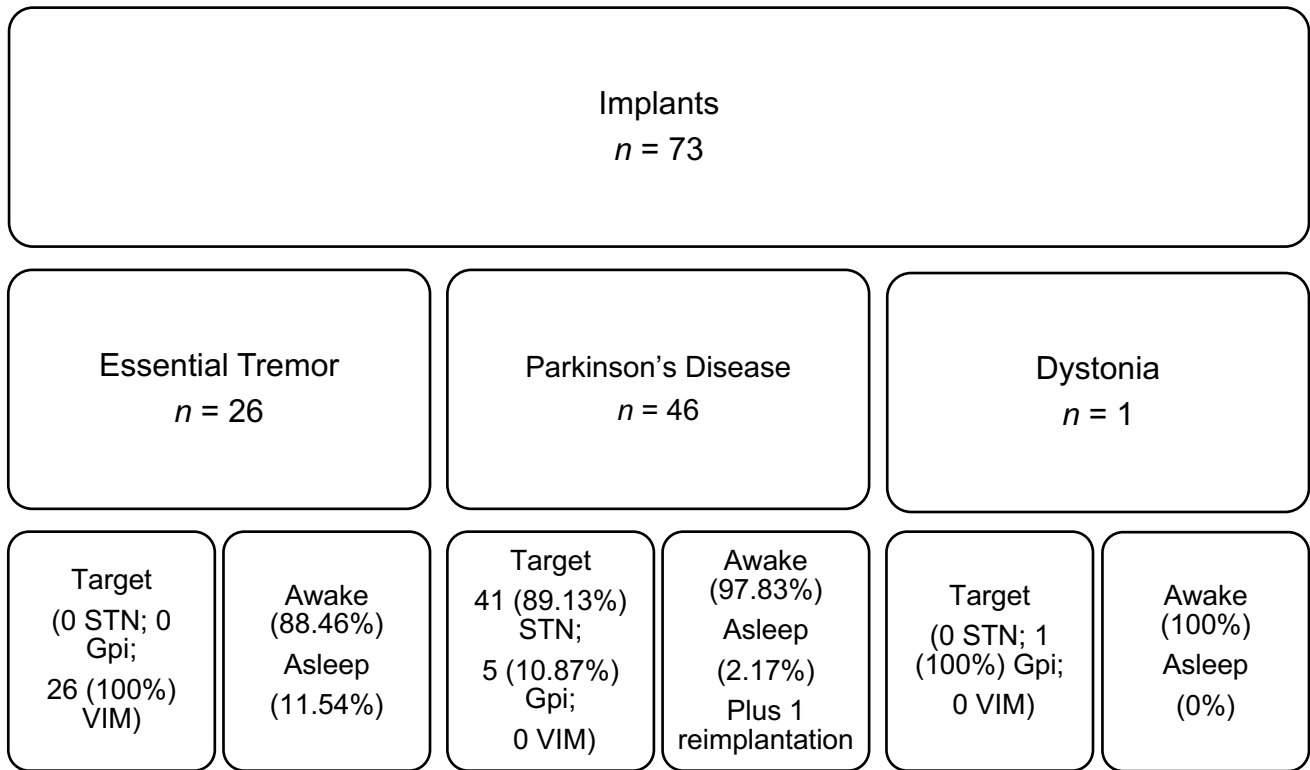


Figure 2. Conditions Treated and Brain Targets in Included Patients

This figure presents brain areas targeted by each DBS electrode and whether the surgery was performed with MER (awake) or without MER (asleep). STN = subthalamic nucleus; Gpi = globus pallidus internus; VIM = ventralis intermedius or ventral intermediate nucleus of the thalamus.

There were fifty-six patients (77%) who underwent bilateral electrode placement and 15 patients (20%) who underwent unilateral electrode placement. Of these, two patients (3%) were scheduled to undergo bilateral electrode placement but surgery was halted after placement of the first electrode, one for patient fatigue and one for equipment failure. Both had a second electrode placed in a later procedure.

Table 1 demonstrates the post-operative complications observed. All patients recovered from their complications, with no mortalities or permanent neurological injuries.

Complications were suffered within 90 days of surgery by six patients (8.2%), while five (6.8%) suffered a complication more than 90 days after surgery. The most frequent complication was wound infection (5.5%), which was treated aggressively with the removal of the affected portions of the stimulation system and antibiotic treatment. There were six patients (8.2%) readmitted within 90 days of surgery (Table 2). Of these six, four required surgery for treatment of a complication, including two infections, one lead fracture, and one generator site hematoma. A single patient was readmitted with poorly defined symptoms which resolved after treatment of pain with nonsteroidal anti-inflammatories. Another patient had bradycardia and hypotension due to cardiac disease not deemed related to surgery or stimulation. In total, 11 patients (15.1%) underwent additional surgery during the follow-up period, nine (12.3%) for a complication, and the remainder for poor stimulation effect (See Fig 3).

Within 90 Days	>90 Days	Total (as of the Last
----------------	----------	-----------------------

	Follow-up)					
	Number	Percent (of all patients)	Number	Percent (of all patients)	Number	Percent (of all patients)
Infection	2	2.7%	2	2.7%	4	5.5%
Lead Fracture	1	1.4%	1	1.4%	2	2.7%
Wound Dehiscence	0	0%	2	2.7%	2	2.7%
Hypotension	1	1.4%	0	0%	1	1.4%
IPG Site Hematoma	1	1.4%	0	0%	1	1.4%
Total	6	8.2%	5	6.8%	11	15.1%

Table 1. Post-op Complications

Table displays complications suffered by patients within 90 days of surgery and at 90 days or longer after surgery.

	Number	Percent (of all patients included)
Infection	2	2.7%
Lead Fracture	1	1.4%
Hypotension	1	1.4%
IPG Site Hematoma	1	1.4%
Pain	1	1.4%
Total	6	8.2%

Table 2. Post-op Readmissions

Table displays readmissions within 90 days of DBS surgery.

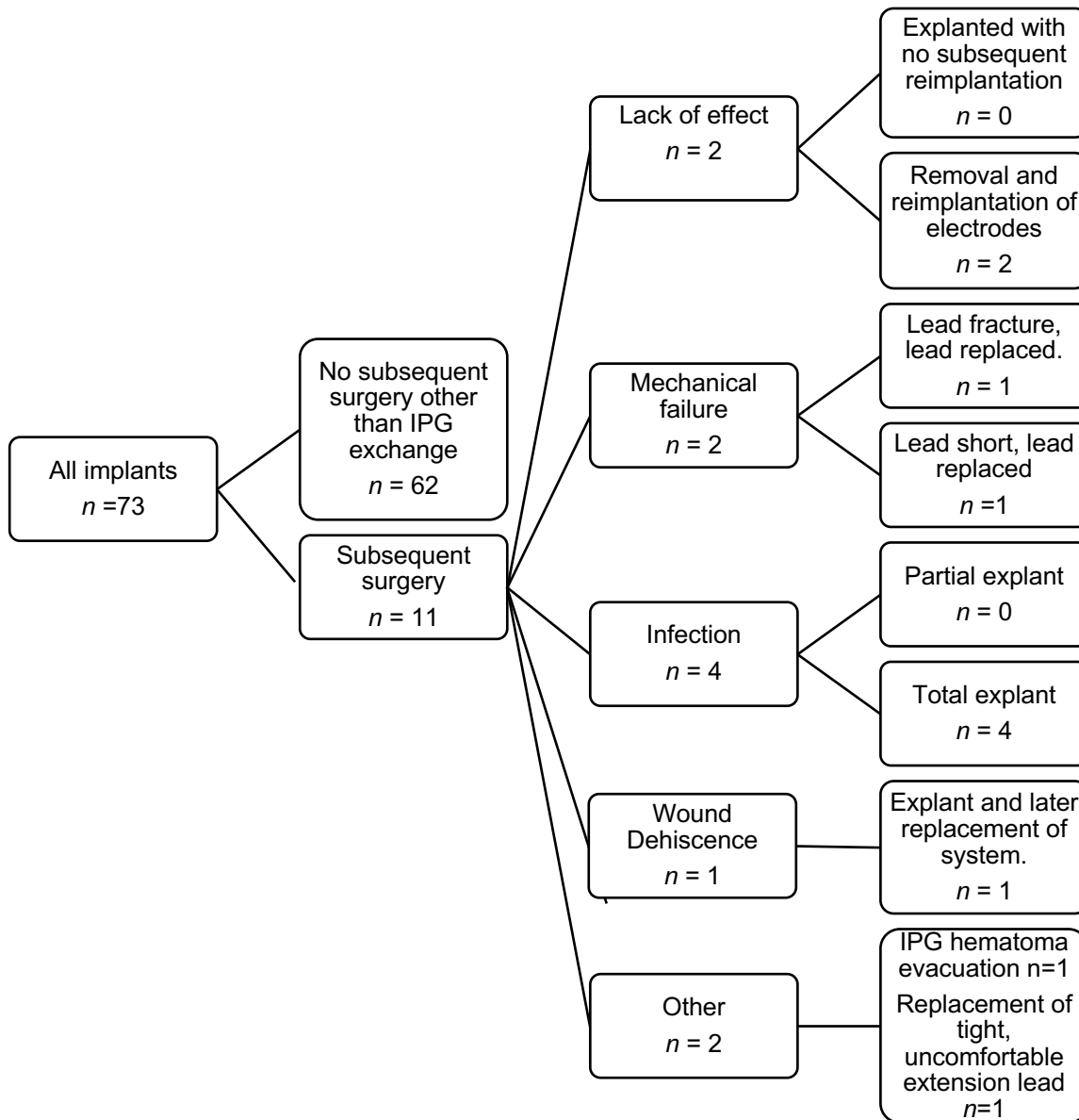


Figure 3. Flow Chart of Outcomes

All patient outcomes following DBS surgeries, including whether a return to surgery was indicated and why.

There were two patients (2.7%) that underwent a revision for poor stimulation effect. The first was a 66-year-old man with a diagnosis of PD. Pre-operative on/off testing resulted had revealed significant a reduction of Unified Parkinson's Disease Rating Scale (UPDRS) motor scores from 55 to 27. He underwent bilateral pallidal stimulator placement but had little improvement in symptoms with stimulation. MRI imaging confirmed lead placement in the desired target bilaterally. He subsequently underwent revision of the electrodes from the pallidum to the subthalamic nucleus, again with only marginal improvement in symptoms.

The second was a 67-year-old man with bilateral upper extremity tremor diagnosed as essential tremor. He underwent bilateral "asleep" thalamic DBS due to a history of severe sleep apnea. Substantial improvement was noted in tremor for about 6 weeks after initial programming, and then tremor appeared to return. Despite multiple programming attempts, the tremor worsened, and he reported persistent headaches. He did not respond to a trial of levodopa. He ultimately underwent bilateral "awake" lead revision with MER, although he had relatively little tremor to test intraoperatively. He again experienced no improvement in tremor despite multiple rounds of programming and ultimately elected to have the DBS removed due to persistent headaches.

Discussion

While DBS is a well-established therapy for movement disorders, there is considerable variation in methods of system placement. Attempts to determine the best methods are hindered by differences in terminology, inconsistent reporting of complications and outcomes, and the individual practices of surgeons. It is clear, however, that the vast majority of patients in the United States have been made to undergo multiple staged

procedures (20). Little data exists to suggest the practice of staging is superior. Arguments for staging have included improved electrode accuracy, reduced operative time, and concerns for increased post-operative confusion or other complications (21, 22).

Some authors have referred to “staging” as individually placing only one of two planned intracranial electrodes at a time, and studies have compared simultaneous bilateral electrode placement with implantation of each hemisphere in two separate surgeries (22, 23). Peng, et al. concluded that there was no significant difference in lead accuracy between unilateral, simultaneous bilateral, and staged bilateral electrode placement (22). Petraglia, et al. reported a higher rate of revision within 90 days with separate unilateral electrode placement than in simultaneous bilateral electrode placement but found no significant difference between these groups in rates of complication or costs (23). Neither author reported when an IPG was implanted (Appendix B).

Similarly, there have been several published comparisons of “awake” surgery including MER and intraoperative neurophysiological testing with “asleep” surgery under general anesthesia. A clearly superior technique has not been established (24). Studies have shown similar outcomes when comparing intraoperative CT (iCT)-guided sub-thalamic nucleus (STN)- or Globus Pallidus (Gpi)-DBS lead implantation to MER-guided DBS (25), as well as when comparing iMRI-guided GPi-DBS to MER-guided DBS (26), with some motor outcomes slightly favoring asleep DBS. Mirzadeh, et al. suggested stereotactic accuracy was better under general anesthesia without MER, compared to the group receiving MER intraoperatively (27, 28). Opposingly, in a retrospective analysis of awake versus asleep DBS for STN stimulation in PD, Blasberg, et al. found motor function improved faster following awake surgery and axial subitems were worse in the

asleep surgery group (29). They concluded awake placement was advantageous over asleep placement in suitable patients. Still, others have reported no significant differences in complications, length of stay, and readmissions between awake and asleep DBS procedures (30).

Based on personal experience, the senior surgeon of this paper maintains that MER and “awake” stimulation testing result in superior electrode placement, particularly in small targets like the STN. As a result, placement under general anesthesia was reserved for patients with significant respiratory comorbidities. In this series, the need for revision due to poor effect was used as a surrogate for stimulation efficacy. There were two patients (2.7%) that underwent a revision for poor effect. A patient with a diagnosis of PD did not have a good response even after revision of the electrodes from the pallidum to the subthalamic nucleus, suggesting that it was not poor placement but the patient’s disease that resulted in lackluster symptom control. A second patient with ET had a transient response to thalamic stimulation and no improvement after revision of the electrode, again suggesting a flaw in patient selection and not in electrode placement.

An increased operative time is a logical consequence of single-stage surgery. While we did observe a longer operative time than is reported in some literature, we did not observe any serious complications intra- or peri-operatively related to this increased time under sedation. On one occasion, a bilateral implantation surgery was halted after placement of a single due to patient somnolence. The patient recovered normally and received the second electrode in a later procedure. One additional patient had bradycardia and hypotension due to cardiac disease not deemed related to the length of surgery. In both instances, placement of the IPG in a second procedure would not have

prevented the event. With an average length of stay of 1.2 days, and 86% of patients returning home on the day after surgery, this increased operative time did not appear to result in significantly longer lengths of stay (Appendix B).

Further, while difficult to quantify, the single-stage approach reduces each patient's total time commitment to DBS placement by avoiding procedures on multiple days. In a similar effort to streamline the implantation process, Van Horne, et al. (31) performed cranial access, IPG placement, and extension lead insertion during an initial procedure and stimulating lead placement using MER in the second stage. An argued benefit was that an entire system was implanted and ready to program within five days. We assert that a nonstaged approach provides similar advantages in a single day.

Variation in how complications are reported frustrates direct comparison to other approaches, but the presented results are similar to published accounts (23, 30, 32-42). (See Appendix B). In a study evaluating factors associated with postoperative confusion and prolonged hospital stay following DBS surgery for PD, Abboud, et al. determined that surgical factors such as implantation laterality, surgical staging, or the number of MER passes did not influence immediate outcomes (43). A European study showed a nonsignificant decrease in infection rate in single stage (entire DBS system placed in one operative session) DBS surgery compared to that in staged DBS surgery (IPG placed in subsequent surgery) (44). In a retrospective analysis of "asleep" DBS, Chen et al. found that staging did not significantly affect hardware-related complications such as infection, erosion, impedance, or lead malposition (30). They also observed a reduction in hemorrhage or seizures with staging. In another study categorizing staging in the same manner described in this study, surgical site infections were shown to be similar in

228 staged and 17 non-staged implantations (6.6% to 5.9%) (40). Their results also showed similar rates of wound dehiscence and post-op seroma between staged and non-staged groups (Appendix B).

Perhaps one of the most important factors to many surgeons' decision to perform staged DBS implantation is financial. Given the complexities of medical economics in the United States, it is very difficult to perform an economic evaluation of cost-effectiveness for DBS as a whole, let alone determining the relative cost-effectiveness of single-stage procedures (45). The current payment structure reimburses hospitals more based on Medicare Severity—Diagnosis Related Group (MS-DRG) codes for staged procedures (46). For example, staged placement of bilateral subthalamic electrodes in one procedure (MS-DRG 027) with later placement of an IPG (MS-DRG 042) results in a 5.7% greater relative weight for reimbursement than nonstaged placement (MS-DRG 024). This payment structure incentivizes hospitals to mandate surgeons to perform staged procedures and unfortunately may result in patients having unnecessarily convoluted care.

While admittedly a small sample, this report constitutes one of the larger series of frame-based bilateral electrode placement with intraoperative MER and neurophysiological testing accompanied by IPG placement in the United States. Direct comparison to staged approaches is limited by the lack of a control group of staged surgeries at the same facility by the same surgeon. Anecdotally, the authors have found avoiding multiple procedures to be attractive to patients. It helps to simplify scheduling and to reduce transportation needs. These factors are particularly attractive when patients may travel several hours to reach the hospital, such as in rural settings. While no formal

assessment has been performed, patients frequently report that they prefer a single-stage approach as the longer procedure does not necessitate a longer hospital stay. Performing a systematic assessment of patients' attitudes toward a longer, single procedure versus several shorter procedures would help support this assertion.

Conclusions

This series expands the body of evidence suggesting placement of a complete DBS system during a single procedure, including bilateral electrodes with MER, which appears to be an efficacious and well-tolerated implantation option. Complication rates, length of stay, and readmission rates appear comparable with published reports of staged procedures while the patient avoids multiple procedures.

CHAPTER 2

CHAPTER INTRODUCTION

The absence of neuro-restorative therapies for disorders of the CNS has motivated research to explore the use of stem cells (SCs) in approaches for cell replacement therapy. Much of the ongoing research in neuroregenerative medicine relies on the implantation of exogenous SCs, including embryonic pluripotent SCs, embryo or fetal-derived neural SCs, and induced pluripotent stem cells (iPSCs). While successful outcomes have been reported using exogenous SC grafts in some preclinical (47-53) and clinical (54, 55) studies of neurological diseases, there remains several complications associated with the implantation of exogenous SCs. Many original issues related to SC implantation have been mitigated, at least in part, such as tumor formation, immunorejection, death of implanted cells due to lack of stromal support (56) and/or trophic factors (57) and failed integration of grafts into local neural network (58), however, other problems have been uncovered such as an indefinite reliance on immunosuppressive agents (49). Accordingly, there persists an unmet need for new cell replacement approaches that circumvent these issues yet provides an effective method for regeneration of neural tissues.

One potential treatment strategy is to target the brain's innate regenerative capacity to reverse the trend of cell loss. Although continued post-natal neurogenesis was first discovered over 50 years ago (59, 60), the fallacy that neurons lost in the adult mammalian brain could never be replaced persisted. Therefore, modulating the endogenous neuroplasticity of the adult brain remains an underdeveloped resource for neural

tissue regeneration and could have major therapeutic implications for many neurological diseases.

While neurogenesis in the adult mammalian brain is relatively limited, endogenous neural progenitors *do* continue to replicate throughout adulthood. These proliferative niches are primarily in two distinct regions: the subventricular zone (SVZ) located along the walls of the lateral ventricles and the subgranular zone (SGZ) located in the dentate gyrus (DG) of the hippocampus. NSCs reside and continue to symmetrically divide throughout adulthood in these regions giving rise to transiently amplifying multipotent neural progenitor cells (NPCs) (59, 61, 62). Neurogenesis in the DG plays a particularly important role in hippocampal-mediated learning (63, 64). In fact, enhanced neurogenesis and survival of newborn cells in the hippocampus is observed in rats trained on hippocampal-dependent tasks (64), and performance on these tasks is impaired by inhibition of cell proliferation (65). Newly generated NPCs in the SVZ give rise to another type of neural precursor called the migrating neuroblast, which travel from the lateral ventricles to the olfactory bulb (OB) along the rostral migratory stream (RMS) where they then mature into neural cells involved in olfaction (60, 66-69). While SVZ NSCs normally follow this migratory route, brain injuries can stimulate SVZ neurogenesis and migration of neural progenitors to sites of injury (70-77). Additionally, it has been postulated that traditionally nonneurogenic regions of the brain such as the cortex (78), retina (79), striatum (80) and substantia nigra (81-83) contain quiescent SCs and/or induce glial reprogramming to produce NPCs in an innate attempt to repair damaged neural tissues (84-87).

While the brain's neuroplastic mechanisms are considerably limited, if the regenerative power of NSCs could be harnessed by targeted recruitment of NSCs/NPCs to specific brain lesions, therein lies significant neuro-restorative potential. Here we discuss one conceivable mechanism of recruiting NPCs to specific brain lesions to recover lost function. First, a modifiable biomaterial compatible with NPC migration is presented. Then, the application of said biomaterial as a cylindrical brain implant for SVZ NSC recruitment to the striatum in hemiparkinson's rodent model is discussed. Finally, a revised implant design for improved SC recruitment is explored.

SECTION 1: MODULATING BIODEGRADATION OF A FIBRIN-BASED SCAFFOLD BY NEURAL CELLS VIA CHEMICALLY IMMOBALIZED APROTININ

Introduction

Whether induced by mechanical trauma, ischemic injury, toxin exposure or neurodegeneration, the death of neurons and loss of axonal connections is central to CNS injury and subsequent neurological deficits. Restoring damaged or diseased tissue through cell replacement therapy is a basic underlying principal of regenerative medicine. Cell replacement approaches include, systemic vascular delivery of SCs (88, 89) or neurogenesis promoting substrates (90-92), direct intracerebral implantation of SCs (48, 49, 88, 93-97) or bioengineered NSC migratory tracts (98), intranasal administration of therapeutic cells (99, 100), and intraventricular or intraparenchymal administration of growth factors (101-105) or recombinant proteins (106, 107). The efficacy of systemic administration of therapeutic factors is limited by blood brain barrier permeability and off-target effects (108, 109). These problems are circumvented in approaches that directly administer cells and/or cytokine into CNS lesions. One obstacle to direct intracerebral administration of chemotactic and/or growth factors is that they can freely migrate/diffuse away from the target area, hindering their therapeutic efficacy (109, 110). Additionally, a drawback to cell implantation into lesions or methods to enhance neurogenesis and progenitor migration to the site of a brain damage is that transplanted exogenous or recruited endogenous cells have limited survival without stromal support (111-113).

These problems have been addressed by incorporating cells and/or therapeutic substrates into biological matrices, which can then function as implantable scaffolds that restrict contents to appropriate anatomical locations and provide the needed stromal support (110, 113-117). One promising application of implantable scaffolds for neuro-regeneration has been to induce endogenous stem cell recruitment to other traditionally nonneurogenic brain regions (98, 111, 118, 119). Various hydrogels, such as Matrigel™ (120), hyaluronic acid (121, 122) and gelatin (123, 124), have been explored for neural tissue engineering. While multiple matrix materials have been found suitable to serve as a scaffold for neural cell migration, survival, differentiation and axon growth (117, 125), we have found that fibrin possess many desirable properties for CNS implantation (126) while also allowing for a simple and inexpensive, yet efficient and versatile, methodology for scaffold creation.

Fibrin is a favorable matrix for use as a scaffold in neurological therapies because it is biocompatible (127), viscoelastic (128), plastic (126), has modifiable flexibility and stiffness (altered by allowing more or less thrombin-induced fibrinogen polymerization) (129) and can be matched to the patient in clinical applications by extraction from autologous blood (130). Further, fibrin has numerous established neurosurgical and other clinical applications (131-135). Fibrin is also, however, highly biodegradable and is rapidly fibrinolysed in the presence of tissues that exhibit robust degradative proteolytic activity such as neural tissues (136-142). Without intervention of these proteolytic processes, the therapeutic application of fibrin would be severely limited. Fortunately, because of fibrin's versatility in bioconjugate reactions (143), certain protease inhibitors capable of slowing or altogether preventing fibrinolysis can be embedded in the

hydrogel. Aprotinin, a small polypeptide serine protease inhibitor of plasmin and matrix metalloproteases (144-146) (the degradative enzymes thought to mediate the breakdown of fibrin (147, 148)) is used in this study.

To prevent the diffusion of aprotinin out of the matrix, rendering the fibrin hydrogel once again susceptible to degradation, aprotinin can be covalently incorporated to fibrin polymers (146, 149-152). Several methods to accomplish such covalent immobilization of aprotinin within fibrin hydrogels have been previously described (150-153). However, some of these methods require involved processes, making synthesis of the aprotinin-linked fibrin scaffolds tedious and timely. One described method involves a complex, multi-step synthesis of conjugated fibrin-protinin via 4-(4-N-maleimidophenyl) butyric acid hydrazide hydrochloride crosslinking (153). This method, however, yields a fibrin-protinin conjugate with limited stability, experiencing significant *in vitro* degradation by day 4 in a chick chorioallantoic membrane angiogenesis assay. We suggest that a more prolonged resistance to degradation will be required for many *in vivo* or clinical applications, particularly in environments that exhibit robust proteolytic activities like the brain. An alternative method to achieve covalent immobilization of aprotinin into fibrin involved the generation of a recombinant version of the protease inhibitor, thus necessitating a bacterial expression system and purification of the material prior to pre-clinical or clinical use (150). Unfortunately, it was also not apparent that this construct could be easily tuned to yield matrices with varying stability against degradation. We postulate a tunable architecture would be more suitable for use in a variety of regenerative applications.

Despite its widespread use in experimental and clinical neurobiology, the stabilization of fibrin hydrogels in the CNS is underreported. We present an efficient and versatile method for the covalent incorporation of aprotinin into fibrin via incorporation of chemical crosslinking agent disuccinimidyl suberate (DSS). The present method does not require specialized laboratory expertise, equipment, or reagents. And importantly, can be optimized to yield matrices of desired biological half-life in neural tissues, ranging from fibrin stability of days to weeks *in vitro* and *in vivo*.

Materials and Methods

Subventricular Zone Neural Progenitor Cell (SVZ-NPC) Culture

All animal procedures were performed following an approved protocol from the Institutional Animal Care and Use Committee of Marshall University. Cell culture reagents were from Life Technologies and growth factors were from R&D Systems. SVZ-NPCs were isolated from 200-275 gm female Sprague-Dawley rats according to standard methodology (154). The cells were maintained in DMEM/F12 media supplemented with B27/N2 according to the manufacturer's recommendation, penicillin/streptomycin (100 U/ml), 2 µg/ml heparin, 20 ng/ml bFGF-2, and 20 ng/ml EGF. The cells were maintained on a constantly rocking (30 rpm) platform at 37°, 5% CO₂ in 6 well non-tissue culture treated plates. Spheroids and aggregates were enzymatically dissociated into single-cell preparations using Accutase® approximately every 2 weeks for propagation or as needed for use in experiments. To accomplish this, spheroids were recovered from culture and allowed to settle at 1 x g for five minutes. The supernatant was removed and 1 ml of Accutase® was added to the sample which was incubated at 37° for

10-15 minutes with frequent trituration. The homogenous cell suspension was centrifuged for 5 minutes at 500 x g at ambient temperature. The pellet was either resuspended in the maintenance media described above or used for seeding tissue culture wells containing fibrin domes (*vide infra*).

Preparation of fibrin matrices

All stock components were dissolved in PBS unless otherwise noted. Solutions containing fibrinogen (from bovine plasma, Sigma-Aldrich) and varying amounts of aprotinin (from bovine lung, Sigma-Aldrich) were prepared as 20 μ l (final volume) aliquots on Parafilm[®] in a humidified chamber. When crosslinker was used, disuccinimidyl suberate (Pierce Chemical Co.) was freshly dissolved in dry DMSO (dried over 4Å, 40 mesh molecular sieves) and added to the sample at a final concentration of 50 μ M. The final fibrinogen concentration 36 μ M and the fibrinogen-fibrin conversion was initiated by the addition of 0.1 U thrombin (1 μ l, from bovine plasma, Sigma- Aldrich). To prepare domes for cell culture experiments, the preparation was quickly transferred into individual wells of 24-well tissue culture plates and the sample allowed to polymerize for 20-30 minutes before the careful addition of media and cells. Fibrin cylinders for surgical implantation were prepared in a similar manner, except that fluorescent fibrinogen (Alexa 488 fibrinogen, Life Technologies) was admixed with the preparation at a final concentration of 0.15 mg/ml. Polymerization was initiated via thrombin and the sample was quickly drawn into quartz tubes (Fiber Optic Center, dimensions, 0.70 mm inner diameter [i.d.] x 3.5 cm) such that a 6 mm long cylinders were crafted.

In vitro assessment of fibrin stability with SVZ-NPCs

Approximately 1×10^4 cells were seeded into wells containing fibrin domes with or without aprotinin and/or DSS, in 600 μ l aliquots of DMEM/F12, B27/N2, penicillin/streptomycin. Media was changed every 3-4 days. Mosaic photomicrographs were taken of each dome at days 2, 3, 4, 7, 9 and 14. Images were acquired using a Zeiss Axio Observer microscope (10x objective) outfitted with a Zeiss PM S1 live cell incubator, controlled by AxioVision software. Dome area was measured using this same software program.

Brain implantation of Fibrin Cylinders

Fibrin cylinders were made as described above and a small disc of PVDF (0.56 mm dia., Berkley) was inserted into the quartz tube and served as a plunger head. Anesthesia of female Sprague Dawley rats (250-300 gm) was induced via 5% isoflurane and maintained with 2.5% isoflurane (oxygen carrier flow rate maintained at 0.8 L/min). The animal's scalp was shaved and, after fitting the animal into a Kopf stereotaxic frame, the scalp was swabbed with Betadine[®]. An approximately 2 cm incision (anterior-posterior) was made in order to expose the skull bregma and lambda suture landmarks. The exposed skull was scrubbed with 3% H₂O₂ to clear away subcutaneous connective tissue. Two stereotaxic frame manipulator arms were used, one on each arm of the Kopf "U" frame, and both were angled 17° to the right of midline. To implant a cylinder into the right hemisphere, the tip of the fibrin cylinder-containing quartz tube (on the first manipulator arm) was moved, relative to the bregma, 0.13 cm anterior and 0.30 cm right of midline. A small hole was drilled using a round dental bur at the location corresponding to these coordinates. The dura was gently pricked with a 25-gauge needle and the tube driven 0.73 cm down the dorsoventral axis on an angle 17° off midline to the right.

A 0.5 mm stainless steel wire, affixed onto the second manipulator arm positioned directly above the first arm, served as a plunger and was lowered into the fibrin cylinder-containing tube. The plunger was lowered until the plunger head reached the top of the fibrin cylinder. The plunger was held immobile by the second manipulator arm while the quartz tube was slowly raised (1/4 turn/45 seconds) via the first manipulator. This maneuver results in the fibrin cylinder being placed in the brain along a predetermined path as the quartz tube is pulled out of the brain with the plunger holding the cylinder in place. The fibrin cylinders are implanted such that they transect the RMS containing SVZ migrating neuroblasts (a location chosen as it exposes the fibrin implants to the same endogenous progenitor cells being investigated for neuroregeneration therapies (98)). After complete extraction of the quartz tube and a five-minute incubation period, the plunger was slowly removed, the skull hole plugged with bone wax and the scalp closed with absorbable sutures plus Histoacryl®. Animals were injected with dexamethasone (0.4 mg/kg s.c. in 0.9% sterile saline) once at the time of anesthesia induction and then each day for four days post-operatively. For pain management, animals were injected with buprenorphine (0.15 mg/kg s.c.) immediately after surgery and then daily for two additional days.

Brain extraction and preservation

The first cohort of animals were sacrificed three weeks post-implant and brains extracted as described below (these brains samples were ultimately cryosectioned, imaged, and two-dimensional (2D) areas of remaining fibrin calculated). The second

cohort of animals were sacrificed at eight weeks post-implant and brains extracted (these brain samples then underwent non-destructive *in situ* imaging using tissue clearing and surface area of remaining three-dimensional (3D) cylinders were measured). Animals sacrificed by bilateral pneumothoracotomy, fixed via transcardial perfusion with 0.9% NaCl with 2U/ml heparin followed by 4% PFA. Brains were then carefully removed and underwent overnight post-fixing in 4% PFA.

Cryosectioning and imaging of brain samples

Following overnight post-fixing in 4% PFA, brains from the first cohort of animals were equilibrated in 30% sucrose until no longer buoyant and sectioned into 20 μm sections using a Leica cryostat. Sections were mounted on SuperfrostTM Plus slides (Fisher Scientific) using Fluoro-Gel II with DAPI (Electron Microscopy Sciences) as a mountant, covered with #1 coverslips and sealed with clear nail polish. Sections were observed on a Zeiss Axio Observer fluorescence microscope using Zeiss filter cube 38HE (470/40 excitation; 525/50 emission; 495 split). The area of fluorescent fibrin remaining in the section was quantitated using AxioVision software (Zeiss). Unfortunately, this method had two major downfalls. The first being that the freezing and manipulation of thin tissues left the embedded fibrin susceptible to falling out of the samples. Secondly, this method could only render a 2D view of a portion of the fibrin cylinder at a time for imaging. Therefore, the second cohort of brains collected underwent an alternative technique for imaging and analysis (*vide infra*).

Passive clearing and refractive index matching of brain samples

Tissue clearing methodology based on/adapted from previously published work (155, 156). Briefly, following post-fixation in PFA, lipid-clearing of whole brain samples was attempted using passive CLARITY technique (PACT), without the use electrophoretic tissue clearing as to not induce undue tissue swelling and disrupt brain implants. Intact brain samples were desired at this time as preliminary work revealed complications in attempts to cryosection portions of histological tissue that contained the cylindrical fibrin implants (notably, portions of the fibrin cylinders falling out of the manipulated tissues slices). As collecting measurements of remaining, undegraded fibrin within the brain samples was necessary, we sought an approach that would allow for imaging without the need for sectioning across the fibrin implants.

Whole rat brains were incubated at 4°C overnight in hydrogel monomer solution (4% acrylamide, 0.05% bis-acrylamide and 4% PFA in PBS) supplemented with 0.25% photoinitiator 2,2'-Azobis[2-(2-imidazolin-2-yl)propane]dihydrochloride (VA-044, Wako Chemicals USA, Inc.) thermal initiator. The hydrogel-infused samples degassed with nitrogen for approximately 30 minutes to ensure consistent hydrogel polymerization. Samples incubated for 2–3 hours at 37 °C to initiate tissue-hydrogel hybridization via VA-044 thermal initiation.

Once tissues were successfully cross-linked to acrylamide, excess hydrogel was gently removed with a Kimwipe and samples were transferred to perforated 50 mL conical tubes to bathe in clearing solution. To extract lipids, hydrogel-embedded brains were then incubated in sodium dodecyl sulphate (SDS) detergent clearing solution (4-8% SDS in 200 mM boric acid solution, pH 8.5 with NaOH) for 5 months. However, at this time it became evident that lipid clearing would not produce completely transparent brain tissue through these means for the internal regions of the whole brain samples.

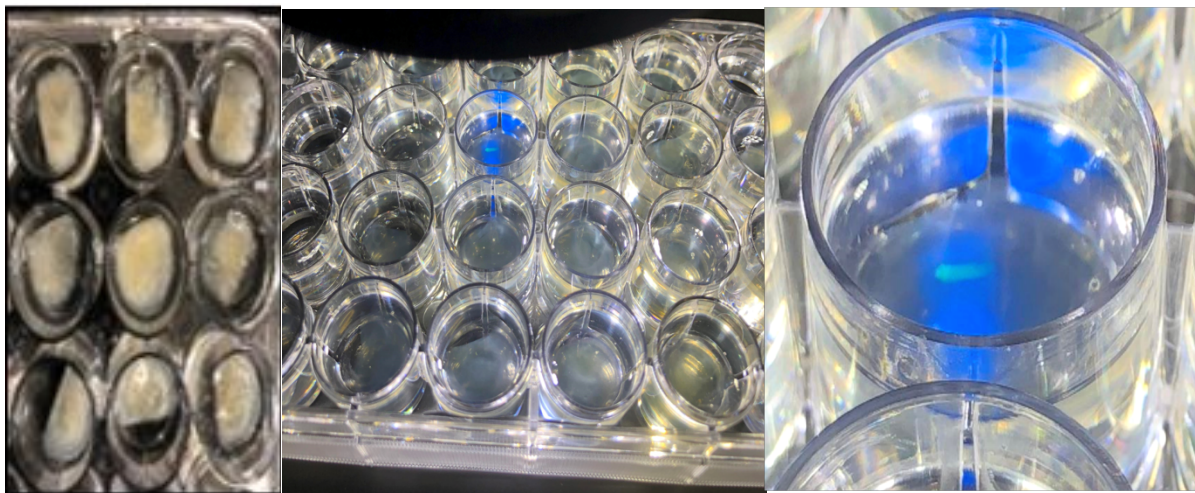


Figure 4. Cleared Brain Samples

Photographs of hemisected coronal brain slices before CLARITY/RIMS (far-left) and after (middle). Far-right image is expanded view from middle image, showing an intact fluorescent cylindrical implant within a single 2mm brain slice (as described in methods).

Taking into account surgical coordinates and brain surface landmarks, brains were hemisected and sliced to 2mm thickness using a brain mold and sharp razor blade. The sections were made so that the entire fibrin cylinder, if remaining, would be contained within one slice preparation (Fig 4). The 2 mm rat brain samples were then

returned to 50ml tubes containing clearing solution for 2 weeks. At that time tissue samples appeared relatively transparent and were washed with PBS and moved to refractive index matching solution (RIMS). RIMS imaging solution contained 40g of Histodenz (Sigma D2158) in 30 ml of 0.02 M PB with 0.1% tween-20 and 0.01% sodium azide, pH to 7.5 with NaOH, resulting in a final concentration of 88% Histodenz w/v. Samples were incubated in RIMS throughout imaging.

Imaging of fibrin brain implants

Images were acquired using Zeiss light sheet microscopy. The 2 mm cleared brain slices were affixed to a straightened section of 4-5 staples using superglue such that the brain sample was suspended by their upper pole and the portion to be imaged hung below. The staple was magnet mounted into a 5X clarity chamber. Images collected using the following parameters: detection objective – EC Plan-Neofluar 5x/0.164908000123; Illumination Objective – LSFM 5x/0.1; 488 nm laser at 20% power; Camera Exposure Time 30 ms; Light sheet thickness 7.32 μm ; zoom 0.56; single-side illumination.

Image and statistical analysis

Images were imported to Imaris (Bitplane) software for surface area analysis of cylinder 3D reconstructions. Surface area of remaining 488Alexa fibrin cylinders for each concentration were compared to each other. Comparisons to starting surface area could not be determined due to the swelling that occurs during the CLARITY process. Graphpad Prism was used for all statistical analysis.

Results

To establish a baseline for these studies, fibrin alone was cultured with SVZ- NPCs and the rate of degradation determined. The data indicate rapid degradation of the matrix, with only 20% of the dome remaining at Day 5 and no observable material remaining after seven days (Fig. 5A and Fig. 6). Very little additional stability was observed when 30 μ M aprotinin was non-covalently included in the fibrin dome (Fig. 5C and Fig. 6). This supports a number of reports indicating that the inhibitor ($M_w = 6500$ dalton) rapidly diffuses out of fibrin or other matrices (150, 153, 157). Figure 5B displays results observed when DSS alone was added to the fibrin. Interestingly, the crosslinker alone imparted slight resistance to SVZ-NPC mediated degradation (Fig. 5B and Fig. 6), suggesting that the DSS crosslinked structure of fibrin is itself somewhat more resistant to proteolytic degradation compared to native fibrin. Finally, aprotinin, at 30 μ M and covalently crosslinked into fibrin, completely resisted degradation throughout the duration of this experiment (7 days; Fig. 5D and Fig. 6). Additional experimentation (data not shown) revealed that fibrin domes crosslinked with 30 μ M aprotinin were completely intact up to 3 weeks in culture.

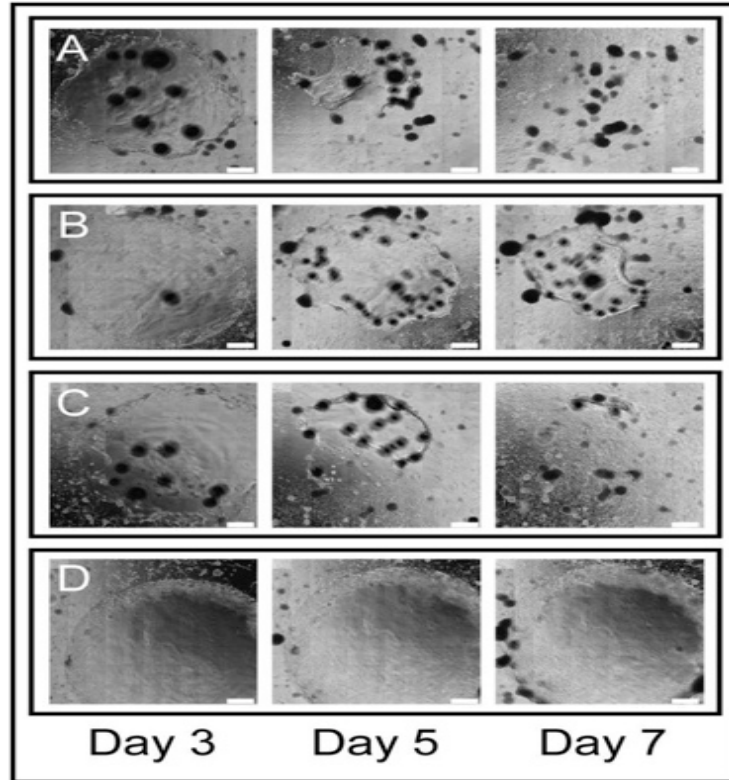


Figure 5. Photomicrographs of Fibrin Domes in SVZ-NPC Culture

Fibrin domes containing aprotinin and/or DSS were cast in 24 well tissue culture plates and seeded with SVZ- NPCs. On the indicated day a 12 x 15 mosaic photomicrograph of each dome was obtained. (A) Fibrin only. (B) Fibrin plus 50 μM DSS. (C) Fibrin plus 30 μM aprotinin. (D) Fibrin plus 50 μM DSS and 30 μM aprotinin. The dark structures seen in some of the images are aggregates of cells that are out of the focal plane.

Scale bar, 500 μm .

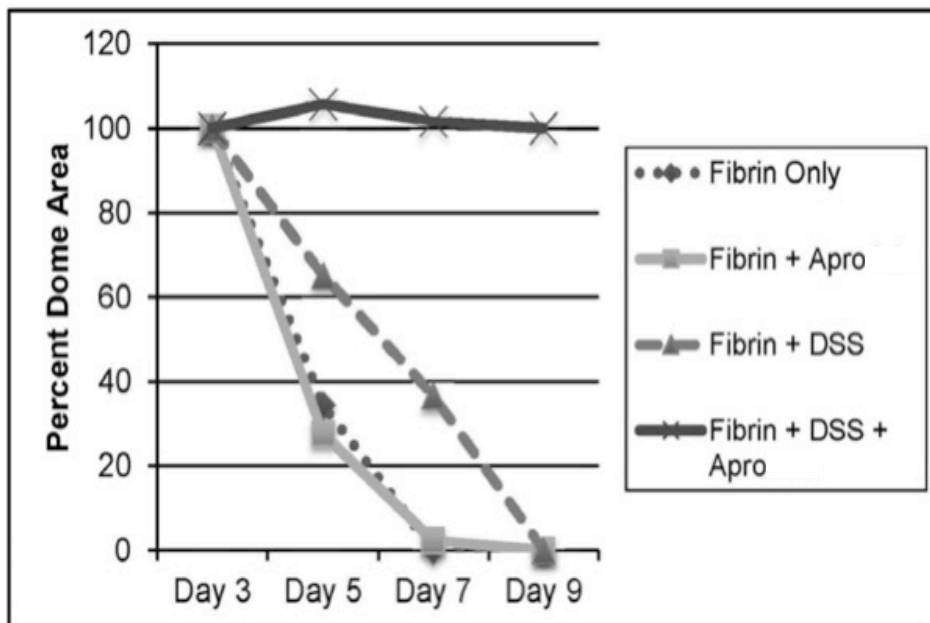


Figure 6. Degradation Rates of Fibrin Domes

Rate of degradation of fibrin-based domes containing immobilized or diffusible aprotinin in SVZ-NPC culture. Samples as described in Figure 5 were analyzed by assessing the area of fibrin dome remaining on a specific day relative to the area of that dome at the start of the experiment and plotted as percent dome remaining according to time.

An *in vitro* aprotinin dose-response experiment was performed over a 14-day period to determine whether it would be possible to develop fibrin hydrogels of varying degrees of stability in the presence of SVZ-NPCs. It was observed that fibrin stability could indeed be readily controlled depending upon the concentration of DSS-crosslinked aprotinin that was incorporated into the hydrogels (Figure 7 & 8). At concentrations 30 and 60 μM , domes were essentially completely resistant to degradation for the entire duration of the experiment. At lower concentrations, the dome half-life varied in a dose-dependent manner with concentrations below 10 μM showing significant degradation

after 1 week. This indicates that it is possible to fine-tune fibrin matrices to a particular stability for *in vitro* NSC experimentation.

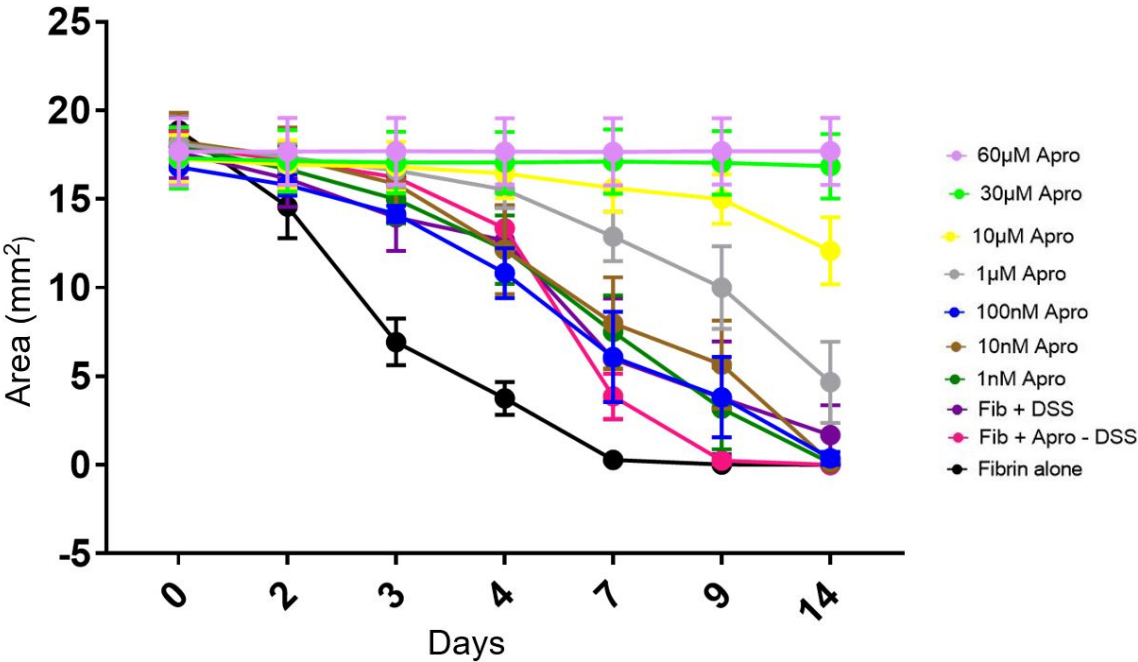


Figure 7. Aprotinin Mediated *In Vitro* Stability of Fibrin in a Dose-Dependent Manner Over the Course of Fourteen Days

Fibrin domes containing fibrin alone, fibrin with DSS, or fibrin with increasing amounts of aprotinin \pm 50 μ M DSS were cast in 24 well tissue culture plates, incubated with SVZ-NPCs for the indicated number of days, and the area of dome remaining on the indicated day.

Area of Fibrin Domes Remaining at Day 14

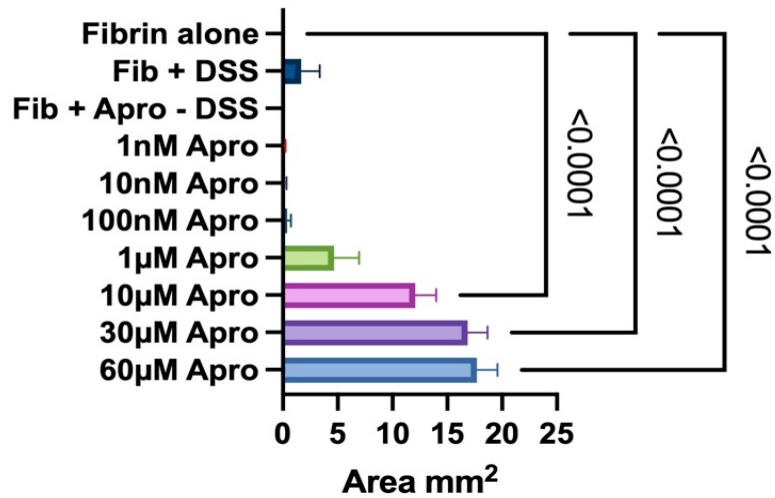


Figure 8. Aprotinin Mediated *In Vitro* Stability of Fibrin in a Dose-Dependent Manner

Fibrin domes with or without DSS and with increasing doses of protease inhibitor aprotinin were seeded with SVZ NPCs in cell culture. Statistically significant differences between areas of fibrin domes remaining at experimental endpoint (day 14) are presented. Data are mean \pm SEM; Ordinary One-way ANOVA

Aprotinin mediated *in vivo* stability of fibrin in a dose-dependent manner was also demonstrated (Fig 9, 10 & 12). All animals recovered fully after the procedure and there were no obvious behavioral sequelae. The first *in vivo* cohort (animals sacrificed 3-weeks post-implant) demonstrated increased resistance to degradation with increasing crosslinked aprotinin included in the fibrin implants (Fig 9 & 10). With the 0.075 μM aprotinin containing implant being nearly completely degraded, Cylinders that were cast with 0.75 μM or 0.075 μM aprotinin were significantly degraded based on Alexa-488

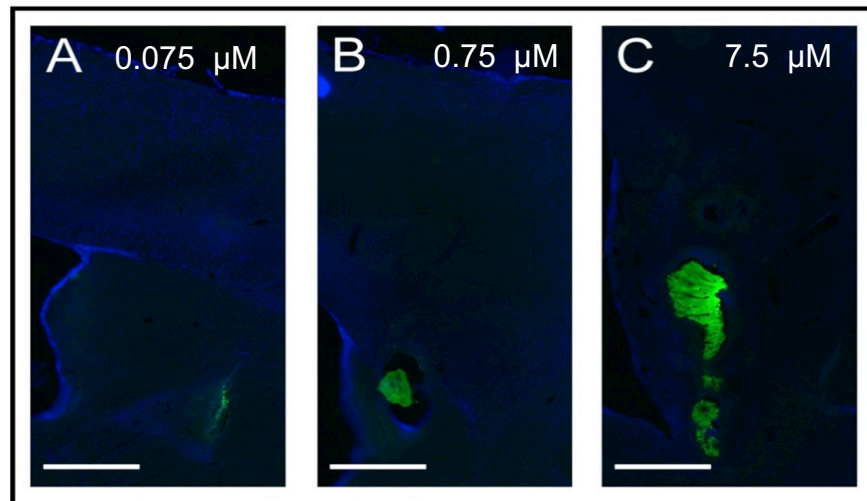


Figure 9. Concentration Dependence of Crosslinked Aprotinin on Fibrin Stability in Brain Implants

Fibrin cylinders made with Alexa 488-fibrinogen and containing increasing amounts of aprotinin crosslinked with 50 μM DSS were implanted into rat brain striatum (right hemisphere). Animals were sacrificed three weeks following surgery and brain sections visualized for Alexa 488 fluorescence. (A) Implanted cylinder containing 0.075 μM aprotinin. (B) Implanted cylinder containing 0.75 μM aprotinin. (C) Implanted cylinder containing 7.5 μM aprotinin. Scale bar, 2 mm.

containing fibrin that was visualized with brain sections collected (Fig 10). When calculations of percent remaining are calculated based on images provided (Fig. 9), cylinders that were cast with 0.75 μM or 0.075 μM aprotinin were 80% and 95% degraded, respectively. These results were complicated by the inability to visualize the intact fibrin cylinder as a whole. However, brain sections immediately adjacent to those depicted (Figure 9) were completely void of Alexa 488 fluorescence in the 0.075 μM and 0.75 μM aprotinin brains. Percent remaining, however, could not be determined for the 7.5 μM aprotinin cylinders due to problems previously discussed. Nonetheless, it is evident that a substantially larger amount of Alexa 488 containing fibrin is detectable in the 7.5 μM aprotinin sample, with an implant area over 3X greater than the next highest aprotinin concentration.

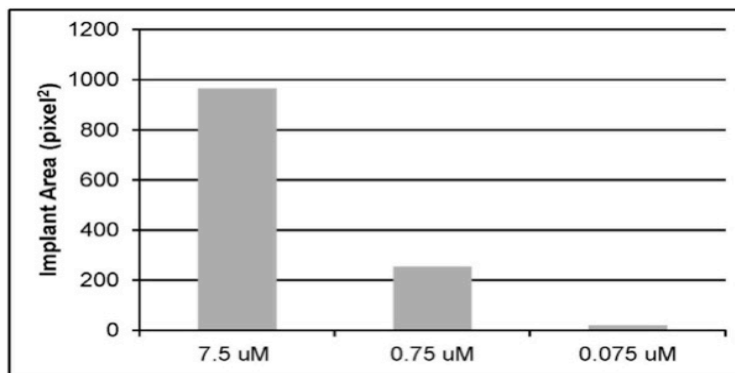


Figure 10. Quantitation of Fibrin Stability in Brain Implants

The area of the implanted fibrin matrix was determined from the images shown in Fig. 6 and presented as total pixels as a function of aprotinin concentration.

For the second cohort (animals sacrificed 8-weeks post-implant and whole brain clearing), 2D representative images of fibrin cylinders containing 30 and 60 μM aprotinin plus DSS are presented (Fig 11). Graphical representation (Fig 12) and raw data (Table 3) of the surface area remaining for each implanted fibrin cylinder containing increasing amounts of chemically crosslinked aprotinin are shown. The data show a dose-dependent resistance to degradation of fibrin in the neural environment with the use of proteolytic inhibitor aprotinin. On average, 46% more Alexa488 fibrin was detected in 60 μM samples than in 30 μM at week 8 post-implant. We suspect that if the fourth 10 μM aprotinin cylinder containing brain was not damaged and would have been included in the analysis that it would have followed the dose-dependent trend. Moreover, these

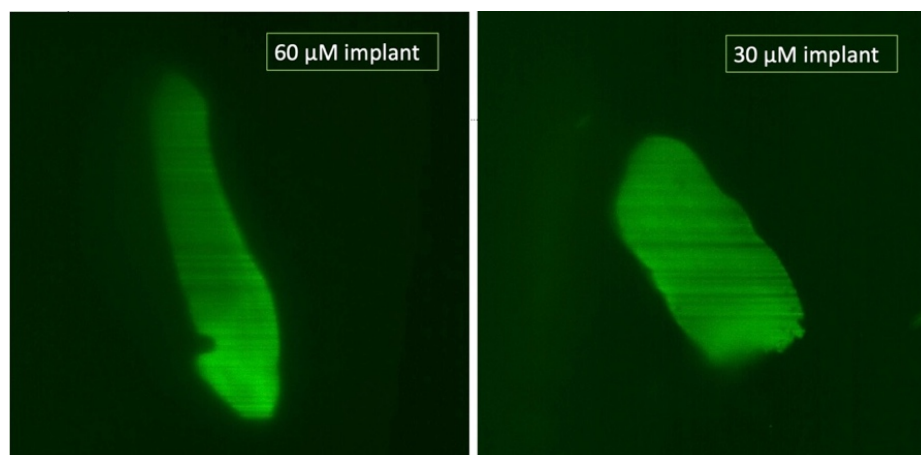


Figure 11. Two-Dimensional Representative Image of Fibrin Cylinders Used for 3D Reconstruction and Surface Area Analysis

data also reveal significant variability between animals. This may be due to any number of biological variabilities such as quantity of SVZ NPCs, varying proteolytic activity or other unknown differences. These data also demonstrate the usefulness of using the simple technique of chemical-crosslinking via addition of DSS to the fibrin/aprotinin mixture before casting implantable matrices.

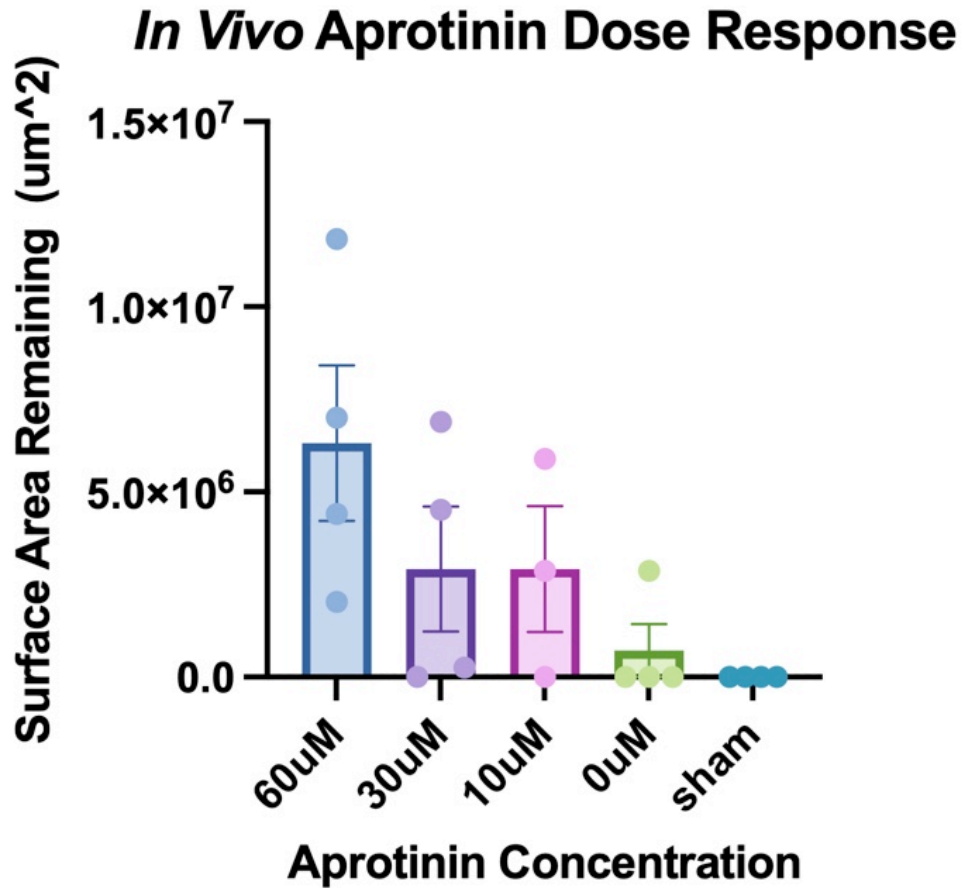


Figure 12. Aprotinin Concentration Dependence of Fibrin Stability Following Brain Implantation

Alexa 488-fibrinogen containing cylinders with increasing amounts of aprotinin cross-linked with 50 μ M DSS were implanted in rat brains such that the cylinders transect the endogenous path of SVZ NPCs and surface area of cylinders remaining 8 weeks after surgery were measured. All datapoints are shown \pm SEM; * p <0.05; One-way

Surface area of Fibrin Cylinders Following CLARITY and 3D Reconstruction					
Aprotinin concentration	60 μM	30 μM	10 μM	0 μM	sham
Surface area of cylinder remaining in each brain (μM^2)	2,031,080	0	-	0	0
	4,410,160	261,334	0	0	0
	7,008,460	4,521,290	2,862,760	0	0
	11,835,200	6,893,400	5,892,140	2,862,760	0
Averages (μM^2)	6,321,225	2,919,006	2,918,300	715,690	0

Table 3. Raw Data *In Vivo* Experiment

Four brain samples were obtained for each treatment. Brains passively cleared and cylinders imaged in their entirety (without sectioning) using light sheet microscopy.

The remaining Alexa488 for each cylinder at experimental end-point (post-implant week 8) are shown. One 10 μM sample was damaged and therefore not included.

Discussion

There are many synthetic and natural polymers that have been used as matrices for the therapeutic delivery of cells, proteins/peptides, or other compounds into tissues. Our laboratory proposes that fibrin is an ideal material for such applications, especially those aimed at furthering our understanding of neurological disorders and the development of associated novel therapies. It is biocompatible and biodegradable, thus appropriate for implantation in clinical applications. Fibrin is easily molded into desired 3D structures, pliable, and readily modified via chemical crosslinking agents such as the amino-directed reagent described here. It is cast and gelled under mild conditions enabling the incorporation of labile peptides, proteins, and cells. Fibrin-based matrices of various mechanical strengths can be prepared by varying the thrombin/fibrinogen ratio (158, 159), therefore fibrin can be cast into a very similar “softness” as brain tissue. Importantly, mechanical cues have been shown to affect many neuronal processes (160) and previous reports indicate matrices with compliance comparable to brain tissue select for and support neuronal growth (158, 161). This report further strengthens the argument that fibrin holds potential as an implantable matrix into the CNS; we demonstrate that degradation rates can be customized by incorporating specific amounts of immobilized aprotinin. Applications such as the transient delivery of a neurotrophin may require a rapidly degraded matrix, while, on the other hand, providing a stable extracellular matrix for regeneration of a complex structure such as a neural migratory pathway may necessitate several weeks of stability.

Fibrin biodegradation or fibrinolysis is a natural process mediated by both secreted (e.g. plasmin) and cell-associated (e.g. matrix metalloproteases) proteolytic enzymes

(147, 162). Aprotinin has been shown to inhibit the activity of both classes of proteases secreted by many cell types including neural cells (150). Robust fibrinolytic activity, thought to be critical in the natural response to stroke (138), is exhibited throughout the brain and aprotinin may provide a solution for the challenge natural fibrinolysis poses on the utilization of fibrin-based scaffolding in CNS regenerative therapies. This study aimed to develop a biocompatible, customizable, easily reproducible, and implantable matrix based on fibrin.

We found that fibrin was rapidly degraded when seeded with SVZ NPCs. The non-covalent addition of aprotinin to the fibrin solution provided no anti-fibrinolytic support, as suspected based on previous reports of rapid diffusion of the 6.5kDa aprotinin out of the fibrin hydrogels (150, 153). Incorporation of disuccinimidyl suberate (DSS), a non-cleavable, homobifunctional amino crosslinking agent (163), was successful at immobilizing aprotinin in the fibrin matrix and thus allowing aprotinin to prevent fibrinolysis in a dose-dependent manner. This trend was observed in both SVZ NPC culture and rat brain implantation models.

As the stabilization of the fibrin matrix was directly proportional to the concentration of proteolytic inhibitor used, this allows for a “tunable” fibrin scaffold. An important quality as we postulate that for their use in potential neuroregenerative therapies, neural implants must be stable enough to provide a suitable time frame for a desired cellular response to cues provided by the implant, but must eventually degrade completely to yield to de novo complex cellular structures. Significantly, over the period between surgery and sacrifice, there were no obvious deleterious postoperative effects of the implants on the animals in terms of overt behavior, tumorigenesis, or significant brain damage.

Conclusion

The current study demonstrates the feasibility of bioengineering implantable fibrin matrices to a modifiable and predetermined degree of stability against biodegradation within the CNS. The method of covalent incorporation of the proteolytic inhibitor, aprotinin, into hydrogel scaffolds presented here is simple, inexpensive, and easily reproducible. Stabilization of fibrin implants in vitro and in vivo is critical for ongoing and future research investigating applications in tissue engineering.

SECTION 2: *IN VIVO* NEURAL TISSUE ENGINEERING: CYLINDRICAL BIOCOMPATIBLE HYDROGELS THAT CREATE NEW NEURAL TRACTS IN THE ADULT MAMMALIAN BRAIN

Introduction

Individuals suffering from neurodegenerative disorders (e.g. Parkinson's, Alzheimer's, or Huntington's) or brain injuries (e.g. stroke or traumatic brain injury) have few effective treatment options. Therapies based on the regeneration or replacement of appropriate neurons have been proposed and many of these rely on implantation of exogenous stem cells into the lesioned area of the brain (54, 126, 164-167). To date, these approaches face serious problems such as immunogenicity, tumorigenicity, functional ineffectiveness, cell availability, and ethical concerns (168-170). We describe in this study, an alternate and potentially transformative procedure for targeted neural cell replacement that is based on the recruitment and guidance of endogenous neural stem cells directly from their natural niche into a specific region of interest. Harnessing these preexisting neural progenitors *in vivo* will bypass the numerous concerns associated with exogenous cell transplantation. When reduced to practice, this unique approach will have tremendous ramifications for patients suffering from neurological disorders who currently face a paucity of beneficial therapies.

This innovation is derived from our understanding of adult neurogenesis in the mammalian brain, which consists of a coordinated series of overlapping steps, including proliferation, differentiation, migration, neuritogenesis, axon guidance, and integration (171). Induced adult neurogenesis has been demonstrated to be a natural response to various activities such as exercise (172) or neurological disorders such as stroke (173-

176) or traumatic brain injury (75, 176, 177), and this has led to the belief that endogenous neural stem cells can be harnessed to repopulate dysfunctional or lesioned nonneurogenic regions of the brain (76, 178). Studies using cultured neural stem cells and genetically engineered animals have identified numerous neurotrophins and extracellular matrix (ECM) components that appear to mediate the maturation of endogenous NPCs into neurons (179, 180). However, few reports integrate this knowledge into an application that can be used to engineer an effective means to recruit these cells to regenerate neural tissue, especially using an in vivo approach. The full potential of therapeutic endogenous neural stem cells requires efficient cell recruitment, targeting, neural subtype-specific differentiation, and long-term cell survival. The results presented in this study represent an important contribution toward achieving these goals.

A renewable source of endogenous neural stem cells is the adult mammalian SVZ. Much of what we currently know about neurogenesis has come through studies of the SVZ/RMS/OB pathway (181, 182). SVZ-derived neural progenitor cells (SVZ-NPCs) are the likely source of nascent neurons, which arise in the typically nonneurogenic striatum following exercise or injury (75, 172-177). This supports the notion that SVZ-NPCs are naturally rerouted to typically nonneurogenic regions in response to an insult to the brain. While a vital observation, the number of SVZ-derived cells naturally recruited to lesioned areas is too low to expect significant therapeutic efficacy in the case of most neuro-degenerative diseases or brain injury.

Recent efforts to deliberately recruit endogenous NPCs into nonneurogenic areas of the brain have met with some success. This approach was in the form of hyaluronic acid engineered to contain neurotrophic factors, made as an injectable low

viscosity polymer (183), which increased neurogenesis in rat cortex and striatum after injection into these regions (184). These authors suggested that the source of new neural cells may be endogenous quiescent NPCs rather than a neurogenic niche such as the SVZ.

The goal of this report is to present research describing a means to reroute and retask endogenous SVZ-NPCs from the RMS to populate nonneurogenic brain regions with new neural cells. Our approach was to develop an implantable, biocompatible, and biodegradable fibrin matrix, which was readily modified to contain judiciously chosen immobilized factors such as neurotrophins, ECM molecules, and aprotinin. Our goal, upon implantation into the brain, was to provide an environment that would create a new migratory path from the renewable neurogenic niche of the SVZ/RMS to a new and distant target region. We chose to include both neurogenic [nerve growth factor (NGF)] and angiogenic [vascular endothelial growth factor (VEGF)] factors in the implantable microenvironment since both developmental processes are inextricably linked to the creation of neural migratory paths (185-188).

We believe that fibrin is an ideal biomaterial for these implantable matrices; it is readily chemically modified to covalently incorporate bioactive peptides and proteins (143); it is biochemically similar to extracellular proteins found in the brain (128, 158); fibrin is biologically compatible and is degraded by well-known and inhibitable proteolytic processes (147, 162); and, it is used clinically in the form of fibrin sealant and has low immunogenicity (132, 189). Furthermore, several groups have successfully used fibrin hydrogel injected into animals to address spinal cord and peripheral nerve injury

(143, 190-195). Finally, it seemed logical to create this implantable biomaterial in the form of a cylinder since the RMS is, in fact, cylindrical.

Materials and Methods

Preparation of implantable cylindrical scaffolds

Fibrinogen (Sigma-Aldrich, St. Louis, MO) was dissolved in phosphate-buffered saline (PBS) at a final concentration of 64 μM , degassed, and stored in aliquots at 80°C. An 8 μL aliquot of fibrinogen was placed on a square of Parafilm® to which was added aprotinin (15 μM Sigma-Aldrich), laminin I (100 $\mu\text{g}/\text{mL}$ Trevigen, Gaithersburg, MD), carrier-free VEGF (10 $\mu\text{g}/\text{mL}$ final concentration; R&D Systems, Minneapolis, MN), and carrier-free NGF (10 $\mu\text{g}/\text{mL}$ final concentration; R&D Systems). The volume of the sample was brought to 18 μL with PBS. The homobifunctional crosslinker disuccinimidyl succinate (DSS; Thermo Scientific Pierce, Rockford, IL) was dissolved in dry dimethyl sulfoxide (dried over 4 Å, 40 mesh molecular sieves) and 1 μL (500 μM final) was added to the sample with thorough mixing. DSS is a chemical crosslinker that is directed toward amino groups, thus facilitating the covalent incorporation of the peptides and proteins used in this study (i.e., VEGF, NGF, laminins, and aprotinin) into the fibrin hydrogel (196-200). The crosslinking reaction was incubated for 10 min at ambient temperature in a humidified chamber. Thrombin (1 μL of 0.1 U/ μL ; Sigma-Aldrich) was added and the sample quickly mixed and injected through a Gilson P20 Pipetman® into a quartz tube (0.7 mm i.d., 3.5 cm long; Fiber Optic Center, Inc., New Bedford, MA) such that a 7 mm long cylinder was created. The dimensions of the final cylinder were 0.7 mm dia. X 6 mm long following the polymerization and concomitant shrinkage of the fibrin.

Cylinders were made within 4h of implant surgery and stored in a humidified chamber until used.

Implantation of cylinders into rat brain

Female Sprague-Dawley rats (175 g; 7 weeks old) were purchased from Hilltop Lab Animals, Inc. (Scottsdale, PA). Animals were acclimated and handled every 1–2 days for 2–3 weeks before experimentation. Cages were provided environmental enrichment in the form of PVC pipe fittings. All animal experiments were carried out in accordance with the National Institutes of Health Guide for the Care and Use of Laboratory Animals and performed under an approved protocol from Marshall University's IACUC. The fibrin cylinders were implanted along a predetermined path in the right hemisphere of each animal (Fig. 1). A short (ca. 0.5mm) length of polyvinylidene difluoride (PVDF) fluorocarbon line (0.56 mm diameter leader material; Berkley, Columbia, SC) was inserted into the quartz tube containing the fibrin cylinder and served as a plunger head and a 20 cm length of stainless-steel wire (0.5mm dia.; AmazonSupply) was used as a plunger (Fig. 13). Animals were anesthetized using isoflurane (5% induction, 2% maintenance) with an oxygen flow of 0.8 L/min.

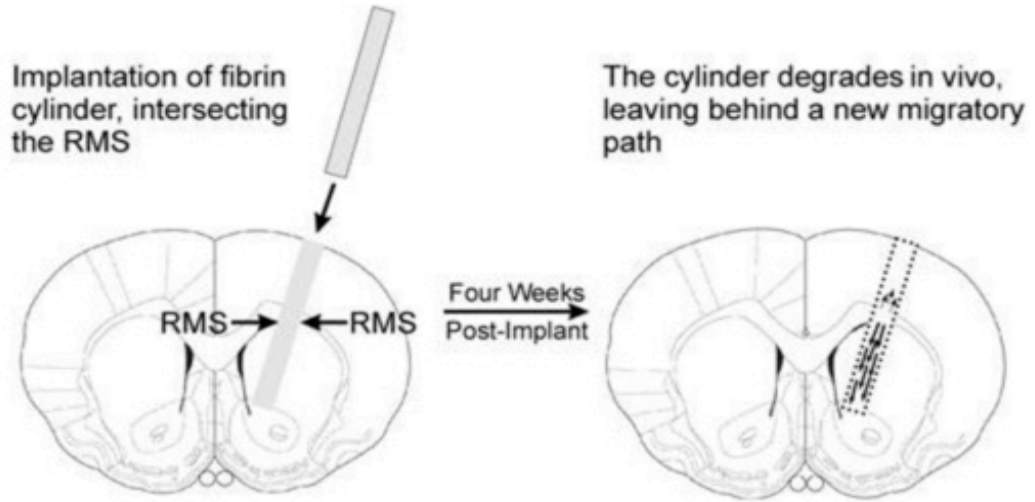
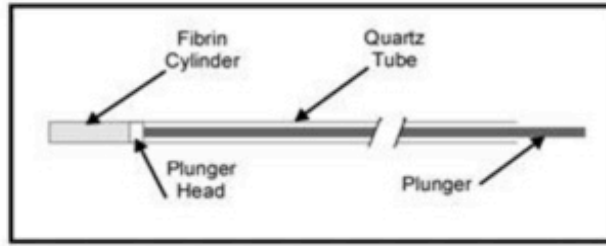


Figure 13. Diagram of Coronal Section of Rat Brain Showing Location of Hydrogel Implant

The relative location of the cylinder is at an angle 17° right of midline, implanted through the skull, relative to bregma, and at 0.13 cm anterior and 0.30 cm lateral right of midline, with the distal end of the implant 0.73 cm dorsoventral to the skull. The cylinder passes through the cortex, corpus callosum, the RMS, and into the striatum. The fibrin-based biomaterial degrades to completion after *4 weeks. Coronal diagram reprinted with permission, originally published in “The Rat Brain in Stereotaxic Coordinates,” George Paxinos and Charles Watson, figure 13, Copyright Elsevier (1998). Inset: Implant assembly. A solution of fibrinogen/thrombin/immobilized factors was injected into quartz tubes (0.7 mm i.d. · 35 mm length) such that 6 mm long fibrin cylinders were produced. A plunger head made of PVDF was inserted into the cylinder and pushed to the top of the fibrin cylinder using a 20 cm long stainless-steel wire (0.5 mm dia.) as a plunger. The plunger was removed and the quartz tube/fibrin cylinder/plunger head assembly was affixed to the right arm of a stereotaxic frame and the plunger wire attached to the left arm. The fibrin cylinders were surgically implanted into rat brains as described in the Materials and Methods sec-

Animals were positioned into a Kopf stereotaxic frame that was outfitted with two manipulators, one on each arm of the Kopf “U” frame, and both were angled 17° to the right of midline. The fibrin cylinder-containing quartz tube was affixed to the right manipulator and the wire plunger was placed on the left manipulator. A small hole was drilled using a round dental bur at, relative to the bregma, 0.13 cm anterior and 0.30 cm lateral

right of midline (201). The dura was gently pricked with a 25-gauge needle and the quartz tube slowly driven 0.73 cm down the dorsoventral axis on an angle 17° off midline to the right. The plunger was lowered into the fibrin cylinder-containing tube until just touching the PVDF plunger head, which itself was just touching the fibrin cylinder. The plunger was held immobile by the left manipulator arm, while the quartz tube was slowly raised (1/4 turn/45 s) by the right manipulator. This maneuver resulted in the 6 mm cylindrical fibrin matrix being placed (not extruded) in the brain along a predetermined path (Fig. 13) as the quartz tube was removed from the brain with the plunger holding the hydrogel cylinder in place.

The final position of the 6 mm long implant started at the surface of the brain and passed through the cortex, corpus callosum, RMS, and striatum. After complete extraction of the quartz tube, the skull hole was plugged with bone wax and the scalp closed with absorbable sutures. Animals were injected with dexamethasone [0.4 mg/kg subcutaneously (s.c.) in 0.9% sterile saline] once at the time of anesthesia induction and then each day for 4 days postoperatively. For pain management, animals were injected with buprenorphine (0.15 mg/kg s.c.) immediately after surgery and then daily for 2 additional days. Ten animals were used in this series; six received fibrin cylinders containing VEGF, NGF, laminin I, and aprotinin; two were implanted with fibrin cylinders containing only immobilized aprotinin and laminins, and two underwent sham surgeries (empty quartz tubes driven to the same coordinates).

6-hydroxydopamine lesions

Twelve rats were prepared for surgery as described above. The hemiparkinson model was generated by 6-hydroxydopamine (6-OHDA) injections into the right medial forebrain bundle (MFB). Desipramine was injected (*i.p.*, 25 mg/ kg in sterile H₂O) just after anesthesia induction. The coordinates for MFB injection were, relative to bregma, -0.44 cm anterior; 0.12 cm right of midline; and -0.84 cm dorsoventral, and 3 mL of 6-OHDA (5mg/mL in freshly made, degassed 0.9% NaCl/ 0.02% ascorbic acid) was injected at a rate on 0.5 mL/min. Following injection, the cannula was left in place for 5 min and then slowly removed (raised 1/4th of a turn every 45 s) and the site closed as described above.

Two weeks postoperative, animals were injected *s.c.* with 5 mg/kg d-amphetamine in 0.9% NaCl and rotations were counted for 90 min in a Rotometer (San Diego Instruments, San Diego, CA). Out of the 12 6-OHDA-lesioned animals, 7 displayed greater than 400 total ipsilateral turns and fewer than 5 total contralateral rotations and were chosen for cylinder implantation as described above. Five animals received fibrin cylinders containing VEGF, NGF, laminin I, and aprotinin, and two animals were implanted with fibrin/aprotinin/laminin as a control. Lesioned and subsequently implanted animals were challenged with d-amphetamine 4 weeks following implant surgery to assess the impact of the cylinders on drug-induced ipsilateral rotations. Correction was reported as percent correction for each animal (number of turns before implant) - (number of turns after implant) / (number of turns before implant).

Immunohistochemistry

Animals were sacrificed 4–5 weeks following surgery, a point at which the cylinders were completely degraded, and we determined the phenotype and anatomical distribution of migrating neuroblasts in coronal sections of the brains. This time frame was chosen to visualize Dcx⁺ cells utilizing a stable migratory path rather than merely responding to the inherent damage of the implant surgery, which should be resolved before the 4–5 week sacrifice time point (76).

Animals were sacrificed by bilateral pneumothoracotomy, fixed by transcardial perfusion with 0.9% NaCl containing 2U/mL heparin followed by 4% freshly prepared paraformaldehyde (PFA), and brains recovered. Following overnight postfixing in 4% PFA, brains were equilibrated in 30% sucrose until no longer buoyant and stored at 4°C until processed into 20 µm sections using a Leica Model 1950 cryostat. Samples were incubated for 15 min in 50 mM NH₄Cl, permeabilized in 0.1% Triton X-100, blocked over-night at 4°C in 5% bovine serum albumin (BSA; Jackson Immunoresearch Laboratories, West Grove, PA) and 5% normal goat serum, and subsequently incubated with primary antibodies (1:200 in 0.1% BSA-cTM; Aurion (Wageningen, The Netherlands); 0.1% normal goat serum) overnight at 4°C. Sources of antibodies were as follows: Doublecortin (Dcx; a marker for immature neurons and neurogenesis), Millipore (Darmstadt, Germany); Neurofilament medium (NF160; a marker for mature neurons), Abcam (Cambridge, MA); tyrosine hydroxylase (TH; a marker for mature dopaminergic neurons), Abcam; microtubule-associated protein 2a and 2b (MAP2ab; a marker enriched in mature neuronal dendrites), Abcam; and glial fibrillary acidic protein (GFAP; a marker for reactive astrocytes), Abcam. Following extensive washing, sections were incubated

overnight at 4°C with Alexa-conjugated fluorescent secondary antibodies (Life Technologies, Carlsbad, CA) diluted 1:500. Following washing, samples were mounted on Superfrost plus glass slides (Fisher Scientific, Pittsburgh, PA) and coverslipped with number 1 glass with Fluoro-Gel II-DAPI (Electron Microscopy Sciences, Hatfield, PA) as the mountant. Slides were sealed with clear nail polish and stored at 4°C until imaged/analyzed using a Zeiss Axio Observer with 10X and 20X LD Plan Neofluar air-interface objectives and AxioVision 4.6.3 software.

Results

Implanted fibrin cylinders recruit neuroblasts that migrate along the implant track

Immunohistochemical analyses of samples from animals implanted with fibrin cylinders containing NGF, VEGF, laminin I, and aprotinin revealed significant numbers of migrating neuroblasts (Dcx⁺; Figs. 14 and 15). These cells exhibited complex, long, and branching neurites and were most numerous along the original location of the cylinder in the striatum. The new path facilitated by the hydrogel implant varied slightly in length between animals and was between ~2.0 and 2.8 mm in length. Evaluation of the Dcx⁺ cells at higher magnification (Figs. 15 and 16) reveals the complexity of the neuroblasts' neurites, many exceeding 100 µm in length and exhibit numerous branch points (Fig. 16). There was no residual mechanical damage due to the surgical procedure nor was there significant GFAP⁺ labeling (data not shown) at the site of the implant, indicating there was not a significant inflammatory response (202) to the matrix.

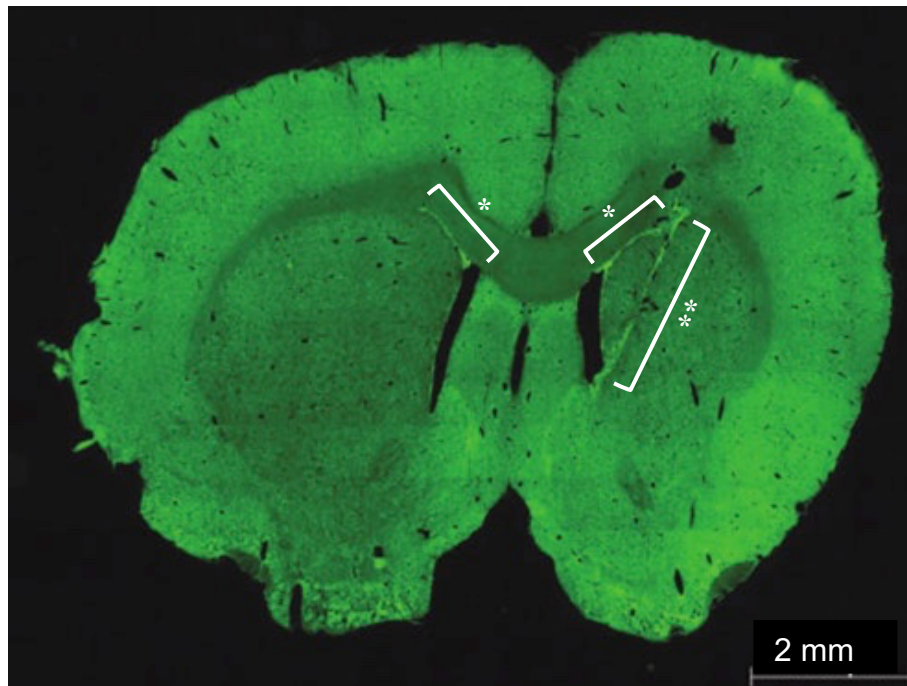


Figure 14. Recruitment of Neural Precursors by the Fibrin Implant

Sections were labeled for migrating neuroblasts with anti-Dcx antibodies. Shown is a whole coronal section revealing both the *left* (contralateral) nonimplanted and *right* implanted hemispheres. Dcx⁺ cells (*green*) were observed in both hemispheres immediately dorsal to the lateral ventricles (indicative of the posterior RMS; signified by the *), while only the implanted hemisphere exhibited significant Dcx⁺ cells in the striatum, along the implant path (indicated by the **). The length of the tract of neuroblasts in this animal is ~2.6 mm. The fibrin cylinder was itself degraded and the majority of labeling was along the track of the implant; additional labeling was observed between the wall of the lateral ventricle and the implant track (Fig. 5). Dcx, double-

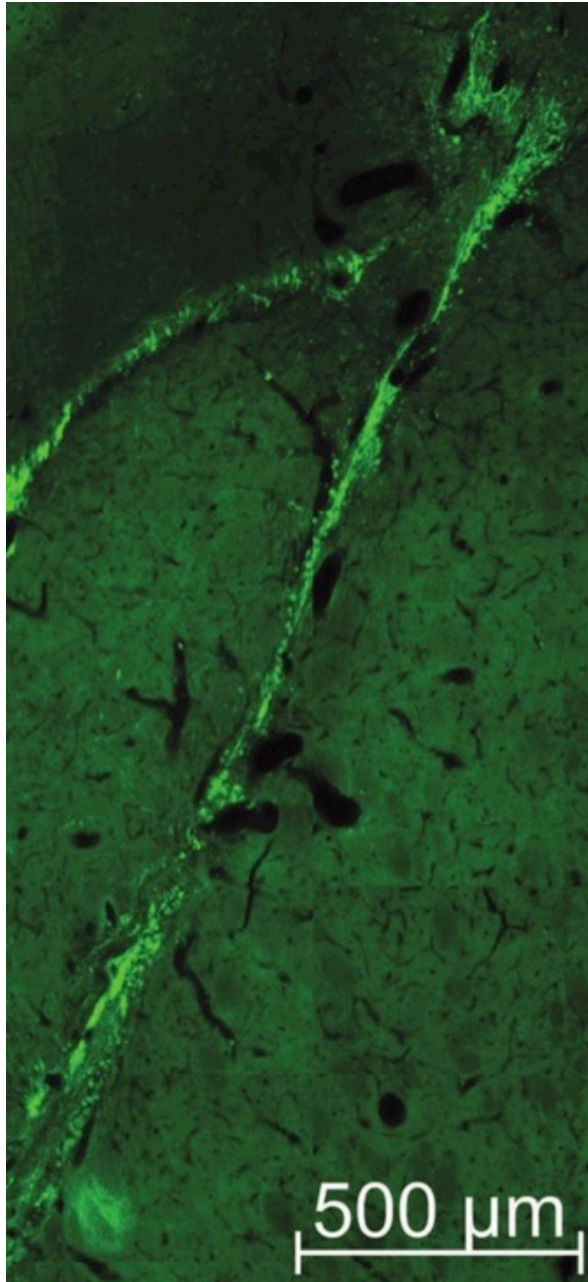


Figure 15. Neuroblasts in the Implant Track Exhibit Complex Neural Morphology

To visualize the neural-like structures of the new cells in the implant region, a high magnification image of the area was generated. Dcx^+ cells (*bright green*) exhibit long neurites along the implant path and many show complex branching, especially those migrating toward and into the corpus callosum. The length of many of these neurites exceeded 100 μm .

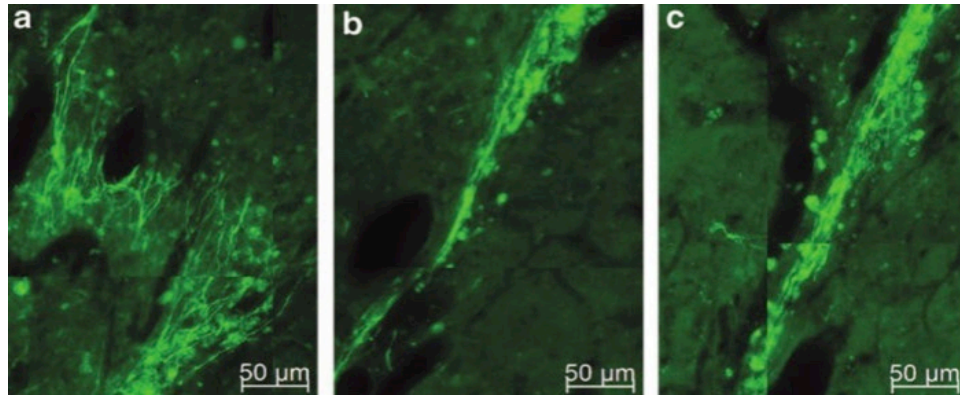


Figure 16. Higher Magnification of Neuroblasts and Neurites in the Implant Region (from Fig 15)

Neuroblasts are prevalent along the implant region and their long neurites project parallel to the original, now degraded, cylinder. (a–c) Representative regions of the implant, dorsal (a) to ventral (c).

Additional Dcx^+ cells were observed in implanted striatum in regions lateral to the lateral ventricle, between the implant path and the ventricle wall (Fig. 17b), which were not observed in the corresponding contralateral striatum (Fig. 17a). These new cells may represent occult neural stem cells residing in the striatum that were stimulated to differentiate due to the implanted microenvironment, or they may have arisen from the lining of the ventricle and migrated directly toward the implant. We noted that many Dcx^+ cells in this intrastriatal region possess long ($>100 \mu\text{m}$) branched neurites with morphology consistent with synaptogenesis (visible upon increased magnification), which possibly suggests the beginning of functional integration of the new neural cells into the existing circuitry (76, 203, 204).

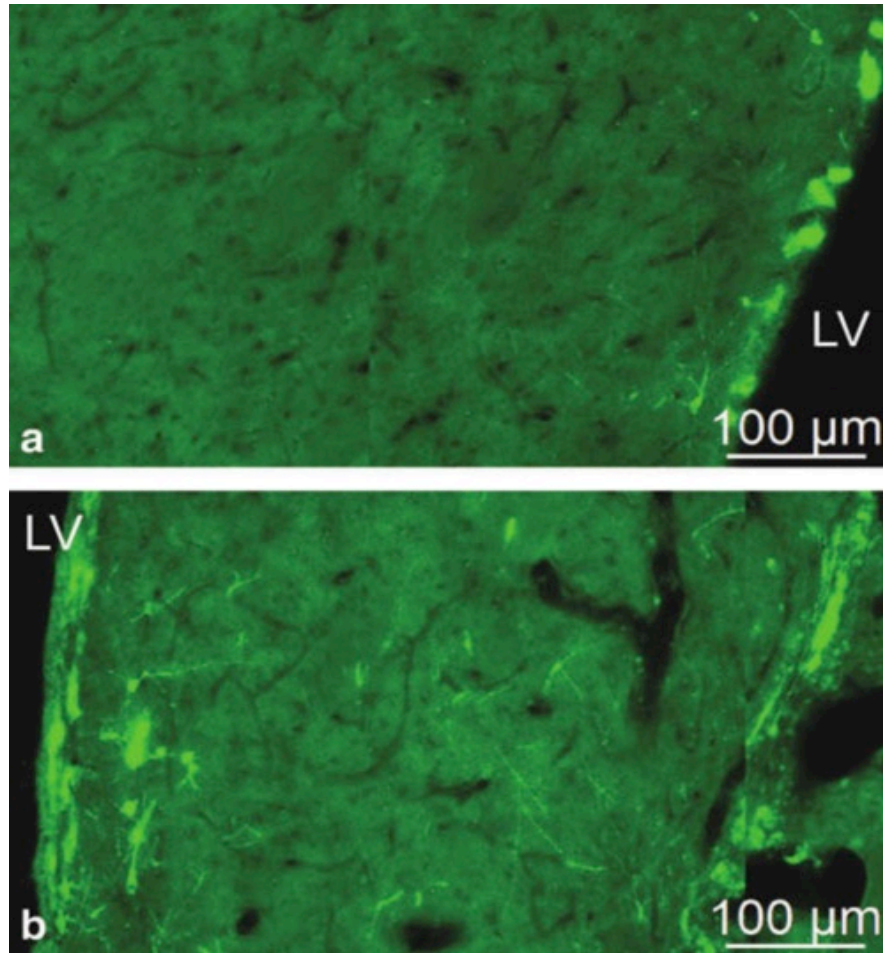


Figure 17. Additional Recruitment of Neuroblasts Between the Lateral Ventricle and Implant Site

(a) Control nonimplanted left hemisphere. (b). Region comparable to that in (a), from the implanted right hemisphere. Compared to the control hemisphere, this intrastriatal region is rich in neuroblasts with complex morphologies. LV, lateral ventricle.

The region of the striatum containing the highest density of new cells was a clearly defined path from the RMS to the bottom of the cylindrical implant region in the ventral striatum. It is of interest to note that, although the cylinder implant also led through the cortex to the dorsal-most aspect of the brain, far fewer new cells were found in the cortical region. Although neurites were clearly visible leading into the cortex, they did not extend significantly into this region, despite being in the implant track (Figs. 14 and 15). Finally, the response of the endogenous SVZ-derived cells to the implant was dependent upon the presence of neurogenic factors; no new neural cells, including dopaminergic (TH⁺) neurons, were observed in factor-free controls (Fig. 18), although there does appear to be a disruption of the NF160-labeled “pencil tracts” (205) in the implanted striatum (Fig. 18a).

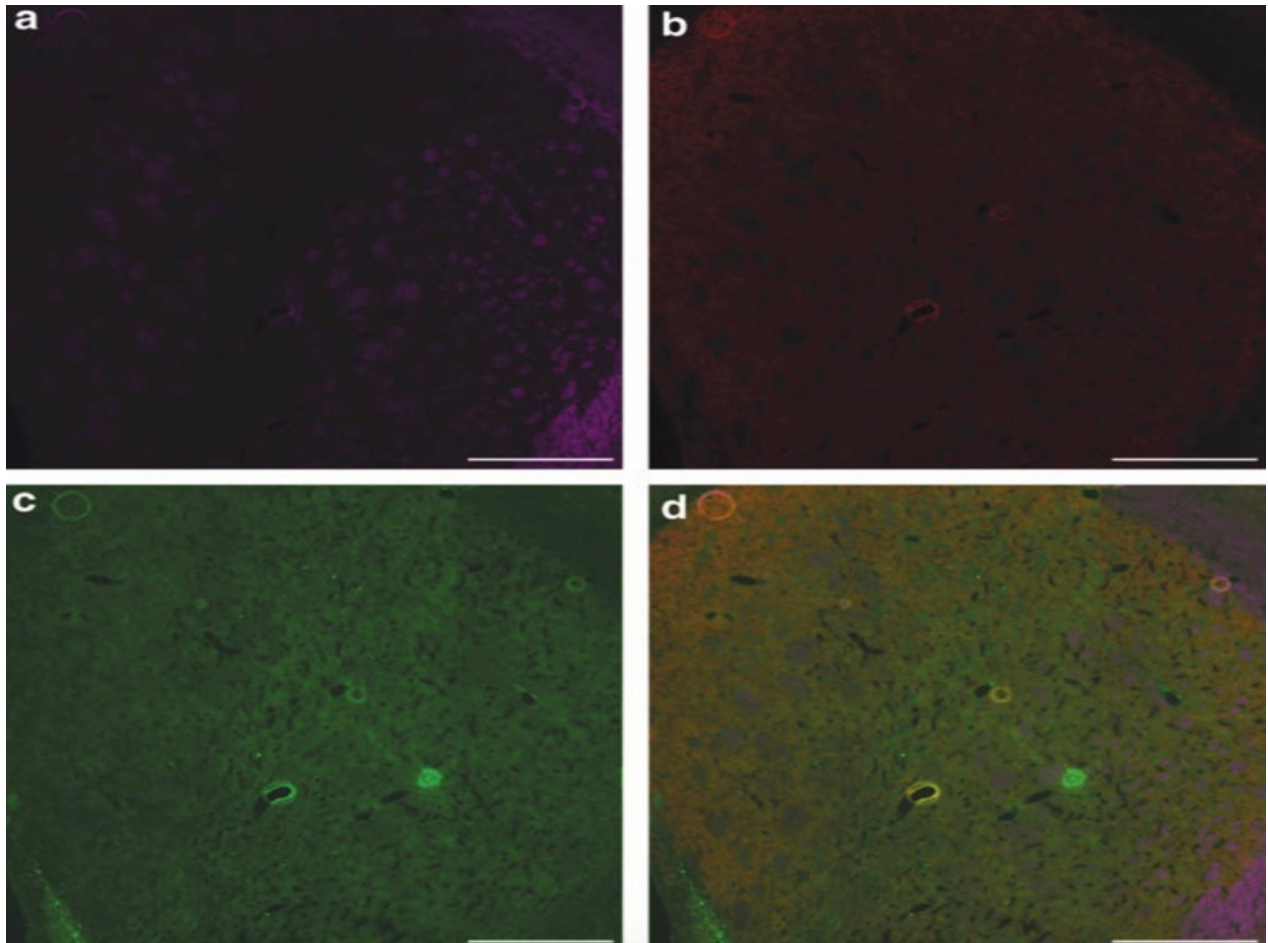


Figure 18. Immunolabeled micrographs of Striatum for Each Treatment

Immunohistochemistry of striatal region of control implant, containing only fibrin, apro-tinin, and laminin. (a) Section probed for NF160 cells (*magenta*). (b) Section probed for Map2ab⁺ cells (*red*). (c) Section probed for tyrosine hydroxylase (*green*). (d) Merged image from (a–c). Scale bar = 500 μm . Map2ab, microtubule-associated protein 2a and 2b.

***In vivo* neural engineering corrects hemiparkinson rat rotational behavior**

The robust neurogenic response to these brain implants suggested a therapeutic application for this technology. We predicted that in an animal model of neurodegeneration, the fibrin cylinders would guide endogenous NPCs into damaged/dysfunctional nonneurogenic regions; these cells would then functionally integrate and restore lost function. We chose the 6-OHDA animal model of Parkinson's disease since the anatomical location of the defect is well characterized (striatum, nigrostriatal pathway, and substantia nigra), the specific neural phenotype that is necessary for therapeutic efficacy is readily assessed (labeling for TH), and correction of the behavioral deficiency is quantifiable (rotometer analysis).

Animals underwent unilateral 6-OHDA lesions to generate hemiparkinson rats and subsequently were subjected to *in vivo* neural engineering by these novel implantable fibrin matrices. This experimental therapeutic approach appeared to correct the asymmetric rotational defect in these animals (Fig. 19a). Immunohistochemical analyses of brains from corrected animals showed cells in the implanted striatum that were decorated with antibodies against TH, suggesting a dopaminergic phenotype (Fig. 19b–d). Control, lesioned animals implanted with fibrin cylinders containing only laminin and aprotinin (and lacking NGF and VEGF) were not corrected by the procedure.

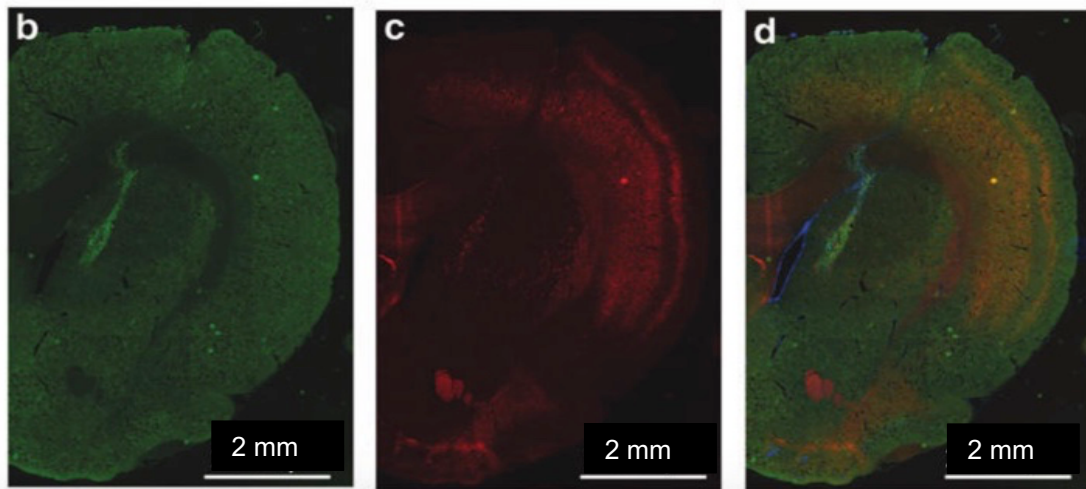
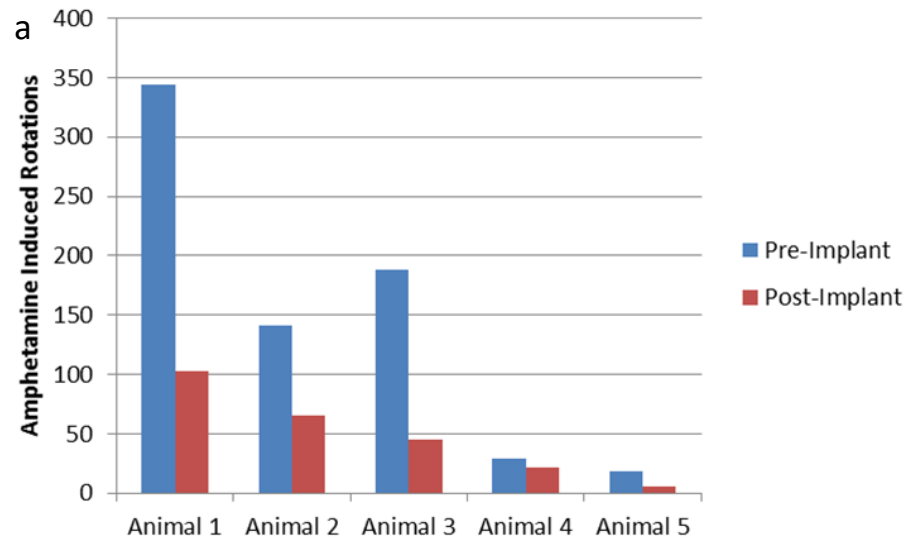


Figure 19. Fibrin Implants Correct Amphetamine-Induced Ipsilateral Rotations in Unilateral 6-OHDA- Lesioned Rats

(a) Shown are individual results from five lesioned animals that were implanted with fibrin cylinders containing laminin, aprotinin, NGF, and VEGF. (b–d) Immunohistochemistry of sections from implanted, corrected animals. (b) Section probed for tyrosine hydroxylase (green). (c) Section probed for Map2ab (red). (d) Merged image showing nuclei (DAPI; blue), tyrosine hydroxylase (green), and Map2ab (red). NGF, nerve growth factor; 6-OHDA, 6- hydroxydopamine; VEGF, vascular endothelial growth factor.

Discussion

Endogenous NPCs from the adult mammalian SVZ/RMS are an untapped source of therapeutic neurons. The restorative potential of these adult neural stem cells can be realized if a portion of the migrating neuroblasts can be steered away from their usual destination (the OB) and into non- neurogenic regions of the brain where disease or injury has reduced the number of functional neurons. The long-term goal of our research is to develop a means to retask these endogenous neural stem cells in the adult brain by engineering new, relatively long migratory paths that lead these cells into nonneurogenic regions of the brain.

Our objectives were threefold; first, we engineered a biocompatible cylindrical matrix that was of sufficient mechanical stability that it could be implanted into the brain in a manner that essentially connected neurogenic to relatively distant nonneurogenic regions. Other types of matrices that have been used to stimulate neurogenesis are relatively fluid and, while straightforward to inject, not likely to generate long engineered pathways targeted to specific regions of the brain. Second, we used an aprotinin-stabilized formulation of fibrin for the implant because we posit that the ideal matrix must be somewhat stable, yet biodegradable such that it will eventually yield newly developed neural paths consisting of complex networks of neural cells and microvasculature. Our data and others (150, 153) have demonstrated the ability of aprotinin, a peptide serine protease inhibitor, to fine-tune the in vitro and in vivo neural cell-mediated degradation rate of fibrin. This information was used in this work to generate a matrix that would be completely degraded within 4–5 weeks. Third, we created an implantable biomaterial with a cylindrical geometry that was readily modified with im- mobilized factors chosen

to recruit endogenous NPCs from the SVZ-RMS and direct them into a typically non-neurogenic region. Since the quintessential neural migratory path in adult mammals is the RMS, and this has a three-dimensional architecture that is relatively cylindrical, we engineered fibrinogen, thrombin, and additional components as small implantable cylinders, cast in quartz tubes.

In this study we describe a biocompatible, biodegradable, modifiable, and implantable matrix, in the shape of a cylinder, which can be surgically placed in the brain such that the implant connects the dorsoposterior RMS with the nonneurogenic striatum. These implants were indeed capable of creating long tracts and enriched regions of new neural cells in the striatum. Such in vivo brain tissue engineering has clear clinical applications for a variety of neurological disorders, especially considering that the source of stem cells would be the patient's own brain, without the need to implant any cells whatsoever. We believe that these deliberately targeted neurons will be repurposed from an olfactory role to a new function specified by the nature of the neurological dysfunction and the signaling cues within the milieu of the targeted niche (206-209).

Cell-replacement therapy in the brain has many hurdles that must be overcome and the work described in this study addresses several of these challenges. Engineered fibrin cylinders can provide both the appropriate three-dimensional architecture and biochemically defined microenvironment to create a migratory path with complex neural cells and vasculature. Upon implantation, this serves to recruit endogenous neural stem cells from their usual location and subsequently target them into specific regions of the brain. Harnessing endogenous adult neural stem cells eliminates the problems

associated with exogenous cell transplants, which include deleterious immune responses and rejection, unavailability of sufficient numbers of cells for transplantation, low survival and integration rates, and, in the case of embryonic or induced pluripotent stem cells, teratoma formation.

We present three key findings in this report. First, as a result of the fibrin implant containing neurotrophins (NGF and VEGF), ECM (laminin I), and protease inhibitor (aprotinin) in normal rats, significant numbers of neuroblasts were found along an extensive (>2.5 mm long) region of the implant track in the striatum, in the striatal region between the implant track and the lateral ventricle, in the corpus callosum, and, to a much lesser degree, in the cortex (Figs. 13-17). Fibrin alone was not sufficient to elicit this effect in terms of attracting neural cells into the implant region [compare control animals (Fig. 18) to implanted animals (Figs. 14-17)] or correcting hemiparkinsonian behavior. Only when VEGF and NGF were incorporated into the cylinders did we observe neuroblasts (Dcx⁺) along the track of the implant, which itself had essentially completely degraded. Second, there were no obvious deleterious neurological sequelae as a result of the implants. We have not observed necrosis, tumors, reactive astrocytes (GFAP⁺), or abnormal behavior in more than 80 animals that have been used during the development of this approach. Regarding inflammation, we attempted to minimize such cellular responses (GFAP⁺ astrocytes) by the administration of an anti-inflammatory agent following the surgery; our unpublished preliminary studies show that GFAP labeling is induced by the surgical procedure and can be subsequently significantly reduced by post-operative dexamethasone administration. Third, 6-OHDA hemiparkinson rats exhibited an attenuation of amphetamine-induced rotations following cylinder implantation (Fig.

19). This provides proof of concept for the idea of creating a new neural migratory stream that connects an abundant source of neural stem cells (the SVZ/RMS) to a dysfunctional brain region.

It is noteworthy to compare the morphology of the Dcx-reactive cells along the implant tract (Fig. 16) with Dcx+ labeled cells along a bona fide migratory path. We observe Dcx+ neuroblasts with long neurites that run parallel to the direction of the implant. Such labeling and morphology are very similar to that observed for Dcx+ cells undergoing chain migration along the rodent RMS (210). It is reasonable to speculate that the neuroblasts that respond to the fibrin implant are undergoing similar migration. The fact that the animals were sacrificed 4 weeks after surgery and Dcx+ neuroblasts were still present along the length of the implant track suggest that the new migratory path is relatively stable over the postoperative time frame.

The likely source of new cells that were in abundance along the implant region is the RMS, which the cylinder was designed to intersect after implantation. It is not clear to us from where the cells that were seen in the striatal region between the implant and the lateral ventricle are derived. We suggest that they may be either from the wall of the lateral ventricle or are occult neural stem cells resident in the striatum that were activated by the implant. Regardless, in addition to the neural cells along the implant track, the new cells in this intrastriatal region are likely to be therapeutically beneficial.

It is of interest to note that, compared to the robust generation of neuroblasts in the striatal region of the implant, there were no nascent neural cells in the cortex. We speculate that the brain itself provides additional signaling molecules that synergize with the factors in the fibrin cylinder, and differential neurogenic responses are due to the

biochemical cues inherent to the adult cortical environment versus those of the striatum. Indeed, these different regions follow different neurogenic mechanisms during brain development (211-214) and this may account for the differential response (cortex vs. striatum) to the implanted fibrin microenvironment.

In conclusion, we present the development and therapeutic application in an animal model of neurodegeneration of an implantable, biocompatible, biodegradable fibrin-based cylinder, which can be readily modified with immobilized factors to create a bioengineered microenvironment that creates *de novo* neural migratory paths for *in vivo* neural tissue engineering. Past efforts to accomplish similar goals have involved the injection of fibrin, usually with factors and exogenous stem cells, into regions of the brain or spinal cord, which then polymerizes *in situ* (126, 191, 215, 216). It is difficult to envision the ability to create new, long migratory paths, which redirect endogenous neural stem cells with such approaches. The safety of these implants remains to be characterized in detail, but we have not observed obvious behavioral problems, mortality, tumor-like masses, significant damage to brain tissue, or other gross abnormalities upon the immunohistological analysis of the implanted brains.

Importantly, the main components of the implant described in this study are currently used in both routine and experimental clinical procedures. Fibrin (derived from fibrinogen and thrombin) and aprotinin (189) are common in many surgical procedures, including neurosurgery. NGF, one of the two neurotrophic factors included in these fibrin implants, has been delivered to patients' brains in clinical trials for traumatic brain injury and Alzheimer's disease (217), while VEGF is being considered for stroke therapy (187, 218, 219). The recruitment of endogenous neural stem cells into regions of the brain

that typically do not have neurogenic potential represents a powerful therapeutic approach for neurological diseases and disorders caused by the loss of specific neurons. The ability to deliberately steer significant numbers of endogenous NPCs from their usual niche into distant nonneurogenic regions of the brain represents a significant advancement for Parkinson's disease, traumatic brain injury, stroke, and other neurological disorders of similar etiology.

Conclusion

Individuals with neurodegenerative disorders or brain injury have few treatment options and it has been proposed that endogenous adult neural stem cells can be harnessed to repopulate dysfunctional nonneurogenic regions of the brain. Here we presented hydrogel implants capable of recruiting endogenous cells from the adult subventricular zone to create new relatively long tracts of neuroblasts targeting them to a specific brain lesion. When these fibrin-based cylinders were implanted into hemiparkinson rats, newly Dcx⁺ neuroblasts were found within the striatum of the implanted hemisphere and correction of parkinsonian behavior was observed.

SECTION 3: BIOENGINEERING FIBRIN CYLINDER-IN-CYLINDER (CinC) BRAIN IMPLANT FOR STRIATAL AND CORTICAL NEURAL STEM CELL RECRUITMENT

Introduction

Neurodegenerative diseases, stroke, and TBI are notoriously difficult to treat due to the brain's limited capacity for regeneration. Once neural tissue is damaged patients experience life-long, often debilitating, deficits. Stroke affects 800,000 people in America annually (220), but currently few treatment options exist for patients following a stroke. To date, most stroke therapies are focused on either preventing further cell death (221) or addressing symptomology due to this loss of neuronal cells (222), however, they do not address neuronal damage once it has occurred. Therefore, the development of new restorative therapies for stroke, and other causes of brain damage, that focus on replacing lost or damaged cells, regenerating brain tissue, and recovering lost function is a crucial next step in the treatment of neural injury.

The present work seeks to use the brain's inherent neuroplasticity to replace neurons lost to injury or disease by exploiting the migratory and regenerative capabilities of endogenous neural stem cells. Although the adult brain undergoes very minimal neurogenesis, small niches of neural stem cells do exist and proliferate throughout the life of mammalian animals. One such proliferative region is the subventricular zone (SVZ). NPCs derived from the SVZ ordinarily travel relatively long distances along the RMS to reach their destination in the OB. We hypothesize that these NPCs that traverse the RMS can be redirected to other nonneurogenic areas of the brain if given an appropriate scaffold and chemotactic cues. Previously we have used an innovative

bioengineered cell-free, implantable fibrin-based matrix capable of redirecting SVZ NPCs from their normal course along the RMS. These fibrin implants create a sort of “off-ramp” for the progenitor cells, thus establishing a new migratory stream in the brain with the cells’ new destination in traditionally nonneurogenic regions. In a hemi-Parkinson rat model, the implantable matrix was able to recruit numerous neuroblasts to the striatum leading to improved motor function (98). This preliminary data indicates that the implantable matrix may be a useful tool for the recruitment of NPCs to areas of the brain damaged from disease or injury.

However, the distance over which NPCs were recruited in our previous work was limited. The implanted matrix spanned the entire length of cortex to midbrain, but newly divided neuroblasts were primarily found along the implant site between RMS and striatum. We hypothesize these limitations can be circumvented with updates to the implant architecture to a design that better promotes NPC migration and survival. NPC recruitment to cortical regions of the brain could prove useful in regenerative strategies following ischemic or traumatic brain injuries.

The physiological RMS structure is tubular, with glial cells extending parallel processes in opposite directions along the RMS to form a cord-like bundle, thus organizing into an astrocytic glial tube (223). Chains of migrating neuroblasts traverse along the RMS ensheathed by astrocytic processes and blood vessels to their destination in the OB (224). Others have sought to recapitulate the RMS structure via fabrication of “living scaffold” constructs composed of longitudinally aligned astrocytes (225) that shows promise for endogenous NPC recruitment and neuronal cell replacement. However, this approach requires complex microtissue engineering, has thus far been limited to *in vitro*

experimentation (226), and poses possible complications related to the implantation of foreign cellular material. Here we demonstrate our acellular, double-barreled “cylinder-in-cylinder” (CinC) fibrin brain implants are capable of NPC recruitment to both striatal and cortical ends of the implant tract.

The CinC is designed such that the inner fiber cylinder is softer and more rapidly degraded than the outer fibrin cylinder (Fig 20), quickly creating a tube-like structure *in vivo*. One advantage of the CinC unique architecture is that it allows for a wide variety of possible ECMs and/or growth factors used to optimize cell recruitment. However, to strictly evaluate the benefit of the double-barreled design, as compared to our previously homogenous cylinder implant, the same components are used as were in former hemi-parkinsonism experiments in both inner and outer cylinder (98).

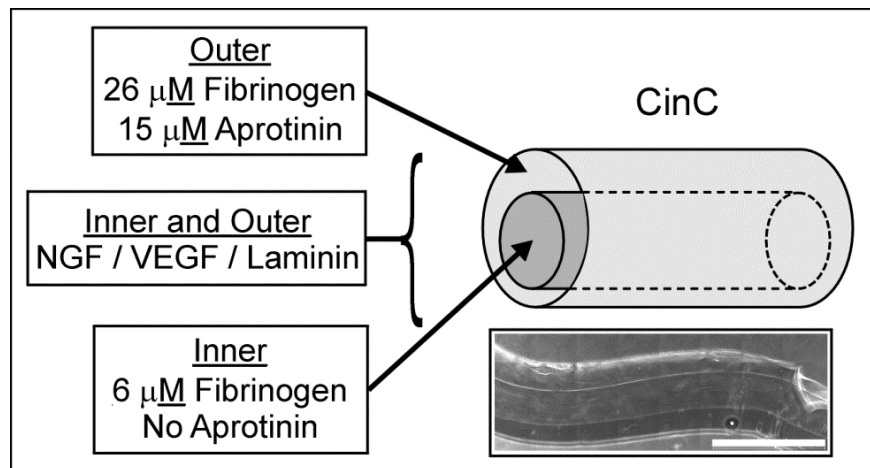


Figure 20. Schematic of Engineered CinC Matrix and Components

Depicted is an example of the double-barreled design for a “CinC” implant. Bottom right reveals a plain photograph of a CinC’s gross appearance.

Material and Methods

Preparation of implantable “CinC” scaffolds

Fibrinogen (Sigma-Aldrich, St. Louis, MO) was dissolved in phosphate-buffered saline (PBS) at a final concentration of 64 μM , degassed, and stored in aliquots at 80°C. Eight μL aliquots of fibrinogen were placed on a square of Parafilm® to which was added aprotinin (15 μM Sigma-Aldrich), laminin I (100 $\mu\text{g}/\text{mL}$ Trevigen, Gaithersburg, MD), carrier-free VEGF (10 $\mu\text{g}/\text{mL}$ final concentration; R&D Systems, Minneapolis, MN), and carrier-free NGF (10 $\mu\text{g}/\text{mL}$ final concentration; R&D Systems). The volume of each sample was brought to 18 μL with PBS. The homobifunctional crosslinker disuccinimidyl suberate (DSS; Thermo Scientific Pierce, Rockford, IL) was dissolved in dry dimethyl sulfoxide (dried over 4 Å, 40 mesh molecular sieves) and 1 μL (500 μM final) was added to the sample with thorough mixing. DSS is a chemical crosslinker that is directed toward amino groups, thus facilitating the covalent incorporation of the peptides and proteins used in this study (i.e., VEGF, NGF, laminins, and aprotinin) into the fibrin hydrogel (196-200). The crosslinking reaction was incubated for 10 min at ambient temperature in a humidified chamber. At this stage, two separate solutions have been prepared for each the inner versus outer cylinders. To one aliquot, thrombin (1 μL of 0.1 U/ μL ; Sigma-Aldrich) was added and the sample was quickly mixed and injected through a Gilson P20 Pipetman® into the larger quartz tube (0.7 mm i.d., 3.5 cm long; Fiber Optic Center, Inc., New Bedford, MA) with the solution surrounding the smaller quartz tube (0.3 mm outer diameter [o.d.]; Fiber Optic Center, Inc., New Bedford, MA) such that a 6 mm long cylinder was created (Fig 21A). The dimensions of the final cylinder were 0.7

mm dia. X 6 mm long following the polymerization and concomitant shrinkage of the fibrin.

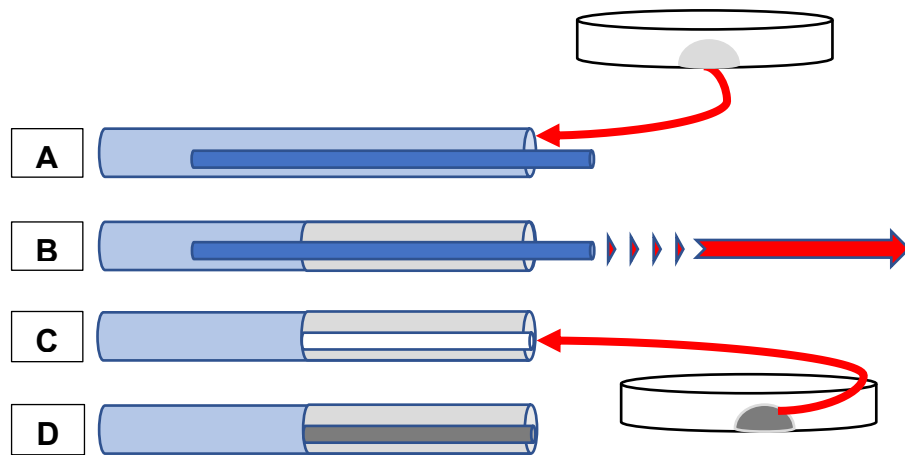


Figure 21. Depiction of Cylinder-in-Cylinder Architecture

A) Fibrin solution is cast within larger quartz tubing and surrounding the smaller quartz tubing. B) Once fibrin has hardened, smaller quartz tubing is removed to establish a hollow tunnel through the casted fibrin. C) Fibrin solution for the “inner” cylinder is injected. D) The final result is a smaller hydrogel cylinder contained within a larger hydrogel cylinder, each of which may contain any variety of matrices and/or growth factors.

After fibrin was polymerized, the inner quartz cylinder was carefully removed leaving a hollow tunnel within the fibrin inside of the larger quartz tubing (Fib 21B). To the remaining fibrinogen aliquot, thrombin ($1 \mu\text{L}$ of $0.1 \text{ U}/\mu\text{L}$; Sigma-Aldrich) was added and the sample was quickly mixed and injected through a Gilson P20 Pipetman[®] into the tunnel within the previously casted “outer” fibrin cylinder (Fib 21C). Therefore,

creating the double-barreled design as depicted in Fig. 21D. Cylinders were made within 4 h of implant surgery and stored in a humidified chamber until used.

Implantation of cylinders into rat brain

Female Sprague-Dawley rats (175 g; 7 weeks old) were purchased from Hilltop Lab Animals, Inc. (Scottsdale, PA). Animals were acclimated and handled every 1–2 days for 2–3 weeks before experimentation. Cages were provided environmental enrichment in the form of PVC pipe fittings. All animal experiments were carried out in accordance with the National Institutes of Health Guide for the Care and Use of Laboratory animals and performed under an approved protocol from Marshall University's IACUC. The fibrin cylinders were implanted along a predetermined path in the right hemisphere of each animal (Fig. 20). A short (ca. 0.5mm) length of polyvinylidene difluoride (PVDF) fluorocarbon line (0.56 mm diameter leader material; Berkley, Columbia, SC) was inserted into the quartz tube containing the fibrin CinC and served as a plunger head and a 20 cm length of stainless steel wire (0.5mm dia.; AmazonSupply) was used as a plunger (Fig. 20). Animals were anesthetized using isoflurane (5% induction, 2% maintenance) with an oxygen flow of 0.8 L/min.

Animals were positioned into a Kopf stereotaxic frame that was outfitted with two manipulators, one on each arm of the Kopf "U" frame, and both were angled 17° to the right of midline. The fibrin cylinder-containing quartz tube was affixed to the right manipulator and the wire plunger was placed on the left manipulator. A small hole was drilled using a round dental bur at, relative to the bregma, 0.13 cm anterior and 0.30 cm lateral right of midline (201). The dura was gently pricked with a 25-gauge needle and the

quartz tube slowly driven 0.73 cm down the dorsoventral axis on an angle 17° off mid-line to the right. The plunger was lowered into the fibrin cylinder-containing tube until just touching the PVDF plunger head, which itself was just touching the fibrin cylinder. The plunger was held immobile by the left manipulator arm, while the quartz tube was slowly raised (1/4 turn/45 s) by the right manipulator. This maneuver resulted in the 6 mm cylindrical fibrin matrix being placed (not extruded) in the brain along a predetermined path (Fig. 20) as the quartz tube was removed from the brain with the plunger holding the hydrogel cylinder in place.

The final position of the 6 mm long implant started at the surface of the brain and passed through the cortex, corpus callosum, RMS, and striatum. After complete extraction of the quartz tube, the skull hole was plugged with bone wax and the scalp closed with absorbable sutures. Animals were injected with dexamethasone [0.4 mg/kg subcutaneously (*s.c.*) in 0.9% sterile saline] once at the time of anesthesia induction and then each day for 4 days postoperatively. For pain management, animals were injected with buprenorphine (0.15 mg/kg *s.c.*) immediately after surgery and then daily for 2 additional days.

EdU (5-ethynyl-2'-deoxyuridine) labeling

To evaluate the ability of our CinC implant to recruit newly divided cells of the brain along its entire course (cortex to deep brain nuclei), we implemented 5-ethynyl-2'-deoxyuridine (EdU) labeling. EdU, a nucleoside analog of thymidine that incorporates into DNA during active DNA synthesis (227), was used to label any cell dividing cell at the time of exposure. Beginning at week 12 following implant surgery, animals were injected

with 50 mg/kg Edu *i.p.* every other day for 2 weeks. At week 14 after surgery animals were sacrificed.

Brain extraction and imaging

Animals were sacrificed by bilateral pneumothoracotomy, fixed by transcardial perfusion with 0.9% NaCl containing 2U/mL heparin followed by 4% freshly prepared paraformaldehyde (PFA), and brains recovered. Following overnight postfixing in 4% PFA, brains were equilibrated in 30% sucrose until no longer buoyant and stored at 4°C until processed into 20 µm sections using a Leica Model 1950 cryostat. Samples were mounted on Superfrost plus glass slides (Fisher Scientific, Pittsburgh, PA) and coverslipped with number 1 glass with Fluoro-Gel II-DAPI (Electron Microscopy Sciences, Hatfield, PA) as the mountant. Slides were sealed with clear nail polish and stored at 4°C until imaged/analyzed using a Zeiss Axio Observer with 10X and 20X LD Plan Neofluar air-interface objectives and AxioVision 4.6.3 software.

Preliminary Results

Edu+ cells were found bilaterally, as expected, along the lateral ventricles where SVZ NSCs normally divide (Fig 22B). Numerous Edu+ cells were also discovered along the implant tract (Fig 22A, C & D). The fibrin implant itself appears to have completely degraded, which is consistent with prior studies (based on previous aprotinin dose response experiments, a fibrin cylinder containing 15 µM aprotinin would expect to be largely degraded by 8 weeks), but in its place were newly replicated cells. Interestingly, unlike the previously used homogenous, single cylinder, the CinC recruited young

neural cells more distally towards the cortex (Fig 22D). On the contralateral, non-implanted hemisphere, Edu+ cells were seen adjacent to the lateral ventricle but few to no Edu-labeled cells were observed elsewhere in the cerebrum. Over the period between surgery and sacrifice, there were no obvious deleterious postoperative effects of the implants on the animals in terms of overt behavior, tumorigenesis or significant brain damage.

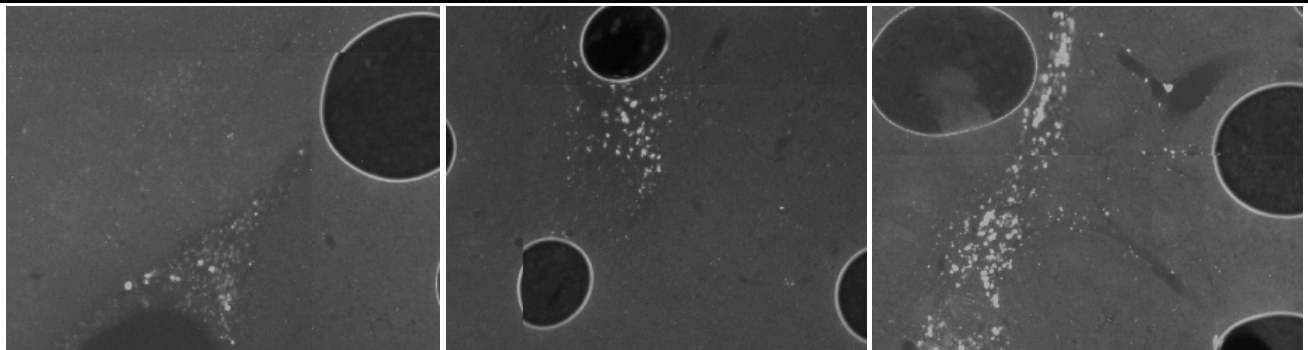
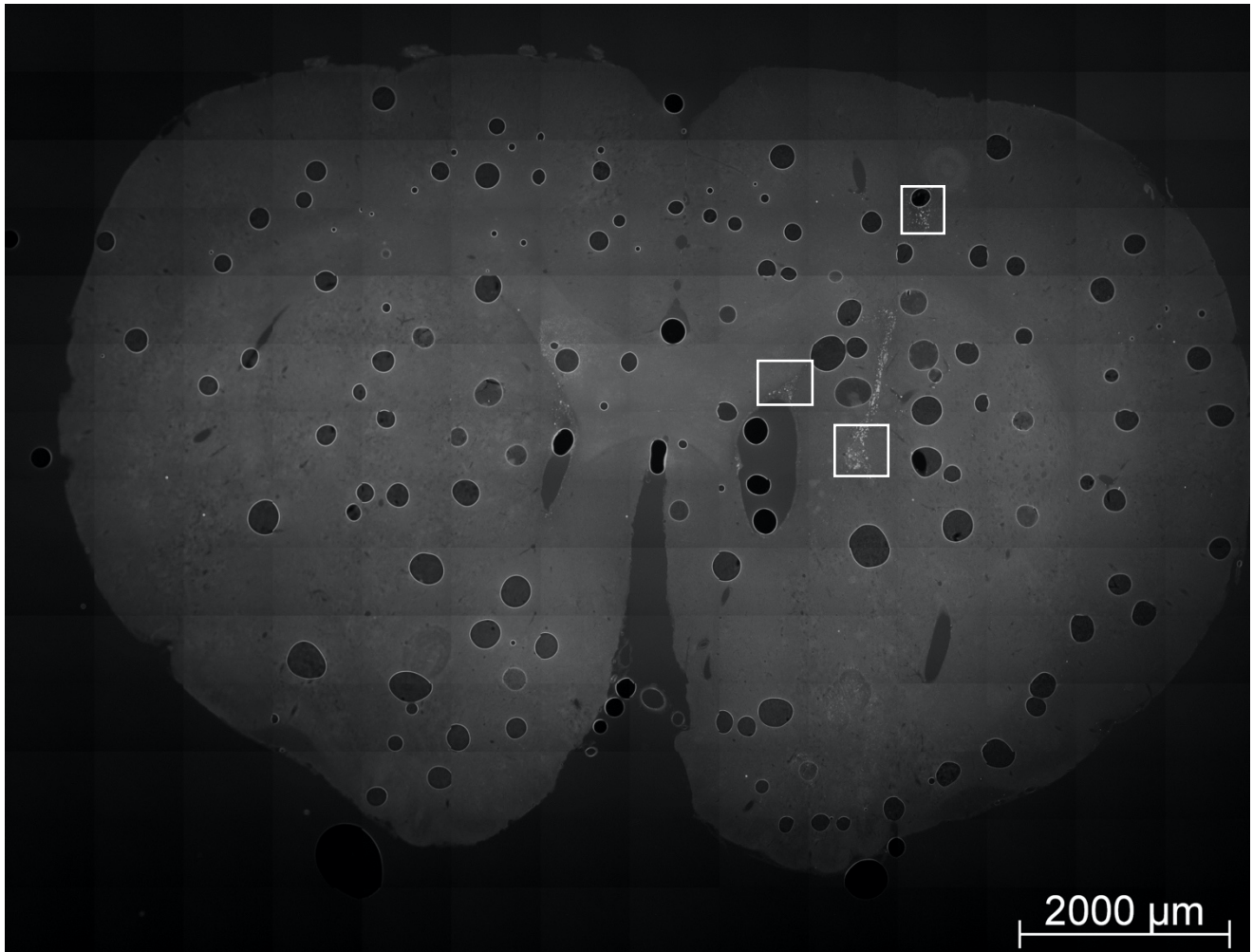


Figure 22. EdU (5-ethynyl-2'-deoxyuridine) Labeled Brain Tissue from Rat Receiving Novel CinC Brain Implant 14 weeks Prior

A) coronal cross-section displaying Edu+ along the longitudinal axis of the fibrin implant tract. B) magnified view of Edu-labeled cells within the SVZ/RMS. C-D) magnified views of populations of Edu+ cells found along the healed implant tract.

Discussion

Many neuropathologies are sequelae of lost neurons due to toxic, ischemic, or mechanical injury. Therefore, many research efforts are focused on techniques to replace these missing neuronal populations via SC transplantation (52, 228, 229), enhancing *de novo* neurogenesis (230-233), or endogenous NSC/NPC recruitment (98, 111, 234). Some success has been demonstrated with SC transplant or endogenous SC recruitment in the striatum of rodent and primate models of PD (48, 49, 98, 164). Transplantation of NSCs and/or mesenchymal SCs into the subdural space or ischemic lesions have also demonstrated some success in functional recovery following stroke in both preclinical and clinical models (51, 216, 235) (for a full review on the effectiveness of SC therapies in stroke see (236)). However, the reliance on immunomodulatory agents following foreign cell transplantation remains an obstacle.

Alternatively, others have focused their research efforts on better harnessing the intrinsic regenerative power of the brain. One approach has been to enhance the brain's innate "self-repair" mechanisms by attempting to increase the post-stroke upregulatory response in neurogenesis and migration of neuronal precursors to ischemic lesions. Numerous cytokines and growth factors, administered systemically, by intraventricular injection or targeted delivery systems into stroke lesions, have been studied with variable success (90, 101, 103, 104, 109, 237, 238). Limitations for these approaches include off-target effects throughout the body (108), inadequate number of progenitors reaching lesion to regenerate, lack of physical scaffold to support migration and/or growth of progenitors (111). This has motivated the application of various biomaterials in neuroregenerative research for both direct recruitment of NSC/NPCs to the area of damage and provide

a physical scaffold to sustain migrating neuroblasts. Poor survival of recruited NPCs to stroke lesions is frequently attributed to the lack of appropriate biological signaling, such as lack of extracellular matrix or structural scaffold (239, 240) and inappropriate biochemical cues (241). Whereas an appropriately designed scaffold can provide these missing components, thus offering a permissive environment for neuroblast migration and survival.

Using electrospun poly- ϵ -caprolactone (PCL) scaffolds containing either vehicle or a BDNF-mimetic, Fon, et al. demonstrated that a physical scaffold is required to provide an accommodating environment for neuroblast survival (111). Observing significant neuroblast infiltration into PCL implants at day 8 post-implantation, an effect seen regardless of incorporation of pro-migratory BDNF-mimetic. Although incorporation of a BDNF-like molecule into their scaffold (PCL+mBDNF) did prolong the persistence of neuroblasts rerouted along the implant tract (significantly more Dcx+ processes remained in PCL+mBDNF than in PCL scaffolds at 21 days post implant) (111). They also revealed direct intersection with the SVZ by a permissive scaffold is required to induce neuroblast migration. As no neuroblast penetration was observed in PCL+mBDNF implants that did not contact the SVZ, signifying the BDNF-like molecule itself was not sufficient to drive NPC migration from SVZ/RMS to site of injury. When the implant contacted the SVZ, neuroblasts were able to travel along the implant, however, the number of Dcx-immunoreactive cells within the scaffold decreased with increasing distance from the intersection of the SVZ.

Feasibility of using scaffolds to re-route neuroblast migration from the SVZ or RMS to targeted brain regions has also been demonstrated using implanted injectable gelatin-

based hydrogels consisting of GDNF (124), graphene coated electrospun poly- ϵ -caprolactone (242), and most recently a new self-assembling peptide hydrogel (243). Unfortunately, the injectable hydrogel was degraded too quickly to promote NPC migration over longer periods. The implant was found to be completely cleared after 3 weeks and the number of neuroblasts around the gelatin matrix decreased from 7 to 21 days. It is unclear however, if there were solely diminishing numbers of immature cells migrating along the implant tract because of discontinued migration, or if the decrease in neuroblasts found around the gelatin matrix tract was also due to differentiation of migrated neuroblasts to neurons.

Another approach employed a hydrogel implant composed of exclusively β -amino acids and a C₁₄hydrophobic acyl tail with or without BDNF. The peptide self-assembles to form a stable, long-lasting and biocompatible matrix (118). They evaluated biocompatibility, neuroblast migration, and cell differentiation at 7- and 35- days post-implant. Transgenic labeling of SVZ NSCs revealed an increase in cell migration in response to sham (injury) at day 7 at appreciably lower numbers and distance of migrating cells than in the plain or BDNF-loaded hydrogel. By day 35 migration was uniform across the BDNF-loaded hydrogel with neuroblasts reaching the far end of the implant located in the cortex. Most SVZ-derived cells along the hydrogels were Dcx+ at day 7, and the population of these Dcx+ cells significantly decreased by day 35. At this time, most of the SVZ-derived cells were colocalized with NeuN+, indicating the neuroblasts differentiated into mature neurons. This differentiation trend was seen in both hydrogels, independent of BDNF.

These results found in the literature are important proof-of-principal that SVZ NSC/NPCs can be re-routed from their normal course to desired brain regions, including

the cortex. Further, recruited cells can differentiate into mature neurons in their new location. Of note, the authors of the aforementioned study speculate that providing stable, long-term support will be essential for continued cell migration and differentiation. In contrast, we have hypothesized that once NPCs are effectively re-routed from the RMS, the cells will continue to migrate as a neuronal chain analogous to their travel along the RMS (244) forming a new, continuous migratory stream in the brain. We posit that the newly established migratory route for SVZ NPCs will be replenishable and cells will continue to travel the carved-out pathway long after the implanted matrix has degraded. Preliminary evidence for this was demonstrated here. The fibrin-based cylinder-in-cylinders (CinC) were implanted such that one terminal landed in striatal tissue and the other end reached through the cortex ending at the most external surface of the brain, whilst intersecting the RMS in the middle. Animals began receiving a 2-week series of Edu injections at week 12 post-implant. This would have been approximately 3-4 weeks, based on previous data, after the fibrin implant itself had degraded. Therefore, Edu+ cells evident along the implant tract must have been derived from an actively dividing population at the time of Edu injection after the implant matrix had degraded yet continued to migrate along the implant tract.

One limitation of this study is that while continued cellular proliferation in the brain is generally limited, at least in substantial amounts, to the SVZ and DG neurogenic niches of the mature mammalian brain, certain inflammatory states also promote glial cell propagation (87). Additionally, it has been proposed that small quiescent SC niches throughout the brain may be activated in response to certain injuries, and thus could contribute to Edu+ cells found along the CinC implant tract. As neither of these cell sources would

likely provide a replenishable source of replacement cells for conditions such as PD or stroke, the origin of Edu-labeled cells should be more definitively confirmed. To determine if cells found along CinC implant tracts were derived from the SVZ, transgenic mice or viral labeling techniques specifically labeling cell populations of the SVZ (245) should be further investigated.

Conclusion

This study demonstrates proof-of-concept for NPC recruitment to non-neurogenic regions of the midbrain and cortex by an implantable matrix. Our “cylinder-in-cylinder” design proved to be more successful at allowing NPC migration to more distal locations than its single, homogenous cylinder predecessor. Importantly, newly divided neural cells were observed close to the gray-white junction of the cortex. A noteworthy finding as our previous fibrin implants were found to only recruit Dcx-labeled NPCs to striatal regions and the new migratory path ranged from only 2.0 to 2.8 mm in length from the implant’s intersection with the RMS. The results of this study reveal the potential application of CinC fibrin implants in neuroregenerative research and an exciting new treatment paradigm for future studies.

CHAPTER 3

CHAPTER INTRODUCTION

It has been postulated that nicotine may play a neuroprotective role in specific neuronal populations (246-249), but may participate in other neurotoxic/neuroinflammatory pathways (250, 251). Moreover, if endogenous NSC/NPCs are to be exploited in regenerative therapies for disorders such as stroke, we must understand the possible implications a main risk factor for stroke, i.e. smoking, may have on these SCs. First, we evaluate the modulation of $\alpha 4$ nicotinic acetylcholine receptor (nAChR) expression in dopaminergic and gamma-aminobutyric (GABA) neurons of the ventral tegmental area (VTA) following nicotine exposure via vapor inhalation in mice. Then we present a systematic literature review of nicotine's effects on NSCs.

SECTION 1: SYSTEMATIC REVIEW OF NICOTINE EXPOSURE'S EFFECTS ON NEURAL STEM AND PROGENITOR CELLS

Introduction

Neurogenesis in the adult mammalian brain primarily occurs in two distinct regions: the SVZ located along the walls of the lateral ventricles and the SGZ located in the DG of the hippocampus. NSCs reside and continue to symmetrically divide throughout adulthood in these regions giving rise to transiently amplifying multipotent NPCs (59, 61, 62). Neurogenesis in the DG plays a particularly important role in hippocampal-mediated learning (63, 64). In fact, enhanced neurogenesis and survival of newborn cells in the hippocampus is observed in rats trained on hippocampal-dependent tasks (64), and performance on these tasks is impaired by inhibition of cell proliferation (65). Newly generated NPCs in the SVZ give rise to another type of neural precursor called the migrating neuroblast, which travel from the lateral ventricles to the OB along the RMS where they then mature into neural cells involved in olfaction (60, 66-69, 252).

Because both clinical and preclinical studies have demonstrated that nicotine elicits improvements in cognitive function (247, 253-258) and possibly offers neuroprotection against neurodegenerative conditions (259, 260), many studies have sought to elucidate the effect of nicotine on neuroplasticity. In contrast to these studies driven by the hypothesis that nicotine is a neuroprotective compound (261-263), others have sought to evaluate nicotine's effects on stem cells. This is due to evidence that nicotine is a neuroteratogen and alters blood-brain barrier (BBB) function (264-266) and potentially contributes toward negative consequences for NSC health. Further, studies have

shown abstinence from smoking in nicotine-dependent individuals leads to profound cognitive impairment (267-269) and disruption of hippocampal and prefrontal cortex (PFC) associated behaviors (270-274), suggesting that chronic nicotine exposure might impair or otherwise alter mechanisms related to learning and memory such as hippocampal neurogenesis.

While the research of possible nicotine-related effects on NSC survival, proliferation and differentiation is understudied, investigation into this area has highly important clinical implications. Although smoking rates have declined in recent decades, the 32nd tobacco-related Surgeon General's report states that 42 million American adults and about 3 million middle and high school students continue to smoke. Additionally, nicotine use in the form of electronic nicotine delivery systems (ENDS) (also known as e-cigarettes (Ecs)) has substantially gained popularity. Recent studies report that youth who use ENDS may have a higher propensity to smoke combustible cigarettes in later life (275). In 2019, over 5 million U.S. middle and high school students had reported ENDS use in the past 30 days, including 10.5% of middle school students and 27.5% of high school students (276). As brain development continues into the mid-twenties, elucidation of the neurological consequences of nicotine exposure is paramount (277, 278).

Nicotine-Related Decreases in NSC Proliferation

An in vitro study showed prolonged exposure to nicotine decreased proliferation of NSCs isolated from embryonic whole brain (279) (Table 4). Brains collected from

Observation	Nicotine Doses	Model System	Ref
Nicotine reduced the proliferation of NSCs via transcriptional mechanisms	100, 400, 800 μ M	Neurospheres	(279)
Nicotine reduced the NSC proliferation in the dentate gyrus (DG)	4 mg/kg/day	Mice	(280)
Nicotine reduced the NSC proliferation in the DG	Variable	Rats	(281)
Nicotine decreases hippocampal neurogenesis	0.1, 0.5, or 1 mg/kg	Rats	(282)

Table 4. Summary of Nicotine-Related Decreases in Neural Stem Cell (NSC) Proliferation

embryonic day 16 mice were enzymatically treated to isolate NSCs and were cultured as neurospheres. Neurospheres were then treated with vehicle or nicotine at 100, 400, and 800 μ M doses, concentrations that greatly exceed that of what is clinically relevant, for five days. In a physiological setting, nicotine in the brain of combustible cigarette and ENDS smokers is typically between 0.05 and 0.5 μ M (283). The proliferative capacity of nicotine treated NSCs was then analyzed via quantity and size measurements of the cultured neurospheres. Nicotine decreased the number and size of newly formed neurospheres as compared to vehicle. Both diminished size and number were dose-dependent and could be restored by application of mecamylamine (MECA), a nonselective

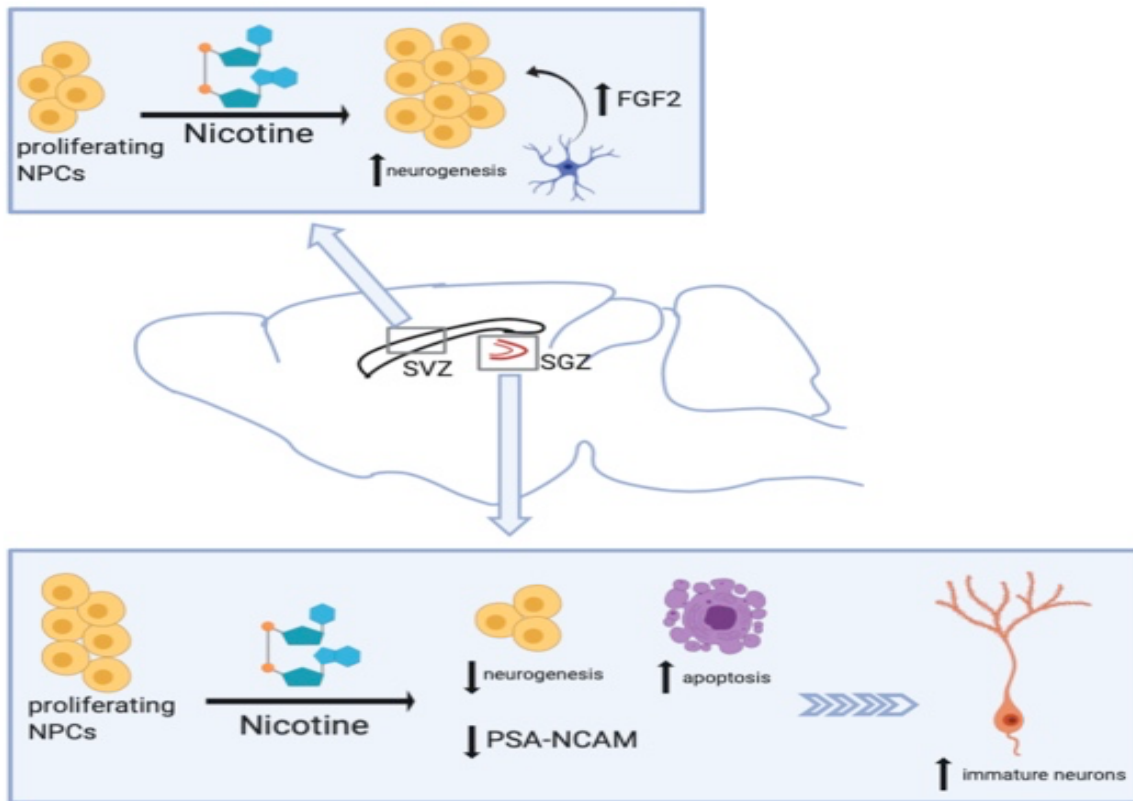
nAChR noncompetitive antagonist. Using RT-PCR to measure mRNA expression of nestin, an NPC marker, and proliferating cell nuclear antigen (PCNA), it was shown that nicotine inhibits proliferation of neurospheres at a transcriptional level. In the RT-PCR analysis, the levels of nestin mRNA were not changed, whereas the level of PCNA was significantly decreased. Additionally, confocal microscopy revealed nicotine treatment increased the number of condensed nuclei and shortened neurogenesis in a dose-dependent manner compared to vehicle. Nicotine also increased the release of certain pro-inflammatory cytokines in NSCs. RT-PCR analysis exposed increased levels of cyclooxygenase-2 (COX-2), tumor necrosis factor alpha (TNF- α), and glutathione reductase mRNA in the nicotine-treated neurosphere cultures. Intriguingly, variable TNF-mediated signal cascades in NSCs have been identified. Depending on which receptor subtype is activated, NSC proliferation can be increased or decreased in response to TNF- α (284, 285). Autocrine signaling of TNF- α is suggested to play a role in the cytokine's influence on neurogenesis (285, 286). In addition to increased transcription of these pro-inflammatory genes, nicotine was shown to increase the mRNA levels of histone deacetylase 1 (HDAC1) and decrease the mRNA levels of sirtuin 1 (SIRT 1, a nicotinamide adenine dinucleotide (NAD)-dependent histone and protein deacetylase) in NSCs. HDAC2 was not changed with nicotine treatment. Nicotine also upregulated levels of inducible nitric oxide synthase (iNOS). When HDAC inhibitors, sodium butyrate (NaB) or valproic acid (VPA), were added to NCS cultures for five days, HDAC1 mRNA was decreased. However, neither NaB nor VPA changed mRNA levels of HDAC2 or SIRT1. Furthermore, HDAC inhibitors partially rescued proliferation of NSCs compared to nicotine without NaB or VPA.

These results are interesting in light of other work that has reported chronic nicotine exposure to decrease HDAC activity in mice (287). Histone acetylation is an epigenetic modification to favor gene expression that is moderated by opposing actions of histone acetyltransferase (HAT) and HDAC, adding and removing acetyl groups, respectively. Therefore, decreased HDAC activity would enhance histone acetylation and promote gene expression. Commonly, activation of HDAC1 would result in transcriptional repression of many gene targets. In the aforementioned study, it is speculated that HDAC1 might deacetylate a repressor bound to an iNOS promoter (288).

Epigenetic regulation has emerged in the literature as an important mechanism underlying brain changes associated with nicotine and other drugs of abuse exposure. In conjunction with the described study, others have demonstrated nicotine to decrease SIRT1 levels in cultured mouse embryos (289). Sirtuins are a family of NAD-dependent enzymes thought to be involved in cell metabolism and regulation of DNA repair, inflammatory response, cell cycle, and apoptosis (290). Interestingly, SIRT1, the sirtuin shown to decrease following nicotine exposure, demonstrates a general neuroprotective effect. In fact, hypermethylation of the SIRT1 gene and significant decrease of SIRT1 expression has been observed in patients with Alzheimer disease (291). Furthermore, epigenetic mechanisms were confirmed in vitro (292). These and other nicotine-induced epigenetic changes could be responsible for the negative effects of nicotine on NSC proliferation.

Nicotine impairment of neural plasticity has also been observed in multiple in vivo studies (280, 282, 293). Abrous et al., found that nicotine self-administration greatly decreased expression of polysialylated (PSA) forms of neural cell adhesion molecule

(NCAM) in the DG in a dose-dependent manner (293). They also observed nicotine-related decreases in neurogenesis and increased cell death (Figure 23). Using male Sprague Dawley rats and an intravenous self-administration (IVSA) model, animals self-administer one of three unitary doses of nicotine (0.02, 0.04, and 0.08 mg/kg per infusion) or vehicle solution, delivered on a contingent basis. Following IVSA, brain sections were collected and analyzed for PSA-NCAM and Brdu (Bromodeoxyuridine/5-bromo-2'-deoxyuridine) immunoreactivity. PSA-NCAM was evaluated because in the adult hippocampus PSA-NCAM is expressed in newborn neurons (294) and in mutant mice, modifications of PSA-NCAM expression causes morphological changes to these hippocampal cells and worsens cognitive function (281). PSA-NCAM immunoreactive cells were located in the deepest region of the granule cell layer at the interface of the hilus within the hippocampus. Nicotine IVSA diminished PSA-NCAM expression in the DG, a decrease up to 44% less than control in the 0.04 mg/kg nicotine dose (Figure 23). Notably, the PSA-NCAM expression was unaltered in the SVZ of nicotine-treated rats. Immunoreactivity for Brdu was decreased in the DG of rats that received nicotine IVSA compared to those receiving vehicle. Again, Brdu-labeling was not altered with nicotine IVSA in the SVZ. Both changes in PSA-NCAM immunoreactivity and Brdu-labeling were most significantly modified by the medium (0.04 mg/kg) dose of nicotine. Evaluation of either neuronal cell marker, NeuN, or astrocytic marker, GFAP, were co-labeled with Brdu to reveal the phenotype of proliferating cells. In control animals, approximately 7% of Brdu-stained cells expressed astroglial marker GFAP, and about 60% of Brdu-stained cells were NeuN-positive. In nicotine IVSA rats, the percentage of Brdu-stained cells co-labeled with GFAP or NeuN was not significantly different than the percentages of that



Created in BioRender.com bio

Figure 23. Graphical Summary of Nicotine's Effects on NSC Proliferation

Nicotine exhibits region-specific effects on neurogenesis. In the subventricular zone (SVZ), nicotine exposure enhances specific effects on neurogenesis. In the subventricular zone (SVZ), nicotine exposure enhances neurogenesis while in the SGZ it decreases neurogenesis. neurogenesis while in the SGZ it decreases neurogenesis.

in control animals. While the total number of Brdu/GFAP-positive cells was also not changed by nicotine administration, the total number of Brdu/NeuN- positive cells was decreased in a dose-dependent manner. The medium dose of nicotine (0.04 mg/kg) had the least amount of Brdu-stained NeuN-positive cells, equaling about half the amount as the Brud/NeuN-positive cells in control. Nicotine IVSA also resulted in greater cell death within the granule cell layer of the DG, demonstrating a significantly increased number of pyknotic cells with dose-dependent nicotine exposure in this region. Again, the greatest number of pyknotic cells within the DG was actually seen in the medium dose of nicotine, with both 0.04 and 0.08 mg/kg nicotine doses resulting in heightened cell death as compared to control or lower dose (0.02 mg/kg) nicotine.

In response to the seemingly controversial work of Abrous et al., as their study appeared inconsistent with prior work that had reported cognitive-enhancing properties of nicotine (255, 256, 295-297), Scerri et al., sought to investigate the effects of constantly infused nicotine on rat spatial learning in the Morris water maze and cell proliferation in the DG (280). In this study, two doses of nicotine were chosen, the high dose (4 mg/kg daily) representing blood nicotine concentrations (approximately 80 ng/mL) found in heavy smokers and the lower dose (0.25 mg/kg daily) to approximate concentrations (approximately 8 ng/mL) commonly found in the plasma of light smokers. They found that only the high dose nicotine (HDN) animals, and not the low dose nicotine (LDN) animals, took longer than controls to find the platform. Moreover, in probe trial, only HDN rats spent significantly less time than control rats in the region where the platform had been located. The group difference was not attributed to changes in swim speed. In all groups (HDN, LDN and control), spatial learning increased the number of Brdu+ cells in

the DG as compared to rats not receiving the learning task. Administration of HDN reduced the number of Brdu+ cells in both trained and non-trained rats. Further, HDN, but not LDN, decreased the number of cells labelled with BrdU compared to controls.

One other study observed nicotine-related decreases in hippocampal neurogenesis (282). Interestingly, Shingo et al. had shown in a prior study that nicotine administration in rats increased mRNA expression of insulin-like growth factor 1 (IGF1) within the hippocampus and cerebral cortex. Here, the authors concluded that this was partially responsible for nicotine's beneficial effects on hippocampal and cortical neurons (298). In their later study, nicotine was injected intraperitoneally (*i.p.*) (doses 0.1, 0.5, or 1 mg/kg) into adult male Wistar rats for two weeks and immunohistochemistry was performed on hippocampal tissue slices to label PSA-NCAM, NeuN, and GFAP (282). The quantity of PSA-NCAM+ and NeuN+ cells were decreased greatly by nicotine (Figure 23). While the actual count of immunolabeled cells was not provided, the values expressed as percent of control revealed a dose-dependent decrease of PSA-NCAM- and NeuN-labelled cells in the DG with nicotine exposure (Figure 23). The highest dose of nicotine used (1 mg/kg) had a nearly 80% decrease in both PSA-NCAM+ and NeuN+ cells, while the percentage of control for GFAP-labelling was unchanged. Although the 0.5 mg/kg nicotine dose alone did reach a statistically significant increase in GFAP-labelling, the increase was not as great a percentage change as that found in PSA-NCAM or NeuN labelling, and the authors thus reported nicotine has no effects on the number of GFAP+ cells. Moreover, Shingo et al., suggest that nicotine may have a "two-sided effect" on neurons, having a positive effect on mature neurons and a negative effect on developing neurons (Figure 23).

Nicotine-Related Increases in NSC Proliferation

In contrast to studies mentioned above that have demonstrated either decreased neural precursor cells number within the hippocampus or no change in NSC number within the SVZ, Mudò et al. reported that acute intermittent nicotine treatment enhanced neural precursor proliferation in the SVZ (299) (Table 5). Adult male Wistar rats were administered a total of four injections given i.p. every 30 min at a dose of 1 mg/kg for the acute intermittent nicotine treatment group and similarly treated with saline for the control group. To evaluate the effect of nicotine on precursor cell proliferation, i.p. injections of BrdU 2 h before sacrifice were also used to label proliferating cells. Changes in neural precursor cell proliferation were measured at 24, 36, 48, and 72 h after acute intermittent nicotine treatments. The time-course study revealed a significant enhancement of SVZ precursor cell proliferation as seen by an increased number of Brdu+ cells in the SVZ of nicotine treated rats versus controls at 36 h after nicotine exposure and maintained at least 72 h after (299). Nicotine did not induce neural precursor proliferation in the SGZ of the adult hippocampus. The enhanced SVZ neural precursor proliferation is thought to be caused by a nicotine-induced increase in fibroblast growth factor 2 (FGF-2) mRNA in the SVZ (Figure 23). Using in situ hybridization for both FGF-2 and fibroblast growth factor receptor 1 (FGFR-1) mRNA in the SVZ, they found that 4 h after acute intermittent nicotine treatment FGF-2 mRNA was upregulated in the SVZ while FGFR-1 mRNA was not. Additionally, the use of a specific monoclonal antibody against FGF-2 administered into the lateral ventricles 24 h after nicotine treatment, blocked the enhancing effects of nicotine on SVZ neural precursor cell proliferation.

Observation	Nicotine Doses	Model System	Ref
Intermittent nicotine exposure increases neural precursor proliferation in the SVZ due to increases in FGF-2	1 mg/kg	Rats	(299)
Nicotine dependence and deprivation increases the number of immature neurons in the SGZ of the DG	Variable, IVSA	Rats	(300)

Table 5. Summary of Nicotine-Related Increases in NSC Proliferation

Administration of a FGFR-1 inhibitor, SU5402, into the lateral ventricles 24 h after nicotine treatment also inhibited nicotine-induced effects on precursor cell proliferation (299). Moreover, a significant reduction of precursor cell proliferation was observed when SU5402 was intraventricularly injected in control rats as well, suggesting a role for endogenous FGF-2 in normal adult SVZ neurogenesis. In order to verify that augmentation of SVZ neural precursor cell proliferation by acute nicotine treatment was mediated by activation of nicotinic receptors, pre-treatment with nonselective nAChR antagonist MECA was injected 30 min prior to acute intermittent nicotine treatments. MECA pre-treatment did counteract the enhancing effects of acute intermittent nicotine on precursor cell proliferation. Further, treatment with MECA alone did not alter precursor cell proliferation in the SVZ compared to control animals (299).

Mudò et al., (299) also sought to identify cell types expressing FGF-2 and FGFR-1 in the SVZ as well as determine nicotine's effect on precursor cell differentiation. Double-labelling of FGF-2 or FGFR-1 in combination with nestin revealed that along the SVZ ventricular epithelium only FGFR-1 was co-expressed with nestin. This suggests that SVZ precursor cells may respond to FGF-2 produced and released by other neural cell types present in and around the SVZ (Figure 23). Double-labelling of FGF-2 with GFAP demonstrated that in the SVZ FGF-2 is expressed in cells also expressing GFAP. Because both astrocytic cells and NSCs within the SVZ are GFAP-positive (as they advance down the neural lineage, NPCs and neural precursors no longer produce GFAP), they examined if Brdu+ cells were also GFAP or nestin-positive. Brdu-labeled cells were GFAP-negative, indicating nicotine-induced enhancement of proliferation in the SVZ was not targeting SCs. On the other hand, all Brdu+ cells were nestin+ cells, signifying that actively proliferating cells are likely the target for nicotine's proliferative effects (Figure 24). These results suggest that nicotine induces release of FGF-2 from GFAP+ cells that target FGFR-1 on nestin+ actively proliferating cells (299).

Lastly in this investigation, rats were treated with acute intermittent nicotine or saline and after 24 h received i.p. Brdu. Rats were sacrificed 12 days following nicotine treatment (299). This resulted in all Brdu-labelled cells residing in the OB with few in the RMS and none in the SVZ. Using NeuN- and GFAP-labelling and co-localization with Brdu, no nicotine effects on differentiation of SVZ NPCs were detected. All Brdu+ cells that had migrated to the OB were NeuN+ in both saline and nicotine treated groups, and no co-localization of Brdu and GFAP were observed in either treatment group. Remarkably, in all experiments performed, the nicotine enhancement of precursor cell

proliferation was not accompanied by an increase in number of apoptotic cells, as shown by comparable TUNEL-labelling in every experimental and control group. Therefore, this study indicates nicotine is not involved in mechanisms underlying fate specification of SVZ neural precursor cells nor does it influence neural precursor cell or their progeny's survival (299).

In another study that reported a nicotine-induced increase in neurogenesis, Cohen et al., (300) demonstrated nicotine dependence and deprivation increases levels of immature neurons in the SGZ of the DG. Here, the authors also observed that nicotine positively correlates with the number of immature neurons in the hippocampus following extended nicotine access in rats. Male Wistar rats received jugular catheter implants for nicotine IVSA or did not undergo intravenous surgery to serve as controls (control animals did not receive saline/vehicle implants). Nicotine infusion were contingent upon nose-poke of active lever in nicotine IVSA group. A periodic deprivation model was used, in which weekly nicotine self-administration was available for either extended access (21 h per day) or limited access (1 h per day) for 4 d, followed by 3 d of abstinence. Nicotine self-administration continued under this model for 14 weeks and then brains were immunohistochemically analyzed. Proliferation marker, Ki-67, and immature neuron marker, neurogenic differentiation factor (NeuroD; transiently expressed in differentiating progenitors between day 1 and 7 after cell birth (301)), were not altered by limited access nicotine self-administration. While extended access nicotine self-administration and deprivation led to significantly higher numbers of Ki-67-labelled cells and NeuroD immunoreactive cells in the SGZ as compared to naïve controls (300). A significant increase in NeuroD+ cells was observed in the SGZ of extended access rats in

both pre-deprivation and post-deprivation stages as compared to controls and limited access rats. Neither limited nor extended access nicotine self-administration and deprivation was shown to induce apoptosis, as the number of activated caspase 3 labelled cells was not altered in these groups compared to naïve animals. Additionally, gliogenesis in the medial prefrontal cortex (mPFC) was evaluated and neither nicotine self-administration groups showed a difference in the number of proliferating progenitors and premyelinating oligodendrocytes. Limited- and extended-access nicotine self-administration did not alter Ki-67-labelling in the mPFC and did not change the number of Oligo2 labeled premyelinating oligodendrocytes in the mPFC compared to control animals (300).

Cohen et al., (300) revealed that in limited access rats, no significant correlation was observed between number of NeuroD+ cells and number of nicotine lever presses following deprivation of nicotine. Alternatively, there was a strong correlation between number of NeuroD-immunoreactive immature neurons and the number of nicotine lever presses post-deprivation during the last week of self-administration in the extended access rats. Consequently, nicotine dependence may have negative effects on the hippocampus leading to aberrant hippocampal neurogenesis. Abnormal proliferation within the SGZ may contribute to maladaptive addiction-like behaviors that are dependent on the hippocampus. This study corroborates clinical studies that have demonstrated that nicotine-dependent individuals show pronounced impairments in hippocampal-associated behaviors such as learning and memory following abstinence from smoking (272-274, 302-305).

Nicotine Attenuates A β -Induced Neurotoxicity in NSCs

Evidence supports nAChRs' role in the differentiation, maturation, survival and integration of newly born neurons in the adult brain (306-308). Immature neurons derived from ongoing neurogenesis within the DG contain $\alpha 7$ nAChRs and receive direct cholinergic innervation that is critical for integration of these adult-born neurons into the DG network (306). Nicotine has demonstrated neuroprotective abilities upon binding nAChRs on numerous cells throughout the brain, acting therapeutically by inducing defense mechanisms against pathology causing Alzheimer's disease (AD) (309, 310), Parkinson's disease (PD) (259, 311-315) and other neuroinflammatory conditions. Nicotine's actions on hippocampal $\alpha 7$ nAChRs has been shown to prevent synaptic impairment induced by A β oligomers through activation of phosphatidylinositol-3-kinase (PI3K) signaling pathways (316) (Table 6). Through its action on astrocytic $\alpha 7$ nAChRs and subsequent PI3K/Akt signaling transduction, nicotine protected against A β aggregation by modulating levels of endogenous astrocytic α B-Crystallin (317). Nicotine has been shown to protect against neuroinflammation that plays a causative role in post-operative cognitive dysfunction (POCD) (318). Nicotine mitigated POCD in partially hepatectomized rats by reducing inflammatory cytokine expression and activating brain-derived neurotrophic factor/tropomyosin receptor kinase B (BDNF/TrkB) signaling, thus preventing neuronal apoptosis in the hippocampi of these animals (262). Nicotine also regulates inflammation via $\alpha 7$ nAChRs on microglia and activating intracellular signaling cascades that ultimately inhibit the production of proinflammatory factors like TNF- α , interleukin (IL)-1 and reactive oxygen species (ROS) (for review on $\alpha 7$ nAChRs immune modulation see (319)). However, less is known about nicotine's contributions, directly or

indirectly, to NSC fate against neurotoxic compounds involved in such neurodegenerative and/or neuroinflammatory states.

Observation	Nicotine Doses	Model System	Ref
Nicotine prevents A β aggregation via hippocampal α 7 nAChRs	10 μ M (cultures), 1 mg/kg (mice)	Cultured hippocampal neurons, mice	(316)
Nicotine is neuroprotective by reducing inflammation by activating BDNF/TrkB and inhibiting TNF- α and IL-1	0.5 mg/kg	Rats	(318)
Nicotine-induced activation of α 7 nAChRs attenuates A β -induced neurotoxicity by reducing A β accumulation in mitochondria	1 μ M	Cultured hippocampal NSCs	(320)

Table 6. Nicotine-Related Neuroprotection and Neurotoxicity in NSCs

Two in vitro studies sought to assess the impact of nicotine on A β -induced neurotoxicity on NSCs through nicotine's effect upon binding microglial α 7 nAChRs (266, 320). The rationale being that following deposition and accumulation of A β , a secondary

phenomenon of inflammation contributes to the loss of cholinergic neurons characteristic in AD pathophysiology (321). It is also known that A β interacts with nicotinic receptors (322, 323) and stimulating nAChRs increases A β internalization and prevents aggregation (213, 324). Additionally, microglia play an important role in regulation of neurogenesis (325). Taken together, cholinergic drugs may promote recovery in AD, at least partially, by restoring NSC populations, as activated nAChRs can improve the microenvironment of the brain by preventing production of microglia-derived inflammatory factors and increasing A β phagocytosis.

The aim of the first study was just that, to improve the survival microenvironment of NSCs co-cultured with microglia by attenuating microglia-derived inflammatory factors mediated by A β peptide accumulation (266). To evaluate this, Jiang et al., (266) used four experimental groups: (1) a control group in which NSCs were cultured with no interventions; (2) A β -treated group in which NSCs were exposed to 10 μ mol/L of A β ₁₋₄₂; (3) co-cultured group in which NSCs were cultured in a transwell system with microglia which had been treated with 10 μ mol/L of A β ₁₋₄₂; and (4) a nicotine pretreated group in which microglia were pretreated with 10 μ mol/L nicotine for 1 h before being treated with 10 μ mol/L of A β ₁₋₄₂ and subsequently co-cultured. They found that low concentration nicotine decreased release of pro-inflammatory cytokines stimulated by A β in primary microglia. Levels of TNF- α and IL-1 were significantly elevated in the microglia co-culture group versus the NSC-only control group, and these levels were decreased when treated with nicotine (10 μ mol/L). Proliferative rates of NSCs were shown to be lower in the A β -treated group and even greatly diminished in the co-cultured group. Nicotine pretreatment was able to partially rescue NSC proliferative rates.

Immunoreactivity for microtubule-associated protein 2 (MAP2), a neuronal marker particularly enriched in the dendrites (326), and choline acetyltransferase (CHAT), used to label cholinergic synapses (327), revealed nicotine mitigates changes in NSC differentiation provoked by microglia-derived factors induced by A β . The control group contained 14.6% MAP2+ cells and 4.0% CHAT+ cells. While the A β -treated group had 10.2% MAP2+ cells and 3.0% CHAT+ cells, and the co-cultured group had 5.6% MAP2+ and 0.9% CHAT+ cells. The nicotine pretreatment group was observed to have partially restored to a condition that resembled cultures without microglia present (8.3% MAP2+ cells and 2.1% CHAT+ cells). Using Annexin V/PI staining and TUNEL assays, the apoptosis rate of each condition was determined. Again, the greatest effect of A β was seen in the presence of microglia, with the percent of apoptotic cells out of total cell population increasing from less than 10% in control to 41.3% in co-culture group. The effect of nicotine on NSC apoptosis also demonstrated the same trend as other series in this study. The apoptosis rate decreased to 29.7% but was still greater than control or A β groups that did not contain microglia. Lastly, the authors examined the Wnt/ β -catenin pathway as the mechanism underlying the observed neuroprotective effects of nicotine. The results demonstrated Axin2 played a negative role in the Wnt/ β -catenin pathway in NSCs co-cultured with A β -treated microglia. Nicotine enhanced Wnt/ β -catenin signaling by upregulating β -catenin, phosphorylating glycogen synthase kinase 3 β (p-GSk-3 β), and downregulating Axin2 and phosphorylated β -catenin. Altogether this partially ameliorates the microglia-activated inflammatory response in NSCs. These data suggest the A β may have some direct negative consequences on NSC

proliferation, differentiation, and survival. However, A β toxicity is primarily mediated through microglial actions.

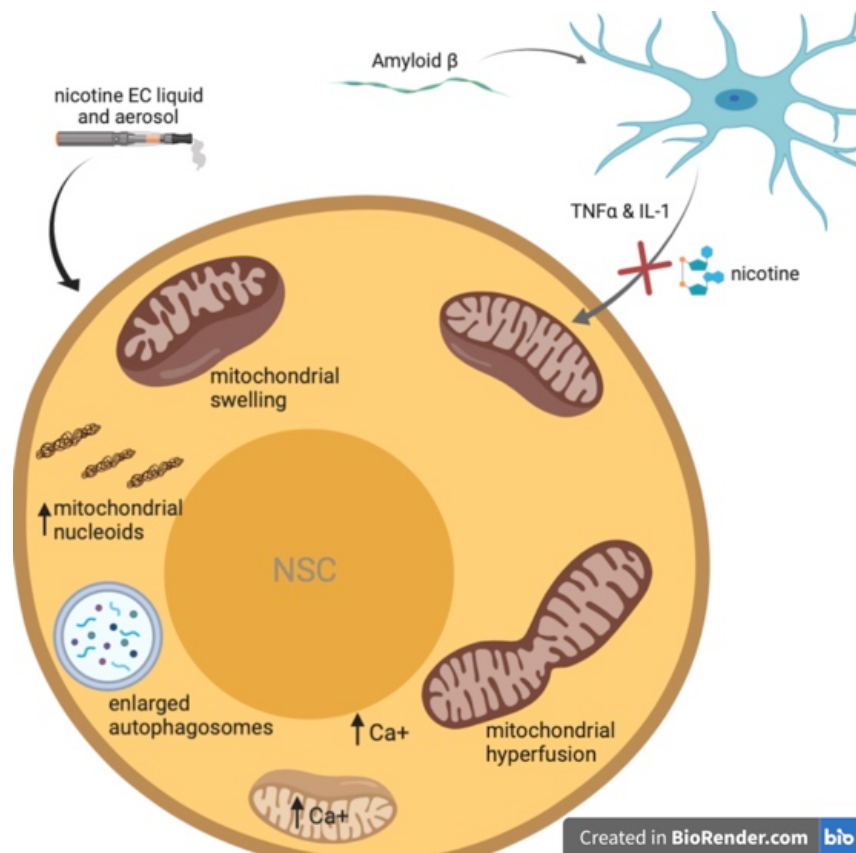


Figure 24. Summary of Described Effects of Nicotine E-Cigarettes (EC) Liquid and Aerosols on NSC Mitochondria

EC treatments led to altered mitochondrial membrane potential (MMP), induced aggregation of mitochondrial nucleoids and mitochondrial DNA, and induced calcium influx leading to plasma membrane retraction and intracellular calcium overload.

The second study also used a transwell system to evaluate the indirect cytotoxicity of A β -mediated microglial activation on NSCs (320). Because many of the microglia-derived proinflammatory factors have been shown to induce neuron death often through mitochondrial dysfunction (328-332), Chen et al. sought to uncover the

mechanism interconnecting mitochondrial function and inflammation-mediated NSC death and how nicotine might therapeutically intervene through its actions on microglial nAChRs. In addition to evidence that the mitochondria is a primary target in inflammation-mediated neural cell death, it has also been shown that A β progressively accumulates in the mitochondria of cells throughout the brain (333). They found that blocking the mitochondrial permeability transition pore (mPTP) (which plays a central role in apoptotic neuronal death (334)) and activating the α 7 nAChRs on microglia attenuated A β -induced neurotoxicity on NSCs (Figure 24).

Interestingly, Chen et al., (320) did not detect α 7 nAChR immunoreactivity on NSCs. This finding is in opposition to previous work that reported α 7-nAChRs are present on undifferentiated stem cells and progenitor cells throughout the body (335). Still yet, others have shown the importance of α 7 nAChRs present on hippocampal NPCs and immature neurons on differentiation, maturation, integration, and survival (306, 336). An exact expression pattern for nAChRs on NSCs and their progeny has not yet been clearly established. Although it appears nAChRs are vital for certain stages of neurogenesis, in this study α 7 nAChR subunit mRNA was only detected on primary microglia, while no detectable expression of α 7 nAChR subunit in primary NSCs was observed.

The results of this study (320) showed blocking the mPTP in NSCs or activating the α 7 nAChR in microglia rescued NSC mitochondrial activity. The NSC mitochondrial membrane potential (MMP) and morphological characteristics were respectively measured by JC-1 staining and transmission electron microscopy. The addition of A β -treated microglia more significantly altered mitochondrial depolarization in NSCs than the

addition of A β directly to NSC culture without microglia present. When A β -treated activated microglia were pretreated with 1 μ M nicotine, their negative effects on NSC mitochondria were partially reversed. The altered NSC mitochondrial membrane permeability was also partially corrected when NSCs were treated with cyclosporine A (CsA), which targets cyclophilin D, an essential regulator of the mPTP opening (337), and ultimately blocked the mPTP. Nicotine or CsA pretreatment was also shown to reverse A β -induced mitochondrial cristae swelling. Lastly, A β -mediated microglial activation greatly increased the apoptotic rate of NSCs compared to control. Nicotine activation of microglial α 7 nAChRs and blocking of the mPTPs by CsA attenuated the observed NSC apoptosis.

Nicotine Induces Mitochondrial Stress in Neural Stem Cells

Changes to SC mitochondrial health could have highly important implications as mitochondria play a key role in regulating stemness (71, 338-343). Recently, in addition to preventing senescence, mitochondria have also been linked to stem cell activation and determining fate/differentiation (342-344). Unfortunately, mitochondria are also sensitive to stress (345), leaving them susceptible to possible damage from nicotine and/or other toxic byproducts from tobacco use. Moreover, a decline in SC mitochondria function could underlie accelerated aging traditionally seen in smokers.

Studies have suggested nicotine exposure affects the mitochondrial respiratory chain, oxidative stress, calcium homeostasis, mitochondrial membrane proteins, mitochondrial association from microtubules, mitochondrial dynamics, biogenesis, and mitophagy (346, 347) (for full review on nicotine's impact on mitochondrial activity see

(348)). However, few studies have specifically examined the impact of nicotine exposure on NSCs and their mitochondria. As discussed in the previous section (Nicotine attenuates A β -induced neurotoxicity in NSCs), Chen et al., demonstrated a link between NSC mitochondrial function and A β -induced neurotoxicity. Interestingly, the results of that study advocate for a protective role of nicotine against microglia-derived proinflammatory factors that have been shown to induce neuron death via mitochondrial dysfunction (Figure 24). In a transwell coculture system, A β -mediated microglial activation led to mitochondrial dysfunction within NSCs and caused NSC apoptosis. These negative effects were attenuated by treatment of microglia with 1 μ M nicotine and treatment of neurospheres with a mitochondrial permeability transition pore inhibitor. This suggests that mitochondria may play a critical role in nicotine's action as a neuroprotective agent for NSCs.

In contrast, Zahedi et al., demonstrated a mitochondrial stress response in NSCs following exposure to electronic cigarette ENDS e-liquids and their aerosols (349). Importantly, they also reported that the effects of ENDS on the mitochondria are mediated by nicotine and not by the transfer of volatile organic chemicals or solvents found in e-liquids (propylene glycol and glycerin). Cultured NSCs were incubated for 4 or 24 h with menthol- or tobacco-flavored e-liquids (0.3%, 0.5% and 1% dilutions) or aerosols (1, 3, and 6 total-puff-equivalents (TPE)). The results of this study revealed that EC liquids and aerosols inhibit proper autophagy in NSCs. Autophagosomes were enlarged in a time-dependent manner, with a greater enlargement seen in e-liquid exposed than aerosol exposed cells. The enlarged autophagosomes also demonstrated an increase in pH. (Figure 24). The decrease in autolysosome acidity could decrease its normal proteolytic

function. This is important as mitophagy, or mitochondrial autophagy, protects cells by removing damaged mitochondria which could induce pro-apoptotic signaling. After 4 and 24 h e-liquid and aerosol treatments mitophagy had not significantly increased, except in the high-dose 1% menthol-flavored nicotine e-liquid group. Using time-lapse imaging and a motion-magnification algorithm they did observe e-liquids and aerosols alter mitochondrial dynamics. Treatment with both e-liquids decreased large motion and increased small motion as compared to controls. While menthol-flavored aerosol decreased small motion and increased large motion of NSC mitochondria, and the same trend was observed in tobacco-flavored aerosol treatment but was not statistically significant when compared to control.

The changes observed in mitochondrial dynamics appear to correlate with alterations in mitochondrial swelling or hyperfusion (Figure 24). Greater motion was seen in hyper-fused mitochondria (aerosol) and less motion was seen in the swollen mitochondria (e-liquids). As hyperfusion has been shown to increase superoxide production (350), they loaded cells with a mitochondrial-targeted dye that produces fluorescence in the presence of superoxide anion. A dose-dependent escalation of fluorescent intensity was observed in e-liquid-treated cells, and a lesser increase also found in the aerosol-treated cells. Using immunoblot analysis, it was determined that cells treated with e-liquid or aerosol also had significantly elevated superoxide dismutase two levels compared to controls. Additionally, a concentration-dependent increase in mitochondrial protein oxidation was observed in all e-liquid and aerosol treatments.

This study also provided evidence that EC e-liquids and aerosols can cause significant and not-easily-reversible damage to the mitochondria of NSCs. EC treatments

led to altered MMP, induced aggregation of mitochondrial nucleoids (Figure 24) and mitochondrial DNA (mtDNA), and induced calcium influx (Figure 24) leading to plasma membrane retraction and intracellular calcium overload. Labelling with tetramethylrhodamine methyl ester (TMRM) dye, a cell-permeable, cationic dye that is sequestered by active mitochondria but leaks out of depolarized mitochondria, revealed changes in MMP in NSCs treated with high-dose e-liquid or aerosol for 24 h. Treatment with aerosols (hyperfused mitochondria) increased TMRM accumulation in the mitochondria. While 1% liquid (swollen mitochondria) had different results. The 1% tobacco-flavored nicotine e-liquid showed no change in TMRM, and the 1% menthol-flavored nicotine e-liquid dose showed a decrease in TMRM signal, suggesting this concentration damages the mitochondria and causes membrane leakage. Because an elevation of ROS can lead to mtDNA damage, a dye was used to label mitochondrial nucleoids. Control cells had multiple small fluorescent nucleoids, whereas e-liquid (0.5%) and aerosol (6TPE) for 24 h treated cells had larger, brighter nucleoids characteristic of mtDNA aggregation.

Lastly, EC- and nicotine-induced alterations to calcium influx were evaluated. NSCs transfected with a fluorescently tagged calcium reporter (GCaMP5) and imaged live before and after exposure to e-liquid (0.5% menthol- or tobacco-flavored), aerosols (6TPE menthol- or tobacco-flavored), and various concentrations of nicotine (220 $\mu\text{g}/\text{mL}$ or 1.1 $\mu\text{g}/\text{mL}$). An increase in intensity was seen at one minute for all conditions and was most pronounced in 0.5% menthol-flavored nicotine e-liquid and 220 $\mu\text{g}/\text{mL}$ nicotine solution. These data also showed that calcium levels did not return to baseline by 20 min after exposure, resulting in calcium overload. Much of the fluorescent signal was seen accumulating in the perinuclear region, which was presumed to be due to

sequestering of calcium by the endoplasmic reticulum. However, because intracellular calcium can also accumulate in the mitochondria which can then trigger ROS production (351), NSCs were then transfected with a genetically encoded calcium indicator called calcium-measuring organelle-entrapped protein indicator (CEPIA). Transfected cells were again imaged live before and after exposure to e-liquid (0.5% menthol- or tobacco-flavored), aerosols (6TPE menthol- or tobacco-flavored), and various concentrations of nicotine (220 $\mu\text{g}/\text{mL}$ or 1.1 $\mu\text{g}/\text{mL}$). All treatments showed an increase in fluorescent signal within 1 min, followed by a decrease by 44 min. Again, the greatest changes were observed 0.5% menthol-flavored nicotine e-liquid and 220 $\mu\text{g}/\text{mL}$ nicotine. Unlike the other treatment, the calcium levels in these groups did not return to resting state by 20 min following exposure. NSCs were then pre-incubated with Ru360, a compound to block calcium uptake through mitochondrial calcium uniporter (MCU) proteins. With calcium uptake through MCU inhibited, the changes in intracellular calcium following e-liquid, aerosol, or nicotine exposure were significantly dampened. Mitochondrial calcium influx was also successfully inhibited by blocking $\alpha 7$ nAChRs with α -bungarotoxin ($\alpha 7$ nAChR competitive antagonist). Lastly, they sought to evaluate if calcium blockage could impede mitochondrial effects of Ecs and nicotine. Thus, NSCs were incubated with 1 μM calcium chelator EGTA (ethylene glycol-bis(β -aminoethyl ether)- N,N,N',N'-tetraacetic acid) and treated with 0.5% e-liquids for 4 h. The results showed a significant decrease in mitochondrial superoxide production when EGTA was present. The authors conclude these data suggest calcium overload contributes to EC-induced mitochondrial defects in NSCs.

Discussion

Adult neurogenesis plays an important role in learning and memory (352), olfaction (252), and the brain's ability to regenerate after injury (353). Albeit limited, the brain does have some capacity to self-heal following insults such as stroke. Ischemic and traumatic lesions within the cortex have been shown to stimulate proliferation in the SVZ (70-72, 175, 354). These newly born neural cells then migrate along blood vessels (355) to the site of injury to where they differentiate primarily into glial cells and fewer become mature neurons (70, 74, 354). One physiological limitation is a substantial lack of integration of these recruited endogenous precursor cells, particularly in the case of stroke as ischemia creates a very hostile microenvironment for the newly arriving cells (74). Since the revelation that neural precursors can migrate to sites of injury within the brain, considerable research efforts have been placed on creating a more robust neurogenic response, promoting NPC migration, and enhancing integrative capacity into damaged regions following stroke and other neurodegenerative conditions (98, 101, 230-232, 356, 357). As this field of regenerative research advances, it will be important to understand what effects the main risk factors for stroke, such as smoking, have on the health of NSCs.

In addition to effects nicotine may have on continued postnatal neurogenesis and its implications for the possible exploitation of NSCs therapeutically in adults, it is also important to consider nicotine-induced changes in prenatal neurogenesis. While the scope of this review primarily focuses on SCs and progenitors of adult neurogenesis, it

is important to note that ENDSs are often used by adolescents and pregnant women. During development, SCs of the nervous system are especially vulnerable to toxicants (358). In attempts to abandon smoking, pregnant women may resort to the use of nicotine patches or ENDSs that are colloquially considered less dangerous (359). These methods nevertheless introduce nicotine, which is considered a neurotoxic and neuroteratogenic agent (360-363), to the developing fetus. Notably, evaluation of maternal nicotine exposure during gestation and lactation period in mice revealed alterations in neurogenesis in offspring (364). Nicotine-exposed offspring were found to have altered behavior, increased cell proliferation in the DG, more disorganized immature double-cortin positive (Dcx+) neurons, and increased microglial markers.

The mRNA for neuronal nicotinic receptor subunits and nicotine receptor binding sites are first detected at the end of neurulation, and at that point the developing brain becomes vulnerable to nicotine exposure (365, 366). Importantly, this process occurs early in pregnancy as primary neurulation begins week 3 of gestation (367). Newly born cells destined for neuronal lineage migrate from the mitotic zone to various regions of the developing brain then nAChR expression becomes regionally specific (368, 369). As previously mentioned, nAChRs play a role in differentiation, maturation, integration, and survival of newly born neurons throughout adulthood (306-308). In the fetal brain acetylcholine signaling is important for coordinating proper assembly of the neural tissues (370). Maternal cigarette smoking has been associated with structural and functional alterations within the brain, including in the mPFC (371), striatum, amygdala, and hippocampus (372), and numerous cognitive and behavioral changes (373, 374), such as deficits in learning and memory (375), auditory dysfunction (363), hyperactivity (376),

and depressive-like behaviors (377), in the offspring (for a full review of pre-clinical and clinical evidence of nicotine's effects on development in the nervous system and more see (378)).

Conclusions

The current state of research on nicotine's effects on neural stem, progenitor and precursor cells is still in its infancy and there is much to be discovered. Presently nicotine appears to have differential effects on these immature cells of neural lineage depending on both location and maturation. Nicotine may exert a protective role for NSCs when exposed to cytotoxic or inflammatory agents. The mitochondria of NSCs appear to also play an important role in these interactions between NSCs, glia, and nicotine. Additionally, nicotine may have differing effects on NSCs depending on route of administration and further research is needed to determine these consequences.

SECTION 2: EXPRESSION OF ALPHA4 NICOTINIC ACETYLCHOLINE RECEPTOR SUBUNITS ON DOPAMINERGIC AND GABAERGIC NEURONS OF THE VENTRAL TEGMENTAL AREA FOLLOWING PASSIVE INHALATION VAPORIZED NICOTINE IN MICE

Introduction

Ventral Tegmental Area and Parkinson's Disease

Parkinson's disease is a neurodegenerative disorder predominantly affecting dopaminergic neurons for which there is no cure (10). While the motor symptoms of PD are generally more familiar to the general public, non-motor symptoms ranging from mild cognitive impairment to severe dementia also occur frequently in PD (379). Just as tremor, bradykinesia, rigidity, facial masking and gait instability progressive over years, cognitive deficits also tend to worsen with disease duration (379, 380). It is important that we uncover and understand the neural networks involved in both motor and cognitive parkinsonian symptoms for more comprehensive treatment of PD patients.

It is thought that selective dopaminergic degeneration within the ventral mesodiencephalon leaves the dopamine (DA) neurons of the VTA partially spared while the DA neurons of the substantia nigra pars compacta (SNc) are much more significantly degenerated in PD (381, 382). While the VTA is more resistant to DA neuron degradation in PD, it does experience about a 50% neuron loss (383, 384). This leads to loss of DA input to the ventral striatum which may cause or contribute to the cognitive decline seen in PD patients, as these connections are important for learned associations, incentive salience and memory consolidation in the brain (385-387).

Further, both SNc and VTA have overlapping projection patterns. The SNc DA neurons are understood to be mainly involved in circuits controlling motor movements while the VTA DA neurons are primarily responsible for regulation of reward, emotional behavior and addiction (388). The majority of SNc neurons project to dorsal striatum and only some nigral fibers project to the ventral striatum and the cortex and, conversely, the VTA sends most projections to the ventral striatum and cortex with fewer going to the dorsal striatum (388, 389). Moreover, both SNc and VTA DA neurons send minor projections to additional brain regions including the globus pallidus, subthalamic nuclei, and habenula (388, 389). Ultimately, the SNc and VTA work together to play a key role in modulating motor behavior through the basal ganglia (390). As such, pathology of the VTA may play a significant role in the motor and/or non-motor symptoms of PD and modulation of this region may prove therapeutically beneficial.

Nicotine and Nicotinic Receptors in the Brain

Several retrospective and prospective population-based epidemiological studies have shown an inverse correlation between patient history of tobacco use and development of PD (249, 391-395). Since 1959, numerous studies have demonstrated this trend in the clinical setting, revealing an approximately twofold decrease in PD risk with tobacco use (396-399). The inverse correlation between smoking and PD has also been shown to be dose-dependent, with a decreased incidence observed with both increased smoking intensity, or number of cigarettes smoked per day, and with number of smoking years (391, 392, 395, 400, 401). Therefore, interrogation of nicotine as a neuroprotective agent and elucidation of possible underlying neuroprotective mechanisms is important. While

causal mechanisms are not fully understood, several studies have observed nicotine-associated neuroprotective effects in *in vivo* models of Parkinsonism (311, 312, 402-404). However, others have suggested that chronic nicotine does not directly protect against degeneration, but rather modifies DA receptor dynamics (405, 406), still others propose nicotine both plays a role in degenerative prevention *and* alters activity at DA synapses to maintain or restore normal function with nigrostriatal damage (407).

Of interest to the present research, is evidence that the decline of $\alpha 4$ nAChR subunits is much less compared to other nAChR subtype expression in the striatum of parkinsonian animals (408). Suggesting $\alpha 4$ nAChRs may be more resistant to PD-related striatal DA neuron degradation and may prove a potential target to ameliorate PD motor symptoms. Additionally, other research has shown pharmacological chaperoning by nicotine upregulate $\alpha 4\beta 2$ nAChRs in the plasma membrane of neurons with chronic nicotine exposure (409). Here we expanded upon evidence that long-term nicotine exposure upregulates $\alpha 4\beta 2$ nAChRs in the brain. Specifically, we have implemented a passive vape inhalation paradigm in which $\alpha 4\beta 2$ nAChR upregulation has not previously been described. With ENDS usage gaining popularity as an alternative to traditional combustible cigarette smoking, alterations in neural nAChRs following ENDS exposure is highly important.

Material and Methods

Reagents

Free-base nicotine (product number – N2472-100ML, lot number – 2AH0278) was obtained from Spectrum. 30% Propylene Glycol and 70% Vegetable glycerin (30/70 PGVG) was obtained from La Jolla Alcohol Research, Inc. (La Jolla, CA).

Mice

All experiments were conducted in accordance with the guidelines for care and use of animals provided by the National Institutes of Health. Protocols were approved by the Institutional Animal Care and Use Committee at Marshall University. Mice were kept on a standard 12/12 h light/dark cycle at 22 °C and given food and water *ad libitum*. Knock-in α 4-mCherry mice originating from a C57/BL/6J background were utilized in all experiments. The creation of the α 4-mCherry knock-in mice has been previously reported (410, 411) and maintained at Marshall University Animal Care Facility. Postnatal day 21 mice were weaned and housed with same-sex littermates. For genotyping, tail biopsies were acquired between postnatal day 16–21 for PCR analysis, using previously published methods (412) by Transnetyx (Cordova, TN). Only mice that were homozygous for α 4-mCherry were selected for use in e-Vape inhalation and confocal assays. For all experiments, both male and female adult (3 - 5 months old) mice were used.

Passive e-liquid vapor inhalation assays

Passive vapor delivery was conducted in four air-tight chambers with interior dimensions of 35 cm L x 25 cm W x 22 cm H (La Jolla Alcohol Research, Inc. La Jolla, CA, USA). The chambers were housed in a dark Plexiglas enclosure that minimized extraneous light and noise. Airflow was vacuum controlled by an electric pump that allowed air

flow at 1 L/min. The air outlet was located at the top back corner of the right wall of the chamber and connected through tubing to a HEPA-Cap filter (product number – 26091, lot number - 3953048) from Midland Scientific. The vapor port was located in the front of the chamber and the e-liquid solutions were contained in a SMOK® baby beast TFV8 X-baby Q2 atomizer tank (0.40 ohms dual coil; Shenzhen IVPS Technology Co., Ltd., Shenzhen, China) that was activated by a custom e-cigarette mod box (La Jolla Alcohol Research, Inc., La Jolla, CA, USA). Vapor delivery settings were controlled by an e-Vape custom controller (La Jolla Alcohol Research, Inc., La Jolla, CA, USA, www.ljari.tech).

Three- to five-month-old $\alpha 4$ -mCherry mice were placed, separating male and female, into passive inhalation chambers for three-hour sessions for a total of 10 days. Sessions ran 5 days consecutively with a 2-day (weekend) abstinence in between. This was done to match the exposure paradigm of e-Vape self-administration assays (413). Time-triggered puffs of e-liquid vapor were performed the same for nicotine and control groups and were as follows: 3-sec puffs administered directly into the passive chambers every 3 min for 3 days, every 2 min for 3 days, and every 1:20 min for 4 days. This escalation of the vapor deliveries within the 3 hr sessions is modeled after the average fixed-ratio 1 escalation of mice in the first 10 sessions of e-Vape self-administration. The nicotine group received puffs of vaporized e-liquid containing 12 mg nicotine. Once 3 hr sessions were completed mice were returned directly to home cages.

Confocal imaging of mouse brain slices

Labeling was derived from direct $\alpha 4$ -mCherry excitation and emission in $\alpha 4$ -mCherry mice. Additionally, immunohistochemistry was performed for tyrosine

hydroxylase to differentiate dopaminergic and GABAergic neurons. Following the completion of the final passive vape inhalation assay, mice were euthanized with CO₂ and subjected to rapid cardiac perfusion with ~10 mL cold saline. This clearance of blood from the cerebrovasculature has been previously shown to significantly reduce the autofluorescence in the mCherry emission range (412). The whole brain was then carefully dissected from the cranium, frozen immediately, and stored at -80 °C. Brains were coronally sectioned (20 µm thickness) using a Leica CM 1950 cryostat, mounted with Vectashield (Vector labs, H-1000), and coverslipped. Bregma range -3.1 mm to -3.3 was collected (only slices containing VTA were imaged in this study, however, we also sought to capture SNr and SNc for storage and future evaluation). A Leica SP5 TCSII confocal microscope was used to excite α4-mCherry at 561 nm. Imaging was performed at 20X magnification with a 5X digital zoom.

Imaging and statistical analysis

A Leica SP5 TCSII confocal microscope was used for imaging of the α4-mCherry and Tyrosine Hydroxylase (TH) stained mouse brain slices. TH and α4-mCherry were excited at 488 and 561 nm, respectively; 10× images with a 5× digital zoom were collected for the quantitative measurements.

Quantitative measurements of α4-mCherry neuron fluorescence intensity were done using ImageJ. The raw integrated density (RID) and mean were recorded from ImageJ analysis and used for the measurements of fluorescence for each neuron. A minimum of 20 VTA neurons were analyzed per mouse. Data for both parameters were averaged for each mouse.

Statistical analyses were performed using Graphpad Prism. Males and females were analyzed separately. Potential sex differences were analyzed using a two-way ANOVA and posthoc Bonferroni for the comparison of means.

Results

The current data yield no statistically significant differences between male or female nicotine of PGVG vehicle treatments (Fig 25). However, a non-statistically significant increase in $\alpha 4$ nAChR expression was observed in female, but not male, mice following passive nicotine vapor inhalation as compared to controls. Future studies are needed to elucidate if such a difference exists.

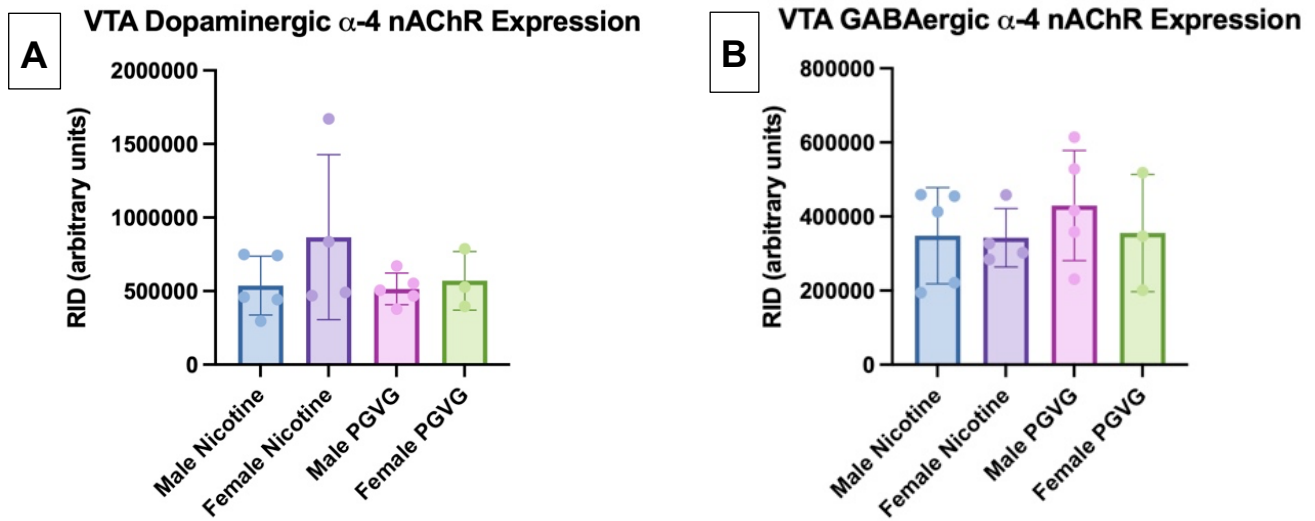


Figure 25. Dopaminergic and GABAergic α 4nAChR Expression in VTA

α 4-mCherry mice were exposed to vaporized PGVG alone or PGVG containing 12 mg nicotine in passive inhalation chambers for three-hour sessions for a total of 10 days.

A) Raw integrated density (RID) values for VTA dopaminergic neurons in males and females following nicotine exposure and vehicle controls. B) Raw integrated density (RID) values for VTA GABAergic neurons in males and females following nicotine exposure and vehicle controls. All data points (average RID for each mouse) are shown \pm SD; * p <0.05; Ordinary Two-way ANOVA.

Discussion

Limitations of this study include a low number of mice included and therefore possibly underpowered data. If the difference in means for female versus male mice passively exposed to vaporized nicotine is truly similar to that presented here, then a power calculation reveals a minimum of 6 subjects per treatment group should be used in future studies. However, we suspect that the greatest drawback of our methodology was the use of larger vape chambers than what has been previously used in our lab. We later found cotinine levels to be lower than expected in mice placed in these particular chambers as compared to previous experiments using smaller vape chambers (data not shown).

Motor symptoms of PD are classically attributed to the death of substantia nigra DA cells and subsequent loss of dopamine signaling within neural circuits essential for proper motor control. Several authors postulate that DA cell death is, at least in part, the result of alterations in the actions of the proapoptotic effector, C/EBP homologous protein (CHOP) (414-418). Activation of CHOP occurs in DA cells as a result of Ca⁺ influx and potentially toxic byproducts of dopamine metabolism that these cells are subjected to which then affect proteostasis (419-421). Proteins involved in the unfolded protein response (UPR), which under normal cellular conditions are responsible for detecting unfolded and misfolded proteins, display sustained activity in DA neurons consequent of these pathophysiologic stressors (416). Unmitigated UPR subsequently activates CHOP, leading to propagation of apoptosis signaling in DA neurons. It is therefore unsurprising that prolonged ER stress and persistent UPR have been implicated in PD pathogenesis (422).

One proposed neuroprotective mechanism of nicotine is through suppression of endoplasmic reticulum (ER) stress and the UPR (423). It has been shown that chronic nicotine exposure leads to nAChR upregulation through intracellular pharmacological chaperoning, but it is only one of several consequences of pharmacological chaperoning by nicotine (409). Nicotinic ligands permeate through cell membranes and exert other pharmacological chaperoning effects including modifications on ER stress and the UPR (409), which was further studied in a cultured model for nicotinic neuroprotection (410). One study found that in cultured ventral midbrain DA neurons given smoking-relevant dose for 2 weeks (200 nM nicotine from 7 to 21 d in culture) pretreatment with nicotine prevents CHOP activation following DA neuron exposure to known ER stress inducer, Tunicamycin (50 or 150 nM for 72 hr). Nicotine's protective effect, however, was limited as only partial suppression of CHOP elevation was noted at the higher concentration. Additionally, they demonstrated mecamylamine (MECA), a broad spectrum nAChR blocker, failed to suppress this effect further supporting evidence that nicotine does not just exert effects following plasma membrane binding, but also acts as an intracellular chaperoning role. Suppressed activity in three arms of the UPR triggered by ER-resident stress sensors, XBP1, ATF6, and protein kinase RNA-like ER kinase (PERK) pathway, by chronic nicotine was also observed. Another important finding of this study was that nAChRs are required for nicotine-induced reduction in ER stress markers, shown by using transfected neuroblastoma cells. Results that are supported by their previous work revealing low-dose nicotine acts as a pharmacological chaperone of NACHRs in the ER, which then suppresses ER stress and UPR (423). Importantly, another indicator

of pharmacological chaperoning by nicotine is the upregulation of $\alpha 4\beta 2$ nAChRs in the plasma membrane of neurons with chronic nicotine exposure (409).

Accruing evidence indicates that nicotine and nAChR ligands may influence PD motor symptoms by two different mechanisms: 1) protection against nigrostriatal damage, and 2) nAChR ligands may directly stimulate the DA system to acutely ameliorate motor-related symptoms. Targeting $\alpha 4$ -containing nAChRs may prove useful for these effects as nigrostriatal damage in PD has been shown to lead to a much lesser decline in certain $\alpha 4$ nAChRs compared to other nAChR subtype expression in the striatum (408). Quick and Wonnacott (399) outline the differential impact on nAChR expression in the striatum in parkinsonian animals following damage to the nigrostriatal DA pathway. Briefly, all $\alpha 6$ -containing nAChRs in the striatum were dramatically diminished following nigrostriatal damage, while $\alpha 4\beta 2$ nAChRs present on striatal DA terminals were more mildly declined. Additionally, no decline was observed for $\alpha 4\beta 2^*$, which are not found on striatal DA terminals, or $\alpha 7$ nAChRs. Therefore, $\alpha 4\beta 2$ nAChRs preserved on other elements, not DA neurons, may contribute to local nAChR-mediated effects in the striatum.

More research is needed to further define nAChR expression patterns in the dorsal versus ventral striatum. As noted previously, multiple dopaminergic networks are affected to varying degrees in PD leading to different motor and non-motor signs and symptoms. It appears $\alpha 4$ -containing neurons and DA neurons of the VTA are more resistant to the cytotoxic pathology in PD. These neurons may prove useful if targeted appropriately in overcoming certain movement and/or cognitive problems PD patients face.

Conclusion

At this time no conclusions can be drawn about the effects of passive vaporized nicotine exposure in mice on $\alpha 4$ nAChR expression on DA or GABAergic neurons within the VTA. More studies are needed to elucidate if this manner of nicotine delivery does or does not alter $\alpha 4$ nAChR expression.

GENERAL DISCUSSION

Here we have discussed multiple facets of current and potential therapies for different neurological conditions with a focus on PD and stroke. PD is the second most common neurodegenerative disease in the world and as it currently stands, is incurable (10). The current standard of care for advanced PD, and other movement disorders, inadequately controlled by pharmacological means is DBS placement (18). We found that while the majority of U.S. surgeons currently split up DBS system implant into multiple surgeries, it is a safe and effective under skilled hands option to perform the entire placement in a single operative session. It has been feared that increased time under anesthesia and longer incision-to-closure time would result in increased length of stay, greater infection rates, and other postoperative complications. However, we found in a single institution study that this was not the case. A single-staged DBS implantation proved non-inferior regarding negative outcomes in a 90-day post-op period. This is important as many of our patients travel long distances from rural locations or have other limitations to transportation. Performing their DBS surgery not only decreases trips to the OR for these patients but also cuts back on pre-and post-op travel to and from the hospital.

Secondly, a novel technique of creating new neural tracts using fibrin-based brain implants for neuroregeneration was discussed. We demonstrated that fibrin can be made predictably stable in neural environments through the incorporation of protease inhibitor aprotinin. Further, a simple and inexpensive method for immobilizing aprotinin in hydrogel implants was described using a chemical crosslinking agent. While every other component found in our fibrin implants has been studied or is currently

being used in clinical application, DSS has not. Future work is needed to evaluate the safety of DSS and/or other chemical crosslinking agents for human use before this method could be translatable.

Thus far, these engineered fibrin implants have been shown effective at recruiting progenitor cells to the striatum and partially improving motor dysfunction in a hemiparkinson rat model. Further, an updated implant architecture was developed, transforming the homogenous, solid fibrin cylinder to a double-barreled, cylinder inside a cylinder design. The CinC is intended to recapitulate the tubular structure of the anatomical RMS (223) and thus better promote SVZ NPC migration. Another advantage of the renovated design is that it allows a great combination of possible matrices and factors that can be incorporated into the implants. As many different cytokines and growth factors have been shown to improve NPC migration, differentiation, and maturation, this structure allows for an assortment of factors to be evaluated. In the future, studies are needed to evaluate these chemotactic and growth factor combinations to determine those optimal for cell differentiation and migration. Additionally, work is needed to determine how effectively recruited NPCs can integrate and function in their new environment.

Next, $\alpha 4$ nAChR expression on DA and GABA neurons in the VTA of mice passively exposed to vaporized nicotine was assessed. In the literature, it has been shown that following chronic nicotine exposure, the high-affinity $\alpha 4\beta 2$ nAChR subtype widely upregulates in the brain (424-426). A trend we expected but did not clearly see here. Further, sex differences are beginning to be reported for drug-induced nAChR expression in various brain regions as well as for nicotine behaviors (427-431). These reports suggest that

it may be beneficial to further explore our nonsignificant findings of nicotine-induced increased $\alpha 4$ nAChR expression on DA neurons of the VTA in female mice only.

While nicotine was discussed in the context of its possible neuroprotective actions on DA cells, nicotine does not reinstate function once nigrostriatal damage has already occurred, its actions are primarily protective in nature not restorative (248, 249). One study showed when a 2- to 3-week nicotine regimen was administered to rats before nigrostriatal lesioning, improved dopamine transporter levels in the striatum were observed (432). Conversely, when the same dose and time intervals of nicotine were administered to rats after lesioning, no change in transporter levels was evident compared to animals not receiving nicotine. Thus, there remains a need for neuroregenerative therapies for striatal (and other brain regions) damage, such as the bioengineered brain implants presented here. Bringing us to the final subject matter discussed, nicotine's potential effects on NSCs.

If endogenous NSC/NPCs are to be used for regenerative purposes in PD or stroke, then we must understand what implications nicotine poses on the health and function of those cells as smoking is thought to be neuroprotective for PD and a main risk factor in the development of stroke. To date the research is limited, but nicotine appears to have differential effects on these immature cells of neural lineage depending on both location and maturation. Nicotine may exert a protective role for NSCs when exposed to cytotoxic or inflammatory agents. An effect that may prove useful for future neurorestorative efforts.

CONCLUSION

There currently remains a paucity of treatment for many neuropathologies resulting from the injury and/or death of neuronal populations. First, we evaluated patient outcomes for the current standard-of-care (*i.e.* DBS) for advanced movement disorders including PD. Our results indicate that single-staged DBS implant surgeries are non-inferior to the more commonly performed multi-staged surgeries. Affording patients the option to condense their DBS system implantation to a single operation without increasing complication risk. A protocol that may prove especially favorable for rural or otherwise underserved populations who often have obstacles surrounding transportation, follow-up care, etc. Our research developing novel potential therapies for regenerating localized brain lesions, such as striatal degeneration in PD or cortical injury in stroke, was discussed. Fibrin-based cylindrical implants were shown to effectively recruit endogenous NPCs from their native location to the striatum and/or cortex. Further, these brain implants were successful in ameliorating motor deficits in a hemiparkinson rodent model. Lastly, we investigated nicotine's effect on $\alpha 4$ nAChR expression in dopaminergic and GABAergic neurons within the VTA following passive vapor inhalation. At present we observed a non-statistically significant increase in $\alpha 4$ nAChR expression on female dopaminergic neurons only. Suggesting sex differences in $\alpha 4$ nAChR expression and AChR functionality within the VTA and other brain regions following nicotine exposure should be further investigated. Nicotine exposure through vapor inhalation is of particular importance regarding the dramatic increase in e-cigarette use in recent years.

REFERENCES

1. Escobar I, Xu J, Jackson CW, Perez-Pinzon MA. Altered Neural Networks in the Papez Circuit: Implications for Cognitive Dysfunction after Cerebral Ischemia. *Journal of Alzheimer's disease: JAD*. 2019;67(2):425-46.
2. Baldassarre A, Ramsey L, Rengachary J, Zinn K, Siegel JS, Metcalf NV, et al. Dissociated functional connectivity profiles for motor and attention deficits in acute right-hemisphere stroke. *Brain: a journal of neurology*. 2016;139(Pt 7):2024-38.
3. Choi EB, Jang SH. Degeneration of core neural tracts for emotional regulation in a patient with traumatic brain injury: A case report. *Medicine (Baltimore)*. 2021;100(4):e24319.
4. Kaplan GB, Leite-Morris KA, Wang L, Rumbika KK, Heinrichs SC, Zeng X, et al. Pathophysiological Bases of Comorbidity: Traumatic Brain Injury and Post-Traumatic Stress Disorder. *J Neurotrauma*. 2018;35(2):210-25.
5. Wang S, Cai H, Cao Z, Li C, Wu T, Xu F, et al. More Than Just Static: Dynamic Functional Connectivity Changes of the Thalamic Nuclei to Cortex in Parkinson's Disease With Freezing of Gait. *Front Neurol*. 2021;12:735999.
6. Lane CA, Hardy J, Schott JM. Alzheimer's disease. *European journal of neurology*. 2018;25(1):59-70.
7. 2020 Alzheimer's disease facts and figures. *Alzheimer's & dementia: the journal of the Alzheimer's Association*. 2020.
8. Hebert LE, Weuve J, Scherr PA, Evans DA. Alzheimer disease in the United States (2010-2050) estimated using the 2010 census. *Neurology*. 2013;80(19):1778-83.
9. Elbaz A, Carcaillon L, Kab S, Moisan F. Epidemiology of Parkinson's disease. *Rev Neurol (Paris)*. 2016;172(1):14-26.
10. Foundation Ps. 2022 [Available from: <https://www.parkinson.org>].
11. Delamarre A, Meissner WG. Epidemiology, environmental risk factors and genetics of Parkinson's disease. *Presse Med*. 2017;46(2 Pt 1):175-81.
12. Yang Q, Tong X, Schieb L, Vaughan A, Gillespie C, Wiltz JL, et al. Vital Signs: Recent Trends in Stroke Death Rates - United States, 2000-2015. *MMWR Morb Mortal Wkly Rep*. 2017;66(35):933-9.
13. Benjamin EJ, Blaha MJ, Chiuve SE, Cushman M, Das SR, Deo R, et al. Heart Disease and Stroke Statistics-2017 Update: A Report From the American Heart Association. *Circulation*. 2017;135(10):e146-e603.
14. Iaccarino C, Carretta A, Nicolosi F, Morselli C. Epidemiology of severe traumatic brain injury. *J Neurosurg Sci*. 2018;62(5):535-41.
15. Peterson AB, Xu L, Daugherty J, Breiding MJ. Surveillance report of traumatic brain injury-related emergency department visits, hospitalizations, and deaths, United States, 2014. 2019.
16. Taylor CA, Bell JM, Breiding MJ, Xu L. Traumatic Brain Injury-Related Emergency Department Visits, Hospitalizations, and Deaths - United States, 2007 and 2013. *MMWR Surveill Summ*. 2017;66(9):1-16.

17. Capizzi A, Woo J, Verduzco-Gutierrez M. Traumatic Brain Injury: An Overview of Epidemiology, Pathophysiology, and Medical Management. *Med Clin North Am.* 2020;104(2):213-38.
18. Guzzi G, Della Torre A, Chirchiglia D, Volpentesta G, Lavano A. Critical reappraisal of DBS targeting for movement disorders. *J Neurosurg Sci.* 2016;60(2):181-8.
19. Lee DJ, Lozano CS, Dallapiazza RF, Lozano AM. Current and future directions of deep brain stimulation for neurological and psychiatric disorders. 2019;131(2):333.
20. Abosch A, Timmermann L, Bartley S, Rietkerk HG, Whiting D, Connolly PJ, et al. An international survey of deep brain stimulation procedural steps. *Stereotactic and functional neurosurgery.* 2013;91(1):1-11.
21. Winkler D, Tittgemeyer M, Schwarz J, Preul C, Strecker K, Meixensberger J. The first evaluation of brain shift during functional neurosurgery by deformation field analysis. *Journal of neurology, neurosurgery, and psychiatry.* 2005;76(8):1161-3.
22. Peng S, Levine D, Ramirez-Zamora A, Chockalingam A, Feustel PJ, Durphy J, et al. A Comparison of Unilateral Deep Brain Stimulation (DBS), Simultaneous Bilateral DBS, and Staged Bilateral DBS Lead Accuracies. *Neuromodulation: journal of the International Neuromodulation Society.* 2017;20(5):478-83.
23. Petraglia FW, 3rd, Farber SH, Han JL, Verla T, Gallis J, Likhnygina Y, et al. Comparison of Bilateral vs. Staged Unilateral Deep Brain Stimulation (DBS) in Parkinson's Disease in Patients Under 70 Years of Age. *Neuromodulation: journal of the International Neuromodulation Society.* 2016;19(1):31-7.
24. Maiti TK, Konar S, Bir S, Kalakoti P, Nanda A. Intra-operative micro-electrode recording in functional neurosurgery: Past, present, future. *Journal of clinical neuroscience : official journal of the Neurosurgical Society of Australasia.* 2016;32:166-72.
25. Brodsky MA, Anderson S, Murchison C, Seier M, Wilhelm J, Vederman A. Clinical outcomes of asleep vs awake deep brain stimulation for Parkinson disease. *Neurology.* 2017;89:1944-50.
26. Bezchlibnyk YB, Sharma VD, Naik KB, Isbaine F, Gale JT, Cheng J, et al. Clinical outcomes of globus pallidus deep brain stimulation for Parkinson disease: a comparison of intraoperative MRI- and MER-guided lead placement. *Journal of neurosurgery.* 2020:1-11.
27. Mirzadeh Z, Chapple K, Lambert M, Evidente VG, Mahant P, Ospina MC, et al. Parkinson's disease outcomes after intraoperative CT-guided "asleep" deep brain stimulation in the globus pallidus internus. *Journal of neurosurgery.* 2016;124(4):902-7.
28. Mirzadeh Z, Chen T, Chapple KM, Lambert M, Karis JP, Dhall R, et al. Procedural Variables Influencing Stereotactic Accuracy and Efficiency in Deep Brain Stimulation Surgery. *Oper Neurosurg (Hagerstown).* 2019;17(1):70-8.
29. Blasberg F, Wojtecki L, Elben S, Slotty PJ, Vesper J, Schnitzler A, et al. Comparison of Awake vs. Asleep Surgery for Subthalamic Deep Brain Stimulation in Parkinson's Disease. *Neuromodulation: journal of the International Neuromodulation Society.* 2018;21(6):541-7.
30. Chen T, Mirzadeh Z, Chapple K, Lambert M, Ponce FA. Complication rates, lengths of stay, and readmission rates in "awake" and "asleep" deep brain simulation. *Journal of neurosurgery.* 2017;127(2):360-9.

31. van Horne CG, Vaughan SW, Massari C, Bennett M, Asfahani WS, Quintero JE, et al. Streamlining deep brain stimulation surgery by reversing the staging order. *Journal of neurosurgery*. 2015;122(5):1042-7.
32. Binder DK, Rau G, Starr PA. Hemorrhagic complications of microelectrode-guided deep brain stimulation. *Stereotactic and functional neurosurgery*. 2003;80(1-4):28-31.
33. Voges J, Waerzeggers Y, Maarouf M, Lehrke R, Koulousakis A, Lenartz D, et al. Deep-brain stimulation: long-term analysis of complications caused by hardware and surgery--experiences from a single centre. *Journal of neurology, neurosurgery, and psychiatry*. 2006;77(7):868-72.
34. Seijo FJ, Alvarez-Vega MA, Gutierrez JC, Fdez-Glez F, Lozano B. Complications in subthalamic nucleus stimulation surgery for treatment of Parkinson's disease. Review of 272 procedures. *Acta Neurochir (Wien)*. 2007;149(9):867-75; discussion 76.
35. Doshi PK. Long-term surgical and hardware-related complications of deep brain stimulation. *Stereotactic and functional neurosurgery*. 2011;89(2):89-95.
36. Fenoy AJ, Simpson RK, Jr. Risks of common complications in deep brain stimulation surgery: management and avoidance. *Journal of neurosurgery*. 2014;120(1):132-9.
37. Tolleson C, Stroh J, Ehrenfeld J, Neimat J, Konrad P, Phibbs F. The factors involved in deep brain stimulation infection: a large case series. *Stereotactic and functional neurosurgery*. 2014;92(4):227-33.
38. Falowski SM, Ooi YC, Bakay RA. Long-Term Evaluation of Changes in Operative Technique and Hardware-Related Complications With Deep Brain Stimulation. *Neuromodulation: journal of the International Neuromodulation Society*. 2015;18(8):670-7.
39. Morishita T, Hilliard JD, Okun MS, Neal D, Nestor KA, Peace D, et al. Postoperative lead migration in deep brain stimulation surgery: Incidence, risk factors, and clinical impact. *PloS one*. 2017;12(9):e0183711.
40. Abode-Iyamah KO, Chiang HY, Woodroffe RW, Park B, Jareczek FJ, Nagahama Y, et al. Deep brain stimulation hardware-related infections: 10-year experience at a single institution. *Journal of neurosurgery*. 2018:1-10.
41. Kochanski RB, Bus S, Brahimaj B, Borghei A, Kraimer KL, Keppetipola KM, et al. The Impact of Microelectrode Recording on Lead Location in Deep Brain Stimulation for the Treatment of Movement Disorders. *World neurosurgery*. 2019.
42. Mostofi A, Evans JM, Partington-Smith L, Yu K, Chen C, Silverdale MA. Outcomes from deep brain stimulation targeting subthalamic nucleus and caudal zona incerta for Parkinson's disease. *NPJ Parkinsons Dis*. 2019;5:17.
43. Abboud H, Genc G, Saad S, Thompson N, Oravivattanakul S, Alsallom F, et al. Factors Associated With Postoperative Confusion and Prolonged Hospital Stay Following Deep Brain Stimulation Surgery for Parkinson Disease. *Neurosurgery*. 2019.
44. Pepper J, Zrinzo L, Mirza B, Foltynie T, Limousin P, Hariz M. The risk of hardware infection in deep brain stimulation surgery is greater at impulse generator replacement than at the primary procedure. *Stereotactic and functional neurosurgery*. 2013;91(1):56-65.

45. Dang TTH, Rowell D, Connelly LB. Cost-Effectiveness of Deep Brain Stimulation With Movement Disorders: A Systematic Review. *Movement disorders clinical practice*. 2019;6(5):348-58.
46. Centers for Medicare & Medicaid Services. Medicare Program: Hospital Inpatient Prospective Payment Systems for Acute Care Hospitals and Policy Changes and FY2020 Rates Final Rule 84 Fed. Reg. 42044–42701. . 2019.
47. Oki K, Tatarishvili J, Wood J, Koch P, Wattananit S, Mine Y, et al. Human-induced pluripotent stem cells form functional neurons and improve recovery after grafting in stroke-damaged brain. *Stem cells*. 2012;30(6):1120-33.
48. Kikuchi T, Morizane A, Doi D, Magotani H, Onoe H, Hayashi T, et al. Human iPS cell-derived dopaminergic neurons function in a primate Parkinson's disease model. *Nature*. 2017;548(7669):592-6.
49. Gonzalez R, Garitaonandia I, Poustovoitov M, Abramihina T, McEntire C, Culp B, et al. Neural Stem Cells Derived from Human Parthenogenetic Stem Cells Engraft and Promote Recovery in a Nonhuman Primate Model of Parkinson's Disease. *Cell transplantation*. 2016;25(11):1945-66.
50. Zeng X, Couture LA. Pluripotent stem cells for Parkinson's disease: progress and challenges. *Stem Cell Res Ther*. 2013;4(2):25.
51. Hermanto Y, Sunohara T, Faried A, Takagi Y, Takahashi J, Maki T, et al. Transplantation of feeder-free human induced pluripotent stem cell-derived cortical neuron progenitors in adult male Wistar rats with focal brain ischemia. *Journal of neuroscience research*. 2018;96(5):863-74.
52. Vonderwalde I, Azimi A, Rolvink G, Ahlfors JE, Shoichet MS, Morshead CM. Transplantation of Directly Reprogrammed Human Neural Precursor Cells Following Stroke Promotes Synaptogenesis and Functional Recovery. *Translational stroke research*. 2019.
53. Darsalia V, Kallur T, Kokaia Z. Survival, migration and neuronal differentiation of human fetal striatal and cortical neural stem cells grafted in stroke-damaged rat striatum. *The European journal of neuroscience*. 2007;26(3):605-14.
54. Kondziolka D, Wechsler L, Goldstein S, Meltzer C, Thulborn KR, Gebel J, et al. Transplantation of cultured human neuronal cells for patients with stroke. *Neurology*. 2000;55(4):565-9.
55. Kondziolka D, Steinberg GK, Wechsler L, Meltzer CC, Elder E, Gebel J, et al. Neurotransplantation for patients with subcortical motor stroke: a phase 2 randomized trial. *Journal of neurosurgery*. 2005;103(1):38-45.
56. Sanchez-Rojas L, Gomez-Pinedo U, Benito-Martin MS, Leon-Espinosa G, Rascon-Ramirez F, Lendinez C, et al. Biohybrids of scaffolding hyaluronic acid biomaterials plus adipose stem cells home local neural stem and endothelial cells: Implications for reconstruction of brain lesions after stroke. *Journal of biomedical materials research Part B, Applied biomaterials*. 2018.
57. Bernstock JD, Peruzzotti-Jametti L, Leonardi T, Vicario N, Ye D, Lee YJ, et al. SUMOylation promotes survival and integration of neural stem cell grafts in ischemic stroke. *EBioMedicine*. 2019.

58. Tornero D, Tsupykov O, Granmo M, Rodriguez C, Gronning-Hansen M, Thelin J, et al. Synaptic inputs from stroke-injured brain to grafted human stem cell-derived neurons activated by sensory stimuli. *Brain : a journal of neurology*. 2017;140(3):692-706.
59. Altman J, Das GD. Autoradiographic and histological evidence of postnatal hippocampal neurogenesis in rats. *The Journal of comparative neurology*. 1965;124(3):319-35.
60. Altman J. Autoradiographic and histological studies of postnatal neurogenesis. IV. Cell proliferation and migration in the anterior forebrain, with special reference to persisting neurogenesis in the olfactory bulb. *The Journal of comparative neurology*. 1969;137(4):433-57.
61. Weiss S, Reynolds BA, Vescovi AL, Morshead C, Craig CG, van der Kooy D. Is there a neural stem cell in the mammalian forebrain? *Trends Neurosci*. 1996;19(9):387-93.
62. Levison SW, Goldman JE. Both oligodendrocytes and astrocytes develop from progenitors in the subventricular zone of postnatal rat forebrain. *Neuron*. 1993;10(2):201-12.
63. Kempermann G, Kuhn HG, Gage FH. More hippocampal neurons in adult mice living in an enriched environment. *Nature*. 1997;386(6624):493-5.
64. Gould E, Beylin A, Tanapat P, Reeves A, Shors TJ. Learning enhances adult neurogenesis in the hippocampal formation. *Nat Neurosci*. 1999;2(3):260-5.
65. Shors TJ, Miesegae G, Beylin A, Zhao M, Rydel T, Gould E. Neurogenesis in the adult is involved in the formation of trace memories. *Nature*. 2001;410(6826):372-6.
66. Doetsch F, Caille I, Lim DA, Garcia-Verdugo JM, Alvarez-Buylla A. Subventricular zone astrocytes are neural stem cells in the adult mammalian brain. *Cell*. 1999;97(6):703-16.
67. Lois C, Alvarez-Buylla A. Long-distance neuronal migration in the adult mammalian brain. *Science*. 1994;264(5162):1145-8.
68. Lois C, Garcia-Verdugo JM, Alvarez-Buylla A. Chain migration of neuronal precursors. *Science*. 1996;271(5251):978-81.
69. Lois C, Alvarez-Buylla A. Proliferating subventricular zone cells in the adult mammalian forebrain can differentiate into neurons and glia. *Proceedings of the National Academy of Sciences of the United States of America*. 1993;90(5):2074-7.
70. Saha B, Peron S, Murray K, Jaber M, Gaillard A. Cortical lesion stimulates adult subventricular zone neural progenitor cell proliferation and migration to the site of injury. *Stem Cell Res*. 2013;11(3):965-77.
71. Arvidsson A, Collin T, Kirik D, Kokaia Z, Lindvall O. Neuronal replacement from endogenous precursors in the adult brain after stroke. *Nat Med*. 2002;8(9):963-70.
72. Ramaswamy S, Goings GE, Soderstrom KE, Szele FG, Kozlowski DA. Cellular proliferation and migration following a controlled cortical impact in the mouse. *Brain research*. 2005;1053(1-2):38-53.
73. Sundholm-Peters NL, Yang HK, Goings GE, Walker AS, Szele FG. Subventricular zone neuroblasts emigrate toward cortical lesions. *J Neuropathol Exp Neurol*. 2005;64(12):1089-100.
74. Faiz M, Acarin L, Villapol S, Schulz S, Castellano B, Gonzalez B. Substantial migration of SVZ cells to the cortex results in the generation of new neurons in the excitotoxically damaged immature rat brain. *Molecular and cellular neurosciences*. 2008;38(2):170-82.

75. Sun D. The potential of endogenous neurogenesis for brain repair and regeneration following traumatic brain injury. *Neural regeneration research*. 2014;9(7):688-92.
76. Yamashita T, Ninomiya M, Hernández Acosta P, García-Verdugo JM, Sunabori T, Sakaguchi M, et al. Subventricular zone-derived neuroblasts migrate and differentiate into mature neurons in the post-stroke adult striatum. *The Journal of neuroscience: the official journal of the Society for Neuroscience*. 2006;26(24):6627-36.
77. Massouh M, Saghatelyan A. De-routing neuronal precursors in the adult brain to sites of injury: role of the vasculature. *Neuropharmacology*. 2010;58(6):877-83.
78. Arsenijevic Y, Villemure JG, Brunet JF, Bloch JJ, Déglon N, Kostic C, et al. Isolation of multipotent neural precursors residing in the cortex of the adult human brain. *Exp Neurol*. 2001;170(1):48-62.
79. Campbell LJ, Levendusky JL, Steines SA, Hyde DR. Retinal regeneration requires dynamic Notch signaling. *Neural regeneration research*. 2022;17(6):1199-209.
80. Palmer TD, Ray J, Gage FH. FGF-2-responsive neuronal progenitors reside in proliferative and quiescent regions of the adult rodent brain. *Molecular and cellular neurosciences*. 1995;6(5):474-86.
81. Maya-Espinosa G, Collazo-Navarrete O, Millán-Aldaco D, Palomero-Rivero M, Guerrero-Flores G, Drucker-Colín R, et al. Mouse embryonic stem cell-derived cells reveal niches that support neuronal differentiation in the adult rat brain. *Stem cells*. 2015;33(2):491-502.
82. Lie DC, Dziewczapolski G, Willhoite AR, Kaspar BK, Shults CW, Gage FH. The adult substantia nigra contains progenitor cells with neurogenic potential. *The Journal of neuroscience : the official journal of the Society for Neuroscience*. 2002;22(15):6639-49.
83. Mourtzi T, Dimitrakopoulos D, Kakogiannis D, Salodimitris C, Botsakis K, Meri DK, et al. Characterization of substantia nigra neurogenesis in homeostasis and dopaminergic degeneration: beneficial effects of the microneurotrophin BNN-20. *Stem Cell Res Ther*. 2021;12(1):335.
84. Leal-Galicia P, Chávez-Hernández ME, Mata F, Mata-Luévanos J, Rodríguez-Serrano LM, Tapia-de-Jesús A, et al. Adult Neurogenesis: A Story Ranging from Controversial New Neurogenic Areas and Human Adult Neurogenesis to Molecular Regulation. *International journal of molecular sciences*. 2021;22(21).
85. Palmer TD, Markakis EA, Willhoite AR, Safar F, Gage FH. Fibroblast growth factor-2 activates a latent neurogenic program in neural stem cells from diverse regions of the adult CNS. *The Journal of neuroscience: the official journal of the Society for Neuroscience*. 1999;19(19):8487-97.
86. Jurkowski MP, Bettio L, E KW, Patten A, Yau SY, Gil-Mohapel J. Beyond the Hippocampus and the SVZ: Adult Neurogenesis Throughout the Brain. *Front Cell Neurosci*. 2020;14:576444.
87. Hu X, Leak RK, Shi Y, Suenaga J, Gao Y, Zheng P, et al. Microglial and macrophage polarization—new prospects for brain repair. *Nat Rev Neurol*. 2015;11(1):56-64.
88. Muir KW. Clinical trial design for stem cell therapies in stroke: What have we learned? *Neurochem Int*. 2017;106:108-13.
89. Li X, Zheng W, Bai H, Wang J, Wei R, Wen H, et al. Intravenous administration of adipose tissue-derived stem cells enhances nerve healing and promotes BDNF expression via the

- TrkB signaling in a rat stroke model. *Neuropsychiatric disease and treatment*. 2016;12:1287-93.
90. Schäbitz W-R, Steigleder T, Cooper-Kuhn CM, Schwab S, Sommer C, Schneider A, et al. Intravenous brain-derived neurotrophic factor enhances poststroke sensorimotor recovery and stimulates neurogenesis. *Stroke*. 2007;38(7):2165-72.
 91. Teramoto T, Qiu J, Plumier J-C, Moskowitz MA. EGF amplifies the replacement of parvalbumin-expressing striatal interneurons after ischemia. *The Journal of clinical investigation*. 2003;111(8):1125-32.
 92. Wang L, Zhang Z, Wang Y, Zhang R, Chopp M. Treatment of stroke with erythropoietin enhances neurogenesis and angiogenesis and improves neurological function in rats. *Stroke*. 2004;35(7):1732-7.
 93. Steinberg GK, Kondziolka D, Wechsler LR, Lunsford LD, Kim AS, Johnson JN, et al. Two-year safety and clinical outcomes in chronic ischemic stroke patients after implantation of modified bone marrow-derived mesenchymal stem cells (SB623): a phase 1/2a study. *Journal of neurosurgery*. 2018:1-11.
 94. Yoon Y, Kim HS, Jeon I, Noh JE, Park HJ, Lee S, et al. Implantation of the clinical-grade human neural stem cell line, CTX0E03, rescues the behavioral and pathological deficits in the quinolinic acid-lesioned rodent model of Huntington's disease. *Stem cells*. 2020.
 95. Kim HS, Jeon I, Noh JE, Lee H, Hong KS, Lee N, et al. Intracerebral Transplantation of BDNF-overexpressing Human Neural Stem Cells (HB1.F3.BDNF) Promotes Migration, Differentiation and Functional Recovery in a Rodent Model of Huntington's Disease. *Experimental neurobiology*. 2020;29(2):130-7.
 96. Salehi MS, Pandamooz S, Safari A, Jurek B, Tamadon A, Namavar MR, et al. Epidermal neural crest stem cell transplantation as a promising therapeutic strategy for ischemic stroke. *CNS Neurosci Ther*. 2020.
 97. Liu XL, Zhang W, Tang SJ. Intracranial transplantation of human adipose-derived stem cells promotes the expression of neurotrophic factors and nerve repair in rats of cerebral ischemia-reperfusion injury. *International journal of clinical and experimental pathology*. 2014;7(1):174-83.
 98. Clark AR, Carter AB, Hager LE, Price EM. In Vivo Neural Tissue Engineering: Cylindrical Biocompatible Hydrogels That Create New Neural Tracts in the Adult Mammalian Brain. *Stem cells and development*. 2016;25(15):1109-18.
 99. Danielyan L, Schäfer R, von Ameln-Mayerhofer A, Bernhard F, Verleysdonk S, Buadze M, et al. Therapeutic efficacy of intranasally delivered mesenchymal stem cells in a rat model of Parkinson disease. *Rejuvenation Res*. 2011;14(1):3-16.
 100. Wei N, Yu SP, Gu X, Taylor TM, Song D, Liu X-F, et al. Delayed intranasal delivery of hypoxic-preconditioned bone marrow mesenchymal stem cells enhanced cell homing and therapeutic benefits after ischemic stroke in mice. *Cell transplantation*. 2013;22(6):977-91.
 101. Benraiss A, Chmielnicki E, Lerner K, Roh D, Goldman SA. Adenoviral brain-derived neurotrophic factor induces both neostriatal and olfactory neuronal recruitment from endogenous progenitor cells in the adult forebrain. *The Journal of neuroscience: the official journal of the Society for Neuroscience*. 2001;21(17):6718-31.

102. Mokhtari T, Akbari M, Malek F, Kashani IR, Rastegar T, Noorbakhsh F, et al. Improvement of memory and learning by intracerebroventricular microinjection of T3 in rat model of ischemic brain stroke mediated by upregulation of BDNF and GDNF in CA1 hippocampal region. *Daru: journal of Faculty of Pharmacy, Tehran University of Medical Sciences*. 2017;25(1):4.
103. Dempsey RJ, Sailor KA, Bowen KK, Tureyen K, Vemuganti R. Stroke-induced progenitor cell proliferation in adult spontaneously hypertensive rat brain: effect of exogenous IGF-1 and GDNF. *Journal of neurochemistry*. 2003;87(3):586-97.
104. Kobayashi T, Ahlenius H, Thored P, Kobayashi R, Kokaia Z, Lindvall O. Intracerebral infusion of glial cell line-derived neurotrophic factor promotes striatal neurogenesis after stroke in adult rats. *Stroke*. 2006;37(9):2361-7.
105. Jin K, Sun Y, Xie L, Childs J, Mao XO, Greenberg DA. Post-ischemic administration of heparin-binding epidermal growth factor-like growth factor (HB-EGF) reduces infarct size and modifies neurogenesis after focal cerebral ischemia in the rat. *Journal of cerebral blood flow and metabolism: official journal of the International Society of Cerebral Blood Flow and Metabolism*. 2004;24(4):399-408.
106. Chen K, Henry RA, Hughes SM, Connor B. Creating a neurogenic environment: the role of BDNF and FGF2. *Molecular and cellular neurosciences*. 2007;36(1):108-20.
107. Henry RA, Hughes SM, Connor B. AAV-mediated delivery of BDNF augments neurogenesis in the normal and quinolinic acid-lesioned adult rat brain. *The European journal of neuroscience*. 2007;25(12):3513-25.
108. Lanfranconi S, Locatelli F, Corti S, Candelise L, Comi GP, Baron PL, et al. Growth factors in ischemic stroke. *Journal of cellular and molecular medicine*. 2011;15(8):1645-87.
109. Rhim T, Lee M. Targeted delivery of growth factors in ischemic stroke animal models. *Expert opinion on drug delivery*. 2016;13(5):709-23.
110. Jhaveri SJ, Hynd MR, Dowell-Mesfin N, Turner JN, Shain W, Ober CK. Release of nerve growth factor from HEMA hydrogel-coated substrates and its effect on the differentiation of neural cells. *Biomacromolecules*. 2009;10(1):174-83.
111. Fon D, Zhou K, Ercole F, Fehr F, Marchesan S, Minter MR, et al. Nanofibrous scaffolds releasing a small molecule BDNF-mimetic for the re-direction of endogenous neuroblast migration in the brain. *Biomaterials*. 2014;35(9):2692-712.
112. Gustafsson E, Andsberg G, Darsalia V, Mohapel P, Mandel RJ, Kirik D, et al. Anterograde delivery of brain-derived neurotrophic factor to striatum via nigral transduction of recombinant adeno-associated virus increases neuronal death but promotes neurogenic response following stroke. *The European journal of neuroscience*. 2003;17(12):2667-78.
113. Soma FA, Wang TY, Niclis JC, Bruggeman KF, Kauhausen JA, Guo H, et al. Peptide-Based Scaffolds Support Human Cortical Progenitor Graft Integration to Reduce Atrophy and Promote Functional Repair in a Model of Stroke. *Cell reports*. 2017;20(8):1964-77.
114. Hansen K, Müller FJ, Messing M, Zeigler F, Loring JF, Lamszus K, et al. A 3-dimensional extracellular matrix as a delivery system for the transplantation of glioma-targeting neural stem/progenitor cells. *Neuro Oncol*. 2010;12(7):645-54.
115. Zhang J, Tokatlian T, Zhong J, Ng QK, Patterson M, Lowry WE, et al. Physically associated synthetic hydrogels with long-term covalent stabilization for cell culture and stem cell transplantation. *Adv Mater*. 2011;23(43):5098-103.

116. Headen DM, Aubry G, Lu H, García AJ. Microfluidic-based generation of size-controlled, biofunctionalized synthetic polymer microgels for cell encapsulation. *Adv Mater.* 2014;26(19):3003-8.
117. Madhusudanan P, Raju G, Shankarappa S. Hydrogel systems and their role in neural tissue engineering. *J R Soc Interface.* 2020;17(162):20190505.
118. Motamed S, Del Borgo MP, Kulkarni K, Habila N, Zhou K, Perlmutter P, et al. A self-assembling β -peptide hydrogel for neural tissue engineering. *Soft Matter.* 2016;12(8):2243-6.
119. Motalleb R, Berns EJ, Patel P, Gold J, Stupp SI, Kuhn HG. In vivo migration of endogenous brain progenitor cells guided by an injectable peptide amphiphile biomaterial. *J Tissue Eng Regen Med.* 2018;12(4):e2123-e33.
120. Jin K, Mao X, Xie L, Galvan V, Lai B, Wang Y, et al. Transplantation of human neural precursor cells in Matrigel scaffolding improves outcome from focal cerebral ischemia after delayed postischemic treatment in rats. *Journal of cerebral blood flow and metabolism: official journal of the International Society of Cerebral Blood Flow and Metabolism.* 2010;30(3):534-44.
121. Centola M, Abbruzzese F, Scotti C, Barbero A, Vadalà G, Denaro V, et al. Scaffold-based delivery of a clinically relevant anti-angiogenic drug promotes the formation of in vivo stable cartilage. *Tissue Eng Part A.* 2013;19(17-18):1960-71.
122. Parajó Y, D'Angelo I, Welle A, Garcia-Fuentes M, Alonso MJ. Hyaluronic acid/Chitosan nanoparticles as delivery vehicles for VEGF and PDGF-BB. *Drug Deliv.* 2010;17(8):596-604.
123. Havenith S, Versnel H, Agterberg MJ, de Groot JC, Sedee RJ, Grolman W, et al. Spiral ganglion cell survival after round window membrane application of brain-derived neurotrophic factor using gelfoam as carrier. *Hear Res.* 2011;272(1-2):168-77.
124. Fon D, Al-Abboodi A, Chan PPY, Zhou K, Crack P, Finkelstein DI, et al. Effects of GDNF-loaded injectable gelatin-based hydrogels on endogenous neural progenitor cell migration. *Adv Healthc Mater.* 2014;3(5):761-74.
125. Nisbet DR, Crompton KE, Horne MK, Finkelstein DI, Forsythe JS. Neural tissue engineering of the CNS using hydrogels. *Journal of biomedical materials research Part B, Applied biomaterials.* 2008;87(1):251-63.
126. Yasuda H, Kuroda S, Shichinohe H, Kamei S, Kawamura R, Iwasaki Y. Effect of biodegradable fibrin scaffold on survival, migration, and differentiation of transplanted bone marrow stromal cells after cortical injury in rats. *Journal of neurosurgery.* 2010;112(2):336-44.
127. Terasaka S, Iwasaki Y, Shinya N, Uchida T. Fibrin glue and polyglycolic acid nonwoven fabric as a biocompatible dural substitute. *Neurosurgery.* 2006;58:134-9.
128. Zuidema JM, Rivet CJ, Gilbert RJ, Morrison FA. A protocol for rheological characterization of hydrogels for tissue engineering strategies. *Journal of biomedical materials research Part B, Applied biomaterials.* 2014;102(5):1063-73.
129. Sproul EP, Hannan RT, Brown AC. Controlling Fibrin Network Morphology, Polymerization, and Degradation Dynamics in Fibrin Gels for Promoting Tissue Repair. *Methods in molecular biology.* 2018;1758:85-99.

130. Roura S, Gálvez-Montón C, Bayes-Genis A. Fibrin, the preferred scaffold for cell transplantation after myocardial infarction? An old molecule with a new life. *J Tissue Eng Regen Med.* 2017;11(8):2304-13.
131. Chalmers RT, Darling Iii RC, Wingard JT, Chetter I, Cutler B, Kern JA, et al. Randomized clinical trial of tranexamic acid-free fibrin sealant during vascular surgical procedures. *Br J Surg.* 2010;97(12):1784-9.
132. Dhillon S. Fibrin sealant (evicel® [quixil®/crosseal™]): a review of its use as supportive treatment for haemostasis in surgery. *Drugs.* 2011;71(14):1893-915.
133. Hoyt AT, LaViolette PS, Lew SM. Fibrin sealant to prevent subdural electrode migration during intracranial electroencephalographic monitoring in a patient with a large arachnoid cyst. *J Neurosurg Pediatr.* 2014;14(1):115-9.
134. Theys T, Van Hoylandt A, Broeckx CE, Van Gerven L, Jonkergouw J, Quirynen M, et al. Plasma-rich fibrin in neurosurgery: a feasibility study. *Acta Neurochir.* 2018;160(8):1497-503.
135. Nakayama N, Yano H, Egashira Y, Enomoto Y, Ohe N, Kanemura N, et al. Efficacy, Reliability, and Safety of Completely Autologous Fibrin Glue in Neurosurgical Procedures: Single-Center Retrospective Large-Number Case Study. *World neurosurgery.* 2018;109:e819-e28.
136. Faber-Elman A, Miskin R, Schwartz M. Components of the plasminogen activator system in astrocytes are modulated by tumor necrosis factor-alpha and interleukin-1 beta through similar signal transduction pathways. *Journal of neurochemistry.* 1995;65(4):1524-35.
137. Le DM, Besson A, Fogg DK, Choi KS, Waisman DM, Goodyer CG, et al. Exploitation of astrocytes by glioma cells to facilitate invasiveness: a mechanism involving matrix metalloproteinase-2 and the urokinase-type plasminogen activator-plasmin cascade. *The Journal of neuroscience: the official journal of the Society for Neuroscience.* 2003;23(10):4034-43.
138. Lo EH, Broderick JP, Moskowitz MA. tPA and proteolysis in the neurovascular unit. *Stroke.* 2004;35(2):354-6.
139. Sun CY, Hu Y, Wang HF, He WJ, Wang YD, Wu T. Brain-derived neurotrophic factor inducing angiogenesis through modulation of matrix-degrading proteases. *Chin Med J (Engl).* 2006;119(7):589-95.
140. Ethell IM, Ethell DW. Matrix metalloproteinases in brain development and remodeling: synaptic functions and targets. *Journal of neuroscience research.* 2007;85(13):2813-23.
141. Gueye Y, Ferhat L, Sbai O, Bianco J, Ould-Yahoui A, Bernard A, et al. Trafficking and secretion of matrix metalloproteinase-2 in olfactory ensheathing glial cells: A role in cell migration? *Glia.* 2011;59(5):750-70.
142. Jeon H, Kim JH, Kim JH, Lee WH, Lee MS, Suk K. Plasminogen activator inhibitor type 1 regulates microglial motility and phagocytic activity. *J Neuroinflammation.* 2012;9:149.
143. Wood MD, MacEwan MR, French AR, Moore AM, Hunter DA, Mackinnon SE, et al. Fibrin matrices with affinity-based delivery systems and neurotrophic factors promote functional nerve regeneration. *Biotechnol Bioeng.* 2010;106(6):970-9.

144. Reichel CA, Lerchenberger M, Uhl B, Rehberg M, Berberich N, Zahler S, et al. Plasmin inhibitors prevent leukocyte accumulation and remodeling events in the postischemic microvasculature. *PloS one*. 2011;6(2):e17229.
145. Lu Z, Korotcova L, Murata A, Ishibashi N, Jonas RA. Aprotinin, but not ϵ -aminocaproic acid and tranexamic acid, exerts neuroprotection against excitotoxic injury in an in vitro neuronal cell culture model. *J Thorac Cardiovasc Surg*. 2014;147(6):1939-45.
146. Thomson KS, Dupras SK, Murry CE, Scatena M, Regnier M. Proangiogenic microtemplated fibrin scaffolds containing aprotinin promote improved wound healing responses. *Angiogenesis*. 2014;17(1):195-205.
147. Hultman K, Cortes-Canteli M, Bounoutas A, Richards AT, Strickland S, Norris EH. Plasmin deficiency leads to fibrin accumulation and a compromised inflammatory response in the mouse brain. *Journal of thrombosis and haemostasis: JTH*. 2014;12(5):701-12.
148. Collen A, Hanemaaijer R, Lupu F, Quax PH, van Lent N, Grimbergen J, et al. Membrane-type matrix metalloproteinase-mediated angiogenesis in a fibrin-collagen matrix. *Blood*. 2003;101(5):1810-7.
149. Willerth SM, Arendas KJ, Gottlieb DI, Sakiyama-Elbert SE. Optimization of fibrin scaffolds for differentiation of murine embryonic stem cells into neural lineage cells. *Biomaterials*. 2006;27(36):5990-6003.
150. Lorentz KM, Kontos S, Frey P, Hubbell JA. Engineered aprotinin for improved stability of fibrin biomaterials. *Biomaterials*. 2011;32(2):430-8.
151. Hyatt AJ, Wang D, van Oterendorp C, Fawcett JW, Martin KR. Mesenchymal stromal cells integrate and form longitudinally-aligned layers when delivered to injured spinal cord via a novel fibrin scaffold. *Neuroscience letters*. 2014;569(100):12-7.
152. Sacchi V, Mittermayr R, Hartinger J, Martino MM, Lorentz KM, Wolbank S, et al. Long-lasting fibrin matrices ensure stable and functional angiogenesis by highly tunable, sustained delivery of recombinant VEGF164. *Proceedings of the National Academy of Sciences of the United States of America*. 2014;111(19):6952-7.
153. Smith JD, Chen A, Ernst LA, Waggoner AS, Campbell PG. Immobilization of aprotinin to fibrinogen as a novel method for controlling degradation of fibrin gels. *Bioconjugate chemistry*. 2007;18(3):695-701.
154. Wachs FP, Couillard-Despres S, Engelhardt M, Wilhelm D, Ploetz S, Vroemen M, et al. High efficacy of clonal growth and expansion of adult neural stem cells. *Lab Invest*. 2003;83(7):949-62.
155. Yang B, Treweek JB, Kulkarni RP, Deverman BE, Chen CK, Lubeck E, et al. Single-cell phenotyping within transparent intact tissue through whole-body clearing. *Cell*. 2014;158(4):945-58.
156. Epp JR, Niibori Y, Liz Hsiang HL, Mercaldo V, Deisseroth K, Josselyn SA, et al. Optimization of CLARITY for Clearing Whole-Brain and Other Intact Organs. *eNeuro*. 2015;2(3).
157. Buchta C, Hedrich HC, Macher M, Höcker P, Redl H. Biochemical characterization of autologous fibrin sealants produced by CryoSeal and Vivostat in comparison to the homologous fibrin sealant product Tissucol/Tisseel. *Biomaterials*. 2005;26(31):6233-41.

158. Georges PC, Miller WJ, Meaney DF, Sawyer ES, Janmey PA. Matrices with compliance comparable to that of brain tissue select neuronal over glial growth in mixed cortical cultures. *Biophys J*. 2006;90(8):3012-8.
159. Mooney R, Tawil B, Mahoney M. Specific fibrinogen and thrombin concentrations promote neuronal rather than glial growth when primary neural cells are seeded within plasma-derived fibrin gels. *Tissue Eng Part A*. 2010;16(5):1607-19.
160. Motz CT, Kabat V, Saxena T, Bellamkonda RV, Zhu C. Neuromechanobiology: An Expanding Field Driven by the Force of Greater Focus. *Adv Healthc Mater*. 2021;10(19):e2100102.
161. Uibo R, Laidmäe I, Sawyer ES, Flanagan LA, Georges PC, Winer JP, et al. Soft materials to treat central nervous system injuries: evaluation of the suitability of non-mammalian fibrin gels. *Biochim Biophys Acta*. 2009;1793(5):924-30.
162. Sashindranath M, Sales E, Daglas M, Freeman R, Samson AL, Cops EJ, et al. The tissue-type plasminogen activator-plasminogen activator inhibitor 1 complex promotes neurovascular injury in brain trauma: evidence from mice and humans. *Brain: a journal of neurology*. 2012;135(Pt 11):3251-64.
163. Mattson G, Conklin E, Desai S, Nielander G, Savage MD, Morgensen S. A practical approach to crosslinking. *Mol Biol Rep*. 1993;17(3):167-83.
164. Kang X, Xu H, Teng S, Zhang X, Deng Z, Zhou L, et al. Dopamine release from transplanted neural stem cells in Parkinsonian rat striatum in vivo. *Proceedings of the National Academy of Sciences of the United States of America*. 2014;111(44):15804-9.
165. Fricker RA, Carpenter MK, Winkler C, Greco C, Gates MA, Björklund A. Site-specific migration and neuronal differentiation of human neural progenitor cells after transplantation in the adult rat brain. *The Journal of neuroscience: the official journal of the Society for Neuroscience*. 1999;19(14):5990-6005.
166. Lepski G, Jannes CE, Strauss B, Marie SK, Nikkhah G. Survival and neuronal differentiation of mesenchymal stem cells transplanted into the rodent brain are dependent upon microenvironment. *Tissue Eng Part A*. 2010;16(9):2769-82.
167. Studer L, Tabar V, McKay RD. Transplantation of expanded mesencephalic precursors leads to recovery in parkinsonian rats. *Nat Neurosci*. 1998;1(4):290-5.
168. Hwang DY, Kim DS, Kim DW. Human ES and iPS cells as cell sources for the treatment of Parkinson's disease: current state and problems. *J Cell Biochem*. 2010;109(2):292-301.
169. Li JY, Christophersen NS, Hall V, Soulet D, Brundin P. Critical issues of clinical human embryonic stem cell therapy for brain repair. *Trends Neurosci*. 2008;31(3):146-53.
170. Master Z, McLeod M, Mendez I. Benefits, risks and ethical considerations in translation of stem cell research to clinical applications in Parkinson's disease. *J Med Ethics*. 2007;33(3):169-73.
171. Belvindrah R, Lazarini F, Lledo PM. Postnatal neurogenesis: from neuroblast migration to neuronal integration. *Rev Neurosci*. 2009;20(5-6):331-46.
172. Farioli-Vecchioli S, Mattera A, Micheli L, Ceccarelli M, Leonardi L, Saraulli D, et al. Running rescues defective adult neurogenesis by shortening the length of the cell cycle of neural stem and progenitor cells. *Stem cells*. 2014;32(7):1968-82.
173. Zhang R, Zhang Z, Zhang C, Zhang L, Robin A, Wang Y, et al. Stroke transiently increases subventricular zone cell division from asymmetric to symmetric and increases neuronal

- differentiation in the adult rat. *The Journal of neuroscience : the official journal of the Society for Neuroscience*. 2004;24(25):5810-5.
174. Darsalia V, Heldmann U, Lindvall O, Kokaia Z. Stroke-induced neurogenesis in aged brain. *Stroke*. 2005;36(8):1790-5.
 175. Zhang RL, Chopp M, Roberts C, Liu X, Wei M, Nejad-Davarani SP, et al. Stroke increases neural stem cells and angiogenesis in the neurogenic niche of the adult mouse. *PLoS one*. 2014;9(12):e113972.
 176. Chirumamilla S, Sun D, Bullock MR, Colello RJ. Traumatic brain injury induced cell proliferation in the adult mammalian central nervous system. *J Neurotrauma*. 2002;19(6):693-703.
 177. Kernie SG, Parent JM. Forebrain neurogenesis after focal Ischemic and traumatic brain injury. *Neurobiology of disease*. 2010;37(2):267-74.
 178. Fabel K, Kempermann G. Physical activity and the regulation of neurogenesis in the adult and aging brain. *Neuromolecular Med*. 2008;10(2):59-66.
 179. Kempermann G. Seven principles in the regulation of adult neurogenesis. *The European journal of neuroscience*. 2011;33(6):1018-24.
 180. Pathania M, Yan LD, Bordey A. A symphony of signals conducts early and late stages of adult neurogenesis. *Neuropharmacology*. 2010;58(6):865-76.
 181. Ming GL, Song H. Adult neurogenesis in the mammalian brain: significant answers and significant questions. *Neuron*. 2011;70(4):687-702.
 182. Mu Y, Lee SW, Gage FH. Signaling in adult neurogenesis. *Curr Opin Neurobiol*. 2010;20(4):416-23.
 183. Shimada E, Matsumura G. Viscosity and molecular weight of hyaluronic acids. *J Biochem*. 1975;78(3):513-7.
 184. Conway A, Schaffer DV. Biomaterial microenvironments to support the generation of new neurons in the adult brain. *Stem cells*. 2014;32(5):1220-9.
 185. Chen J, Zacharek A, Zhang C, Jiang H, Li Y, Roberts C, et al. Endothelial nitric oxide synthase regulates brain-derived neurotrophic factor expression and neurogenesis after stroke in mice. *The Journal of neuroscience: the official journal of the Society for Neuroscience*. 2005;25(9):2366-75.
 186. Udo H, Yoshida Y, Kino T, Ohnuki K, Mizunoya W, Mukuda T, et al. Enhanced adult neurogenesis and angiogenesis and altered affective behaviors in mice overexpressing vascular endothelial growth factor 120. *The Journal of neuroscience: the official journal of the Society for Neuroscience*. 2008;28(53):14522-36.
 187. Lee HJ, Kim KS, Park IH, Kim SU. Human neural stem cells over-expressing VEGF provide neuroprotection, angiogenesis and functional recovery in mouse stroke model. *PLoS one*. 2007;2(1):e156.
 188. Ohab JJ, Fleming S, Blesch A, Carmichael ST. A neurovascular niche for neurogenesis after stroke. *The Journal of neuroscience: the official journal of the Society for Neuroscience*. 2006;26(50):13007-16.
 189. Bektas H, Nadalin S, Szabo I, Ploder B, Sharkhawy M, Schmidt J. Hemostatic efficacy of latest-generation fibrin sealant after hepatic resection: a randomized controlled clinical study. *Langenbecks Arch Surg*. 2014;399(7):837-47.

190. Moore AM, Wood MD, Chenard K, Hunter DA, Mackinnon SE, Sakiyama-Elbert SE, et al. Controlled delivery of glial cell line-derived neurotrophic factor enhances motor nerve regeneration. *J Hand Surg Am.* 2010;35(12):2008-17.
191. Johnson PJ, Parker SR, Sakiyama-Elbert SE. Fibrin-based tissue engineering scaffolds enhance neural fiber sprouting and delay the accumulation of reactive astrocytes at the lesion in a subacute model of spinal cord injury. *J Biomed Mater Res A.* 2010;92(1):152-63.
192. McCreedy DA, Wilems TS, Xu H, Butts JC, Brown CR, Smith AW, et al. Survival, Differentiation, and Migration of High-Purity Mouse Embryonic Stem Cell-derived Progenitor Motor Neurons in Fibrin Scaffolds after Sub-Acute Spinal Cord Injury. *Biomater Sci.* 2014;2(11):1672-82.
193. Sakiyama SE, Schense JC, Hubbell JA. Incorporation of heparin-binding peptides into fibrin gels enhances neurite extension: an example of designer matrices in tissue engineering. *Faseb j.* 1999;13(15):2214-24.
194. Lu P, Woodruff G, Wang Y, Graham L, Hunt M, Wu D, et al. Long-distance axonal growth from human induced pluripotent stem cells after spinal cord injury. *Neuron.* 2014;83(4):789-96.
195. Lu P, Wang Y, Graham L, McHale K, Gao M, Wu D, et al. Long-distance growth and connectivity of neural stem cells after severe spinal cord injury. *Cell.* 2012;150(6):1264-73.
196. Cierniewski CS, Budzynski AZ. Localization of the cross-linking site of GPRVVERHK in the gamma-chain of human fibrinogen. *Eur J Biochem.* 1993;218(2):321-5.
197. Panda D, Kundu GC, Lee BI, Peri A, Fohl D, Chackalaparampil I, et al. Potential roles of osteopontin and alphaVbeta3 integrin in the development of coronary artery restenosis after angioplasty. *Proceedings of the National Academy of Sciences of the United States of America.* 1997;94(17):9308-13.
198. McKenna KA, Hinds MT, Sarao RC, Wu PC, Maslen CL, Glanville RW, et al. Mechanical property characterization of electrospun recombinant human tropoelastin for vascular graft biomaterials. *Acta Biomater.* 2012;8(1):225-33.
199. Yaqoob M, Snell CR. Purification and characterisation of B2 bradykinin receptor from rat uterus. *Journal of neurochemistry.* 1994;62(1):17-26.
200. Mädler S, Seitz M, Robinson J, Zenobi R. Does chemical cross-linking with NHS esters reflect the chemical equilibrium of protein-protein noncovalent interactions in solution? *J Am Soc Mass Spectrom.* 2010;21(10):1775-83.
201. C PGaW. *The Rat Brain in Stereotaxic Coordinates.* San Diego, CA: Academic Press; 1998.
202. Brahmachari S, Fung YK, Pahan K. Induction of glial fibrillary acidic protein expression in astrocytes by nitric oxide. *The Journal of neuroscience: the official journal of the Society for Neuroscience.* 2006;26(18):4930-9.
203. Wolff EF, Gao XB, Yao KV, Andrews ZB, Du H, Elsworth JD, et al. Endometrial stem cell transplantation restores dopamine production in a Parkinson's disease model. *Journal of cellular and molecular medicine.* 2011;15(4):747-55.
204. Goffin D, Ali AB, Rampersaud N, Harkavyi A, Fuchs C, Whitton PS, et al. Dopamine-dependent tuning of striatal inhibitory synaptogenesis. *The Journal of neuroscience: the official journal of the Society for Neuroscience.* 2010;30(8):2935-50.

205. Ivkovic S, Canoll P, Goldman JE. Constitutive EGFR signaling in oligodendrocyte progenitors leads to diffuse hyperplasia in postnatal white matter. *The Journal of neuroscience: the official journal of the Society for Neuroscience*. 2008;28(4):914-22.
206. Aumann T, Horne M. Activity-dependent regulation of the dopamine phenotype in substantia nigra neurons. *Journal of neurochemistry*. 2012;121(4):497-515.
207. Porcheri C, Suter U, Jessberger S. Dissecting integrin-dependent regulation of neural stem cell proliferation in the adult brain. *The Journal of neuroscience: the official journal of the Society for Neuroscience*. 2014;34(15):5222-32.
208. Kohwi M, Doe CQ. Temporal fate specification and neural progenitor competence during development. *Nature reviews Neuroscience*. 2013;14(12):823-38.
209. Andressen C. Neural stem cells: from neurobiology to clinical applications. *Curr Pharm Biotechnol*. 2013;14(1):20-8.
210. Li T, Pan YW, Wang W, Abel G, Zou J, Xu L, et al. Targeted deletion of the ERK5 MAP kinase impairs neuronal differentiation, migration, and survival during adult neurogenesis in the olfactory bulb. *PLoS one*. 2013;8(4):e61948.
211. Onorati M, Castiglioni V, Biasci D, Cesana E, Menon R, Vuono R, et al. Molecular and functional definition of the developing human striatum. *Nat Neurosci*. 2014;17(12):1804-15.
212. Jiao Q, Xie WL, Wang YY, Chen XL, Yang PB, Zhang PB, et al. Spatial relationship between NSCs/NPCs and microvessels in rat brain along prenatal and postnatal development. *Int J Dev Neurosci*. 2013;31(4):280-5.
213. Ma KG, Qian YH. Alpha 7 nicotinic acetylcholine receptor and its effects on Alzheimer's disease. *Neuropeptides*. 2019;73:96-106.
214. McKinsey GL, Lindtner S, Trzcinski B, Visel A, Pennacchio LA, Huylebroeck D, et al. Dlx1&2-dependent expression of Zfhx1b (Sip1, Zeb2) regulates the fate switch between cortical and striatal interneurons. *Neuron*. 2013;77(1):83-98.
215. Bhang SH, Lee YE, Cho SW, Shim JW, Lee SH, Choi CY, et al. Basic fibroblast growth factor promotes bone marrow stromal cell transplantation-mediated neural regeneration in traumatic brain injury. *Biochem Biophys Res Commun*. 2007;359(1):40-5.
216. Chen SJ, Chang CM, Tsai SK, Chang YL, Chou SJ, Huang SS, et al. Functional improvement of focal cerebral ischemia injury by subdural transplantation of induced pluripotent stem cells with fibrin glue. *Stem cells and development*. 2010;19(11):1757-67.
217. Aloe L, Rocco ML, Bianchi P, Manni L. Nerve growth factor: from the early discoveries to the potential clinical use. *J Transl Med*. 2012;10:239.
218. Wang HB, Yang L, Wu J, Sun L, Wu J, Tian H, et al. Reduced ischemic injury after stroke in mice by angiogenic gene delivery via ultrasound-targeted microbubble destruction. *J Neuropathol Exp Neurol*. 2014;73(6):548-58.
219. Giacca M, Zacchigna S. VEGF gene therapy: therapeutic angiogenesis in the clinic and beyond. *Gene Ther*. 2012;19(6):622-9.
220. National Center for Chronic Disease Prevention and Health Promotion DfHDaSP. Stroke [Available from: <https://www.cdc.gov/stroke/index.htm>].
221. Ekundayo OJ, Saver JL, Fonarow GC, Schwamm LH, Xian Y, Zhao X, et al. Patterns of Emergency Medical Services Use and Its Association With Timely Stroke Treatment. *Circulation: Cardiovascular Quality and Outcomes*. 2013;6(3):262-9.

222. Hasan TF, Hasan H, Kelley RE. Overview of Acute Ischemic Stroke Evaluation and Management. *Biomedicines*. 2021;9(10).
223. O'Donnell JC, Katiyar KS, Panzer KV, Cullen DK. A tissue-engineered rostral migratory stream for directed neuronal replacement. *Neural regeneration research*. 2018;13(8):1327-31.
224. Gengatharan A, Bammann RR, Saghatelian A. The Role of Astrocytes in the Generation, Migration, and Integration of New Neurons in the Adult Olfactory Bulb. *Frontiers in neuroscience*. 2016;10:149-.
225. Katiyar KS, Winter CC, Gordián-Vélez WJ, O'Donnell JC, Song YJ, Hernandez NS, et al. Three-dimensional Tissue Engineered Aligned Astrocyte Networks to Recapitulate Developmental Mechanisms and Facilitate Nervous System Regeneration. *Journal of visualized experiments: JoVE*. 2018(131):55848.
226. Purvis EM, O'Donnell JC, Chen HI, Cullen DK. Tissue Engineering and Biomaterial Strategies to Elicit Endogenous Neuronal Replacement in the Brain. *Front Neurol*. 2020;11:344.
227. Salic A, Mitchison TJ. A chemical method for fast and sensitive detection of DNA synthesis in vivo. *Proceedings of the National Academy of Sciences of the United States of America*. 2008;105(7):2415-20.
228. Borlongan CV, Fournier C, Stahl CE, Yu G, Xu L, Matsukawa N, et al. Gene therapy, cell transplantation and stroke. *Frontiers in bioscience : a journal and virtual library*. 2006;11:1090-101.
229. Hara K, Yasuhara T, Maki M, Matsukawa N, Masuda T, Yu SJ, et al. Neural progenitor NT2N cell lines from teratocarcinoma for transplantation therapy in stroke. *Progress in neurobiology*. 2008;85(3):318-34.
230. Wu KJ, Yu S, Lee JY, Hoffer B, Wang Y. Improving Neurorepair in Stroke Brain Through Endogenous Neurogenesis-Enhancing Drugs. *Cell transplantation*. 2017;26(9):1596-600.
231. Koh S-H, Park H-H. Neurogenesis in Stroke Recovery. *Translational stroke research*. 2017;8(1):3-13.
232. Zhao L-R, Willing A. Enhancing endogenous capacity to repair a stroke-damaged brain: An evolving field for stroke research. *Progress in neurobiology*. 2018;163-164:5-26.
233. Lu J, Manaenko A, Hu Q. Targeting Adult Neurogenesis for Poststroke Therapy. *Stem Cells Int*. 2017;2017:5868632.
234. Fon D, Al-Abboodi A, Chan PP, Zhou K, Crack P, Finkelstein DI, et al. Effects of GDNF-loaded injectable gelatin-based hydrogels on endogenous neural progenitor cell migration. *Adv Healthc Mater*. 2014;3(5):761-74.
235. Kalladka D, Sinden J, Pollock K, Haig C, McLean J, Smith W, et al. Human neural stem cells in patients with chronic ischaemic stroke (PISCES): a phase 1, first-in-man study. *Lancet*. 2016;388(10046):787-96.
236. Chrostek MR, Fellows EG, Crane AT, Grande AW, Low WC. Efficacy of stem cell-based therapies for stroke. *Brain research*. 2019;1722:146362.
237. Pencea V, Bingaman KD, Wiegand SJ, Luskin MB. Infusion of brain-derived neurotrophic factor into the lateral ventricle of the adult rat leads to new neurons in the parenchyma of the striatum, septum, thalamus, and hypothalamus. *The Journal of neuroscience: the official journal of the Society for Neuroscience*. 2001;21(17):6706-17.

238. Ohab JJ, Carmichael ST. Poststroke neurogenesis: emerging principles of migration and localization of immature neurons. *The Neuroscientist: a review journal bringing neurobiology, neurology and psychiatry*. 2008;14(4):369-80.
239. Kaneko N, Sawada M, Sawamoto K. Mechanisms of neuronal migration in the adult brain. *Journal of neurochemistry*. 2017;141(6):835-47.
240. Fujioka T, Kaneko N, Sawamoto K. Blood vessels as a scaffold for neuronal migration. *Neurochemistry international*. 2019;126:69-73.
241. Yang L, Tucker D, Dong Y, Wu C, Lu Y, Li Y, et al. Photobiomodulation therapy promotes neurogenesis by improving post-stroke local microenvironment and stimulating neuroprogenitor cells. *Exp Neurol*. 2018;299(Pt A):86-96.
242. Zhou K, Motamed S, Thouas GA, Bernard CC, Li D, Parkington HC, et al. Graphene Functionalized Scaffolds Reduce the Inflammatory Response and Supports Endogenous Neuroblast Migration when Implanted in the Adult Brain. *PLoS one*. 2016;11(3):e0151589-e.
243. Motamed S, Del Borgo MP, Zhou K, Kulkarni K, Crack PJ, Merson TD, et al. Migration and Differentiation of Neural Stem Cells Diverted From the Subventricular Zone by an Injectable Self-Assembling β -Peptide Hydrogel. *Front Bioeng Biotechnol*. 2019;7:315-.
244. Kaneko N, Sawada M, Sawamoto K. Mechanisms of neuronal migration in the adult brain. *Journal of neurochemistry*. 2017;141(6):835-47.
245. Lacar B, Young SZ, Platel JC, Bordey A. Imaging and recording subventricular zone progenitor cells in live tissue of postnatal mice. *Frontiers in neuroscience*. 2010;4.
246. Bono F, Mutti V, Fiorentini C, Missale C. Dopamine D3 Receptor Heteromerization: Implications for Neuroplasticity and Neuroprotection. *Biomolecules*. 2020;10(7).
247. Alkadhi KA. Neuroprotective Effects of Nicotine on Hippocampal Long-Term Potentiation in Brain Disorders. *J Pharmacol Exp Ther*. 2018;366(3):498-508.
248. Kume T, Takada-Takatori Y. Nicotinic Acetylcholine Receptor Signaling: Roles in Neuroprotection. In: Akaike A, Shimohama S, Misu Y, editors. *Nicotinic Acetylcholine Receptor Signaling in Neuroprotection*. Singapore: Springer Copyright 2018, The Author(s). 2018. p. 59-71.
249. Ascherio A, Schwarzschild MA. The epidemiology of Parkinson's disease: risk factors and prevention. *The Lancet Neurology*. 2016;15(12):1257-72.
250. Pimentel E, Sivalingam K, Doke M, Samikkannu T. Effects of Drugs of Abuse on the Blood-Brain Barrier: A Brief Overview. *Frontiers in neuroscience*. 2020;14:513.
251. Ruskiewicz JA, Zhang Z, Gonçalves FM, Tizabi Y, Zelikoff JT, Aschner M. Neurotoxicity of e-cigarettes. *Food Chem Toxicol*. 2020;138:111245.
252. Lim DA, Alvarez-Buylla A. The Adult Ventricular-Subventricular Zone (V-SVZ) and Olfactory Bulb (OB) Neurogenesis. *Cold Spring Harbor perspectives in biology*. 2016;8(5).
253. Valentine G, Sofuoglu M. Cognitive Effects of Nicotine: Recent Progress. *Curr Neuropharmacol*. 2018;16(4):403-14.
254. Sutton SK, Van Rensburg KJ, Jentink KG, Drobles DJ, Evans DE. Nicotine-induced cortical activation among nonsmokers with moderation by trait cognitive control. *Psychopharmacology*. 2016;233(12):2301-8.
255. Warburton DM, Rusted JM. Cholinergic control of cognitive resources. *Neuropsychobiology*. 1993;28(1-2):43-6.

256. Hahn B, Stolerman IP. Nicotine-induced attentional enhancement in rats: effects of chronic exposure to nicotine. *Neuropsychopharmacology : official publication of the American College of Neuropsychopharmacology*. 2002;27(5):712-22.
257. Gandelman JA, Kang H, Antal A, Albert K, Boyd BD, Conley AC, et al. Transdermal Nicotine for the Treatment of Mood and Cognitive Symptoms in Nonsmokers With Late-Life Depression. *J Clin Psychiatry*. 2018;79(5).
258. Cooper C, Li R, Lyketsos C, Livingston G. Treatment for mild cognitive impairment: systematic review. *Br J Psychiatry*. 2013;203(3):255-64.
259. Quik M, Perez XA, Bordia T. Nicotine as a potential neuroprotective agent for Parkinson's disease. *Movement disorders: official journal of the Movement Disorder Society*. 2012;27(8):947-57.
260. Gao J, Adam BL, Terry AV, Jr. Evaluation of nicotine and cotinine analogs as potential neuroprotective agents for Alzheimer's disease. *Bioorg Med Chem Lett*. 2014;24(6):1472-8.
261. Majdi A, Kamari F, Vafaei MS, Sadigh-Eteghad S. Revisiting nicotine's role in the ageing brain and cognitive impairment. *Rev Neurosci*. 2017;28(7):767-81.
262. Wei P, Zheng Q, Liu H, Wan T, Zhou J, Li D, et al. Nicotine-Induced Neuroprotection against Cognitive Dysfunction after Partial Hepatectomy Involves Activation of BDNF/TrkB Signaling Pathway and Inhibition of NF-kappaB Signaling Pathway in Aged Rats. *Nicotine Tob Res*. 2018;20(4):515-22.
263. Takarada T, Nakamichi N, Kawagoe H, Ogura M, Fukumori R, Nakazato R, et al. Possible neuroprotective property of nicotinic acetylcholine receptors in association with predominant upregulation of glial cell line-derived neurotrophic factor in astrocytes. *J Neurosci Res*. 2012;90(11):2074-85.
264. Lockman PR, Van der Schyf CJ, Abbruscato TJ, Allen DD. Chronic nicotine exposure alters blood-brain barrier permeability and diminishes brain uptake of methyllycaconitine. *Journal of neurochemistry*. 2005;94(1):37-44.
265. Sajja RK, Rahman S, Cucullo L. Drugs of abuse and blood-brain barrier endothelial dysfunction: A focus on the role of oxidative stress. *Journal of cerebral blood flow and metabolism: official journal of the International Society of Cerebral Blood Flow and Metabolism*. 2016;36(3):539-54.
266. Jiang DQ, Wei MD, Wang KW, Lan YX, Zhu N, Wang Y. Nicotine contributes to the neural stem cells fate against toxicity of microglial-derived factors induced by Abeta via the Wnt/beta-catenin pathway. *Int J Neurosci*. 2016;126(3):257-68.
267. Campos MW, Serebrisky D, Castaldelli-Maia JM. Smoking and Cognition. *Curr Drug Abuse Rev*. 2016;9(2):76-9.
268. Leventhal AM, Waters AJ, Boyd S, Moolchan ET, Lerman C, Pickworth WB. Gender differences in acute tobacco withdrawal: effects on subjective, cognitive, and physiological measures. *Exp Clin Psychopharmacol*. 2007;15(1):21-36.
269. Heishman SJ, Kleykamp BA, Singleton EG. Meta-analysis of the acute effects of nicotine and smoking on human performance. *Psychopharmacology*. 2010;210(4):453-69.
270. Hendricks PS, Ditre JW, Drobles DJ, Brandon TH. The early time course of smoking withdrawal effects. *Psychopharmacology*. 2006;187(3):385-96.

271. Hughes JR, Keenan RM, Yellin A. Effect of tobacco withdrawal on sustained attention. *Addict Behav.* 1989;14(5):577-80.
272. Jacobsen LK, Mencil WE, Constable RT, Westerveld M, Pugh KR. Impact of smoking abstinence on working memory neurocircuitry in adolescent daily tobacco smokers. *Psychopharmacology (Berl)*. 2007;193(4):557-66.
273. Mendrek A, Monterosso J, Simon SL, Jarvik M, Brody A, Olmstead R, et al. Working memory in cigarette smokers: comparison to non-smokers and effects of abstinence. *Addict Behav.* 2006;31(5):833-44.
274. Merritt PS, Cobb AR, Moissinac L, Hirshman E. Evidence that episodic memory impairment during tobacco abstinence is independent of attentional mechanisms. *J Gen Psychol.* 2010;137(4):331-42.
275. Miech R, Patrick ME, O'Malley PM, Johnston LD. E-cigarette use as a predictor of cigarette smoking: results from a 1-year follow-up of a national sample of 12th grade students. *Tob Control.* 2017;26(e2):e106-e11.
276. Cullen KA, Gentzke AS, Sawdey MD, Chang JT, Anic GM, Wang TW, et al. e-Cigarette Use Among Youth in the United States, 2019. *Jama.* 2019.
277. Willett JG, Bennett M, Hair EC, Xiao H, Greenberg MS, Harvey E, et al. Recognition, use and perceptions of JUUL among youth and young adults. *Tob Control.* 2019;28(1):115-6.
278. Xu C, Loh HH, Law PY. Effects of addictive drugs on adult neural stem/progenitor cells. *Cell Mol Life Sci.* 2016;73(2):327-48.
279. Lee H, Park JR, Yang J, Kim E, Hong SH, Woo HM, et al. Nicotine inhibits the proliferation by upregulation of nitric oxide and increased HDAC1 in mouse neural stem cells. *In Vitro Cell Dev Biol Anim.* 2014;50(8):731-9.
280. Scerri C, Stewart CA, Breen KC, Balfour DJ. The effects of chronic nicotine on spatial learning and bromodeoxyuridine incorporation into the dentate gyrus of the rat. *Psychopharmacology.* 2006;184(3-4):540-6.
281. Cremer H, Chazal G, Lledo PM, Rougon G, Montaron MF, Mayo W, et al. PSA-NCAM: an important regulator of hippocampal plasticity. *Int J Dev Neurosci.* 2000;18(2-3):213-20.
282. Shingo AS, Kito S. Effects of nicotine on neurogenesis and plasticity of hippocampal neurons. *J Neural Transm.* 2005;112(11):1475-8.
283. St Helen G, Havel C, Dempsey DA, Jacob P, 3rd, Benowitz NL. Nicotine delivery, retention and pharmacokinetics from various electronic cigarettes. *Addiction.* 2016;111(3):535-44.
284. Widera D, Mikenberg I, Elvers M, Kaltschmidt C, Kaltschmidt B. Tumor necrosis factor alpha triggers proliferation of adult neural stem cells via IKK/NF-kappaB signaling. *BMC Neurosci.* 2006;7:64-.
285. Iosif RE, Ekdahl CT, Ahlenius H, Pronk CJH, Bonde S, Kokaia Z, et al. Tumor Necrosis Factor Receptor 1 Is a Negative Regulator of Progenitor Proliferation in Adult Hippocampal Neurogenesis. *The Journal of Neuroscience.* 2006;26(38):9703.
286. Klassen HJ, Imfeld KL, Kirov, II, Tai L, Gage FH, Young MJ, et al. Expression of cytokines by multipotent neural progenitor cells. *Cytokine.* 2003;22(3-4):101-6.
287. Volkow ND. Epigenetics of nicotine: another nail in the coughing. *Science translational medicine.* 2011;3(107):107ps43.

288. Pance A, Chantome A, Reveneau S, Bentrari F, Jeannin JF. A repressor in the proximal human inducible nitric oxide synthase promoter modulates transcriptional activation. *Faseb j.* 2002;16(6):631-3.
289. Lin C, Yon JM, Jung AY, Lee JG, Jung KY, Kang JK, et al. Resveratrol prevents nicotine-induced teratogenesis in cultured mouse embryos. *Reprod Toxicol.* 2012;34(3):340-6.
290. Wątroba M, Dudek I, Skoda M, Stangret A, Rzodkiewicz P, Szukiewicz D. Sirtuins, epigenetics and longevity. *Ageing Research Reviews.* 2017;40:11-9.
291. Hou Y, Chen H, He Q, Jiang W, Luo T, Duan J, et al. Changes in methylation patterns of multiple genes from peripheral blood leucocytes of Alzheimer's disease patients. *Acta Neuropsychiatrica.* 2013;25(2):66-76.
292. Hou Y, Wang F, Cheng L, Luo T, Xu J, Wang H. Expression Profiles of SIRT1 and APP Genes in Human Neuroblastoma SK-N-SH Cells Treated with Two Epigenetic Agents. *Neuroscience Bulletin.* 2016;32(5):455-62.
293. Abrous DN, Adriani W, Montaron MF, Aurousseau C, Rougon G, Le Moal M, et al. Nicotine self-administration impairs hippocampal plasticity. *The Journal of neuroscience : the official journal of the Society for Neuroscience.* 2002;22(9):3656-62.
294. Seki T, Arai Y. Highly polysialylated neural cell adhesion molecule (NCAM-H) is expressed by newly generated granule cells in the dentate gyrus of the adult rat. *The Journal of neuroscience: the official journal of the Society for Neuroscience.* 1993;13(6):2351-8.
295. Levin ED. Nicotinic systems and cognitive function. *Psychopharmacology.* 1992;108(4):417-31.
296. Levin ED, Briggs SJ, Christopher NC, Rose JE. Persistence of chronic nicotine-induced cognitive facilitation. *Behav Neural Biol.* 1992;58(2):152-8.
297. Levin ED, Rezvani AH. Development of nicotinic drug therapy for cognitive disorders. *Eur J Pharmacol.* 2000;393(1-3):141-6.
298. Shingo AS, Kito S. Estrogen induces insulin-like growth factor-1 mRNA expression in the immortalized hippocampal cell: determination by quantitative real-time polymerase chain reaction. *Neurochemical research.* 2003;28(9):1379-83.
299. Mudo G, Belluardo N, Mauro A, Fuxe K. Acute intermittent nicotine treatment induces fibroblast growth factor-2 in the subventricular zone of the adult rat brain and enhances neuronal precursor cell proliferation. *Neuroscience.* 2007;145(2):470-83.
300. Cohen A, Soleiman MT, Talia R, Koob GF, George O, Mandyam CD. Extended access nicotine self-administration with periodic deprivation increases immature neurons in the hippocampus. *Psychopharmacology.* 2015;232(2):453-63.
301. Seki T. Hippocampal adult neurogenesis occurs in a microenvironment provided by PSA-NCAM-expressing immature neurons. *Journal of neuroscience research.* 2002;69(6):772-83.
302. Snyder FR, Davis FC, Henningfield JE. The tobacco withdrawal syndrome: performance decrements assessed on a computerized test battery. *Drug Alcohol Depend.* 1989;23(3):259-66.
303. Hamidovic A, Candelaria L, Rodriguez I, Yamada M, Nawarskas J, Burge MR. Learning and memory performance following acute intranasal insulin administration in abstinent smokers. *Hum Psychopharmacol.* 2018;33(2):e2649.

304. Hirshman E, Rhodes DK, Zinser M, Merritt P. The effect of tobacco abstinence on recognition memory, digit span recall, and attentional vigilance. *Exp Clin Psychopharmacol.* 2004;12(1):76-83.
305. Myers CS, Taylor RC, Moolchan ET, Heishman SJ. Dose-related enhancement of mood and cognition in smokers administered nicotine nasal spray. *Neuropsychopharmacology : official publication of the American College of Neuropsychopharmacology.* 2008;33(3):588-98.
306. Campbell NR, Fernandes CC, Halff AW, Berg DK. Endogenous signaling through alpha7-containing nicotinic receptors promotes maturation and integration of adult-born neurons in the hippocampus. *The Journal of neuroscience: the official journal of the Society for Neuroscience.* 2010;30(26):8734-44.
307. Harri A, Beech RD, King SL, Zanardi A, Cleary MA, Caldarone BJ, et al. Alteration of hippocampal cell proliferation in mice lacking the beta 2 subunit of the neuronal nicotinic acetylcholine receptor. *Synapse.* 2004;54(4):200-6.
308. Mechawar N, Saghatelian A, Grailhe R, Scoriels L, Gheusi G, Gabellec MM, et al. Nicotinic receptors regulate the survival of newborn neurons in the adult olfactory bulb. *Proceedings of the National Academy of Sciences of the United States of America.* 2004;101(26):9822-6.
309. Shim SB, Lee SH, Chae KR, Kim CK, Hwang DY, Kim BG, et al. Nicotine leads to improvements in behavioral impairment and an increase in the nicotine acetylcholine receptor in transgenic mice. *Neurochemical research.* 2008;33(9):1783-8.
310. Brown D, Ramlochan Singh C, Manaye KF, Tizabi Y. Nicotine promotes survival of cells expressing amyloid precursor protein and presenilin: implication for Alzheimer's disease. *Neuroscience letters.* 2013;535:57-61.
311. Quik M, Parameswaran N, McCallum SE, Bordia T, Bao S, McCormack A, et al. Chronic oral nicotine treatment protects against striatal degeneration in MPTP-treated primates. *Journal of neurochemistry.* 2006;98(6):1866-75.
312. Quik M, Mallela A, Chin M, McIntosh JM, Perez XA, Bordia T. Nicotine-mediated improvement in L-dopa-induced dyskinesias in MPTP-lesioned monkeys is dependent on dopamine nerve terminal function. *Neurobiology of disease.* 2013;50:30-41.
313. Quik M, Bordia T, Zhang D, Perez XA. Nicotine and Nicotinic Receptor Drugs: Potential for Parkinson's Disease and Drug-Induced Movement Disorders. *Int Rev Neurobiol.* 2015;124:247-71.
314. Dong J, Cui Y, Li S, Le W. Current Pharmaceutical Treatments and Alternative Therapies of Parkinson's Disease. *Curr Neuropharmacol.* 2016;14(4):339-55.
315. Barreto GE, Iarkov A, Moran VE. Beneficial effects of nicotine, cotinine and its metabolites as potential agents for Parkinson's disease. *Front Aging Neurosci.* 2014;6:340.
316. Inestrosa NC, Godoy JA, Vargas JY, Arrazola MS, Rios JA, Carvajal FJ, et al. Nicotine prevents synaptic impairment induced by amyloid-beta oligomers through alpha7-nicotinic acetylcholine receptor activation. *Neuromolecular Med.* 2013;15(3):549-69.
317. Ren Z, Yang M, Guan Z, Yu W. Astrocytic alpha7 Nicotinic Receptor Activation Inhibits Amyloid-beta Aggregation by Upregulating Endogenous alphaB-crystallin through the PI3K/Akt Signaling Pathway. *Curr Alzheimer Res.* 2019;16(1):39-48.

318. Wei P, Liu Q, Li D, Zheng Q, Zhou J, Li J. Acute nicotine treatment attenuates lipopolysaccharide-induced cognitive dysfunction by increasing BDNF expression and inhibiting neuroinflammation in the rat hippocampus. *Neuroscience letters*. 2015;604:161-6.
319. Kalkman HO, Feuerbach D. Modulatory effects of $\alpha 7$ nAChRs on the immune system and its relevance for CNS disorders. *Cellular and molecular life sciences: CMLS*. 2016;73(13):2511-30.
320. Chen Q, Wang K, Jiang D, Wang Y, Xiao X, Zhu N, et al. Blocking mPTP on Neural Stem Cells and Activating the Nicotinic Acetylcholine Receptor alpha7 Subunit on Microglia Attenuate Abeta-Induced Neurotoxicity on Neural Stem Cells. *Neurochemical research*. 2016;41(6):1483-95.
321. Forloni G, Balducci C. Alzheimer's Disease, Oligomers, and Inflammation. *Journal of Alzheimer's disease: JAD*. 2018;62(3):1261-76.
322. Kozin SA, Barykin EP, Mitkevich VA, Makarov AA. Anti-amyloid Therapy of Alzheimer's Disease: Current State and Prospects. *Biochemistry*. 2018;83(9):1057-67.
323. Lombardo S, Maskos U. Role of the nicotinic acetylcholine receptor in Alzheimer's disease pathology and treatment. *Neuropharmacology*. 2015;96(Pt B):255-62.
324. Takata K, Amamiya T, Mizoguchi H, Kawanishi S, Kuroda E, Kitamura R, et al. Alpha7 nicotinic acetylcholine receptor-specific agonist DMXBA (GTS-21) attenuates Abeta accumulation through suppression of neuronal gamma-secretase activity and promotion of microglial amyloid-beta phagocytosis and ameliorates cognitive impairment in a mouse model of Alzheimer's disease. *Neurobiology of aging*. 2018;62:197-209.
325. Sato K. Effects of Microglia on Neurogenesis. *Glia*. 2015;63(8):1394-405.
326. Mondello S, Hayes RL. Chapter 16 - Biomarkers. In: Grafman J, Salazar AM, editors. *Handbook of clinical neurology*. 127: Elsevier; 2015. p. 245-65.
327. Wainer BH, Levey AI, Mufson EJ, Mesulam MM. CHAPTER 5 - CHOLINERGIC SYSTEMS IN MAMMALIAN BRAIN IDENTIFIED WITH ANTIBODIES AGAINST CHOLINE ACETYLTRANSFERASE. In: Osborne NN, editor. *Selected Topics from Neurochemistry*. Amsterdam: Pergamon; 1985. p. 85-109.
328. Stadler J, Bentz BG, Harbrecht BG, Di Silvio M, Curran RD, Billiar TR, et al. Tumor necrosis factor alpha inhibits hepatocyte mitochondrial respiration. *Ann Surg*. 1992;216(5):539-46.
329. Xie Z, Smith CJ, Van Eldik LJ. Activated glia induce neuron death via MAP kinase signaling pathways involving JNK and p38. *Glia*. 2004;45(2):170-9.
330. Hunter RL, Dragicevic N, Seifert K, Choi DY, Liu M, Kim HC, et al. Inflammation induces mitochondrial dysfunction and dopaminergic neurodegeneration in the nigrostriatal system. *Journal of neurochemistry*. 2007;100(5):1375-86.
331. Samavati L, Lee I, Mathes I, Lottspeich F, Huttemann M. Tumor necrosis factor alpha inhibits oxidative phosphorylation through tyrosine phosphorylation at subunit I of cytochrome c oxidase. *The Journal of biological chemistry*. 2008;283(30):21134-44.
332. Voloboueva LA, Lee SW, Emery JF, Palmer TD, Giffard RG. Mitochondrial protection attenuates inflammation-induced impairment of neurogenesis in vitro and in vivo. *The Journal of neuroscience: the official journal of the Society for Neuroscience*. 2010;30(37):12242-51.

333. Manczak M, Anekonda TS, Henson E, Park BS, Quinn J, Reddy PH. Mitochondria are a direct site of A beta accumulation in Alzheimer's disease neurons: implications for free radical generation and oxidative damage in disease progression. *Hum Mol Genet.* 2006;15(9):1437-49.
334. Halestrap A. Biochemistry: a pore way to die. *Nature.* 2005;434(7033):578-9.
335. Lin W, Hirata N, Sekino Y, Kanda Y. Role of alpha7-nicotinic acetylcholine receptor in normal and cancer stem cells. *Curr Drug Targets.* 2012;13(5):656-65.
336. Narla ST, Klejbor I, Birkaya B, Lee Y-W, Morys J, Stachowiak EK, et al. Activation of developmental nuclear fibroblast growth factor receptor 1 signaling and neurogenesis in adult brain by $\alpha 7$ nicotinic receptor agonist. *Stem cells translational medicine.* 2013;2(10):776-88.
337. Gao J, Sana R, Calder V, Calonge M, Lee W, Wheeler LA, et al. Mitochondrial permeability transition pore in inflammatory apoptosis of human conjunctival epithelial cells and T cells: effect of cyclosporin A. *Invest Ophthalmol Vis Sci.* 2013;54(7):4717-33.
338. Lisowski P, Kannan P, Mlody B, Prigione A. Mitochondria and the dynamic control of stem cell homeostasis. *EMBO Rep.* 2018;19(5).
339. Garcia-Prat L, Sousa-Victor P, Munoz-Canoves P. Proteostatic and Metabolic Control of Stemness. *Cell Stem Cell.* 2017;20(5):593-608.
340. Margineantu DH, Hockenbery DM. Mitochondrial functions in stem cells. *Curr Opin Genet Dev.* 2016;38:110-7.
341. Seo BJ, Yoon SH, Do JT. Mitochondrial Dynamics in Stem Cells and Differentiation. *International journal of molecular sciences.* 2018;19(12).
342. Zhang H, Menzies KJ, Auwerx J. The role of mitochondria in stem cell fate and aging. *Development.* 2018;145(8).
343. Xu X, Duan S, Yi F, Ocampo A, Liu GH, Izpisua Belmonte JC. Mitochondrial regulation in pluripotent stem cells. *Cell Metab.* 2013;18(3):325-32.
344. Wanet A, Arnould T, Najimi M, Renard P. Connecting Mitochondria, Metabolism, and Stem Cell Fate. *Stem cells and development.* 2015;24(17):1957-71.
345. Meyer JN, Hartman JH, Mello DF. Mitochondrial Toxicity. *Toxicol Sci.* 2018;162(1):15-23.
346. Godoy JA, Valdivieso AG, Inestrosa NC. Nicotine Modulates Mitochondrial Dynamics in Hippocampal Neurons. *Molecular neurobiology.* 2018;55(12):8965-77.
347. Bhattacharjee A, Prasad SK, Banerjee O, Singh S, Banerjee A, Bose A, et al. Targeting mitochondria with folic acid and vitamin B12 ameliorates nicotine mediated islet cell dysfunction. *Environ Toxicol.* 2018;33(9):988-1000.
348. Malinska D, Wieckowski MR, Michalska B, Drabik K, Prill M, Patalas-Krawczyk P, et al. Mitochondria as a possible target for nicotine action. *J Bioenerg Biomembr.* 2019;51(4):259-76.
349. Zahedi A, Phandthong R, Chaili A, Leung S, Omaie E, Talbot P. Mitochondrial Stress Response in Neural Stem Cells Exposed to Electronic Cigarettes. *iScience.* 2019;16:250-69.
350. Bahl V, Johnson K, Phandthong R, Zahedi A, Schick SF, Talbot P. From the Cover: Thirdhand Cigarette Smoke Causes Stress-Induced Mitochondrial Hyperfusion and Alters the Transcriptional Profile of Stem Cells. *Toxicol Sci.* 2016;153(1):55-69.

351. Rizzuto R, De Stefani D, Raffaello A, Mammucari C. Mitochondria as sensors and regulators of calcium signalling. *Nat Rev Mol Cell Biol.* 2012;13(9):566-78.
352. Marin-Burgin A, Schinder AF. Requirement of adult-born neurons for hippocampus-dependent learning. *Behavioural brain research.* 2012;227(2):391-9.
353. Liang H, Zhao H, Gleichman A, Machnicki M, Telang S, Tang S, et al. Region-specific and activity-dependent regulation of SVZ neurogenesis and recovery after stroke. *Proceedings of the National Academy of Sciences of the United States of America.* 2019;116(27):13621-30.
354. Salman H, Ghosh P, Kernie SG. Subventricular zone neural stem cells remodel the brain following traumatic injury in adult mice. *J Neurotrauma.* 2004;21(3):283-92.
355. Thored P, Wood J, Arvidsson A, Cammenga J, Kokaia Z, Lindvall O. Long-term neuroblast migration along blood vessels in an area with transient angiogenesis and increased vascularization after stroke. *Stroke.* 2007;38(11):3032-9.
356. Saha B, Jaber M, Gaillard A. Potentials of endogenous neural stem cells in cortical repair. *Front Cell Neurosci.* 2012;6:14.
357. Wang Y, Jin K, Mao XO, Xie L, Banwait S, Marti HH, et al. VEGF-overexpressing transgenic mice show enhanced post-ischemic neurogenesis and neuromigration. *Journal of neuroscience research.* 2007;85(4):740-7.
358. Rodier PM. Developing brain as a target of toxicity. *Environ Health Perspect.* 1995;103 Suppl 6:73-6.
359. Pericot-Valverde I, Gaalema DE, Priest JS, Higgins ST. E-cigarette awareness, perceived harmfulness, and ever use among U.S. adults. *Prev Med.* 2017;104:92-9.
360. Berger F, Gage FH, Vijayaraghavan S. Nicotinic receptor-induced apoptotic cell death of hippocampal progenitor cells. *The Journal of neuroscience: the official journal of the Society for Neuroscience.* 1998;18(17):6871-81.
361. Joschko MA, Dreosti IE, Tulsi RS. The teratogenic effects of nicotine in vitro in rats: a light and electron microscope study. *Neurotoxicol Teratol.* 1991;13(3):307-16.
362. Slotkin TA. If nicotine is a developmental neurotoxicant in animal studies, dare we recommend nicotine replacement therapy in pregnant women and adolescents? *Neurotoxicol Teratol.* 2008;30(1):1-19.
363. Dwyer JB, Broide RS, Leslie FM. Nicotine and brain development. *Birth Defects Res C Embryo Today.* 2008;84(1):30-44.
364. Liu F, Tao X, Pang G, Wu D, Hu Y, Xue S, et al. Maternal Nicotine Exposure During Gestation and Lactation Period Affects Behavior and Hippocampal Neurogenesis in Mouse Offspring. *Front Pharmacol.* 2019;10:1569.
365. Zoli M, Le Novere N, Hill JA, Jr., Changeux JP. Developmental regulation of nicotinic ACh receptor subunit mRNAs in the rat central and peripheral nervous systems. *The Journal of neuroscience: the official journal of the Society for Neuroscience.* 1995;15(3 Pt 1):1912-39.
366. Tribollet E, Bertrand D, Marguerat A, Raggenbass M. Comparative distribution of nicotinic receptor subtypes during development, adulthood and aging: an autoradiographic study in the rat brain. *Neuroscience.* 2004;124(2):405-20.

367. Yuskaitis CJ, Pomeroy SL. 131 - Development of the Nervous System. In: Polin RA, Abman SH, Rowitch DH, Benitz WE, Fox WW, editors. *Fetal and Neonatal Physiology (Fifth Edition)*: Elsevier; 2017. p. 1294-313.e2.
368. Naeff B, Schlumpf M, Lichtensteiger W. Pre- and postnatal development of high-affinity [3H]nicotine binding sites in rat brain regions: an autoradiographic study. *Brain Res Dev Brain Res*. 1992;68(2):163-74.
369. Zhang X, Liu C, Miao H, Gong ZH, Nordberg A. Postnatal changes of nicotinic acetylcholine receptor alpha 2, alpha 3, alpha 4, alpha 7 and beta 2 subunits genes expression in rat brain. *Int J Dev Neurosci*. 1998;16(6):507-18.
370. Hohmann CF. A morphogenetic role for acetylcholine in mouse cerebral neocortex. *Neurosci Biobehav Rev*. 2003;27(4):351-63.
371. Bryden DW, Burton AC, Barnett BR, Cohen VJ, Hearn TN, Jones EA, et al. Prenatal Nicotine Exposure Impairs Executive Control Signals in Medial Prefrontal Cortex. *Neuropsychopharmacology: official publication of the American College of Neuropsychopharmacology*. 2016;41(3):716-25.
372. Dwyer JB, McQuown SC, Leslie FM. The dynamic effects of nicotine on the developing brain. *Pharmacol Ther*. 2009;122(2):125-39.
373. Eskenazi B, Castorina R. Association of prenatal maternal or postnatal child environmental tobacco smoke exposure and neurodevelopmental and behavioral problems in children. *Environ Health Perspect*. 1999;107(12):991-1000.
374. Ernst M, Moolchan ET, Robinson ML. Behavioral and neural consequences of prenatal exposure to nicotine. *J Am Acad Child Adolesc Psychiatry*. 2001;40(6):630-41.
375. Mojica C, Bai Y, Lotfipour S. Maternal nicotine exposure effects on adolescent learning and memory are abolished in alpha(alpha)2* nicotinic acetylcholine receptor-null mutant mice. *Neuropharmacology*. 2018;135:529-35.
376. Dong T, Hu W, Zhou X, Lin H, Lan L, Hang B, et al. Prenatal exposure to maternal smoking during pregnancy and attention-deficit/hyperactivity disorder in offspring: A meta-analysis. *Reprod Toxicol*. 2018;76:63-70.
377. Zhang M, Xu W, He G, Zhang D, Zhao X, Dai J, et al. Maternal nicotine exposure has severe cross-generational effects on offspring behavior. *Behavioural brain research*. 2018;348:263-6.
378. McGrath-Morrow SA, Gorzkowski J, Groner JA, Rule AM, Wilson K, Tanski SE, et al. The Effects of Nicotine on Development. *Pediatrics*. 2020;145(3).
379. Hely MA, Reid WG, Adena MA, Halliday GM, Morris JG. The Sydney multicenter study of Parkinson's disease: the inevitability of dementia at 20 years. *Movement disorders : official journal of the Movement Disorder Society*. 2008;23(6):837-44.
380. Hobson P, Meara J. Mild cognitive impairment in Parkinson's disease and its progression onto dementia: a 16-year outcome evaluation of the Denbighshire cohort. *Int J Geriatr Psychiatry*. 2015;30(10):1048-55.
381. Veenvliet JV, Smidt MP. Molecular mechanisms of dopaminergic subset specification: fundamental aspects and clinical perspectives. *Cell Mol Life Sci*. 2014;71(24):4703-27.
382. Mesman S, Smidt MP. Acquisition of the Midbrain Dopaminergic Neuronal Identity. *International journal of molecular sciences*. 2020;21(13).

383. Hirsch E, Graybiel AM, Agid YA. Melanized dopaminergic neurons are differentially susceptible to degeneration in Parkinson's disease. *Nature*. 1988;334(6180):345-8.
384. Damier P, Hirsch EC, Agid Y, Graybiel AM. The substantia nigra of the human brain. II. Patterns of loss of dopamine-containing neurons in Parkinson's disease. *Brain : a journal of neurology*. 1999;122 (Pt 8):1437-48.
385. Babić Leko M, Hof PR, Šimić G. Alterations and interactions of subcortical modulatory systems in Alzheimer's disease. *Prog Brain Res*. 2021;261:379-421.
386. Castillo Díaz F, Caffino L, Fumagalli F. Bidirectional role of dopamine in learning and memory-active forgetting. *Neurosci Biobehav Rev*. 2021;131:953-63.
387. Lin R, Liang J, Luo M. The Raphe Dopamine System: Roles in Salience Encoding, Memory Expression, and Addiction. *Trends Neurosci*. 2021;44(5):366-77.
388. Brichta L, Greengard P. Molecular determinants of selective dopaminergic vulnerability in Parkinson's disease: an update. *Front Neuroanat*. 2014;8:152.
389. Bentivoglio M, Bloom FE, Owman C, Dunnett SB, Kaczmarek L, Kuhar MJ, et al. *Handbook of chemical neuroanatomy*: Elsevier; 1988.
390. Pérez-Fernández J, Barandela M, Jiménez-López C. The Dopaminergic Control of Movement-Evolutionary Considerations. *International journal of molecular sciences*. 2021;22(20).
391. Morens DM, Grandinetti A, Reed D, White LR, Ross GW. Cigarette smoking and protection from Parkinson's disease: false association or etiologic clue? *Neurology*. 1995;45(6):1041-51.
392. Gorell JM, Rybicki BA, Johnson CC, Peterson EL. Smoking and Parkinson's disease: a dose-response relationship. *Neurology*. 1999;52(1):115-9.
393. Breckenridge CB, Berry C, Chang ET, Sielken RL, Jr., Mandel JS. Association between Parkinson's Disease and Cigarette Smoking, Rural Living, Well-Water Consumption, Farming and Pesticide Use: Systematic Review and Meta-Analysis. *PloS one*. 2016;11(4):e0151841.
394. Gallo V, Vineis P, Cancellieri M, Chiodini P, Barker RA, Brayne C, et al. Exploring causality of the association between smoking and Parkinson's disease. *Int J Epidemiol*. 2019;48(3):912-25.
395. Allam MF, Campbell MJ, Hofman A, Del Castillo AS, Fernández-Crehuet Navajas R. Smoking and Parkinson's disease: systematic review of prospective studies. *Movement disorders : official journal of the Movement Disorder Society*. 2004;19(6):614-21.
396. Hernán MA, Takkouche B, Caamaño-Isorna F, Gestal-Otero JJ. A meta-analysis of coffee drinking, cigarette smoking, and the risk of Parkinson's disease. *Annals of neurology*. 2002;52(3):276-84.
397. Ritz B, Ascherio A, Checkoway H, Marder KS, Nelson LM, Rocca WA, et al. Pooled analysis of tobacco use and risk of Parkinson disease. *Archives of neurology*. 2007;64(7):990-7.
398. Tanner CM, Goldman SM, Aston DA, Ottman R, Ellenberg J, Mayeux R, et al. Smoking and Parkinson's disease in twins. *Neurology*. 2002;58(4):581-8.
399. Quik M, Wonnacott S. $\alpha 6\beta 2^*$ and $\alpha 4\beta 2^*$ nicotinic acetylcholine receptors as drug targets for Parkinson's disease. *Pharmacol Rev*. 2011;63(4):938-66.

400. Chen H, Huang X, Guo X, Mailman RB, Park Y, Kamel F, et al. Smoking duration, intensity, and risk of Parkinson disease. *Neurology*. 2010;74(11):878-84.
401. Morozova N, O'Reilly EJ, Ascherio A. Variations in gender ratios support the connection between smoking and Parkinson's disease. *Movement disorders: official journal of the Movement Disorder Society*. 2008;23(10):1414-9.
402. Maggio R, Riva M, Vaglini F, Fornai F, Molteni R, Armogida M, et al. Nicotine prevents experimental parkinsonism in rodents and induces striatal increase of neurotrophic factors. *Journal of neurochemistry*. 1998;71(6):2439-46.
403. Visanji NP, O'Neill MJ, Duty S. Nicotine, but neither the alpha4beta2 ligand RJR2403 nor an alpha7 nAChR subtype selective agonist, protects against a partial 6-hydroxydopamine lesion of the rat median forebrain bundle. *Neuropharmacology*. 2006;51(3):506-16.
404. Ryan RE, Ross SA, Drago J, Loiacono RE. Dose-related neuroprotective effects of chronic nicotine in 6-hydroxydopamine treated rats, and loss of neuroprotection in alpha4 nicotinic receptor subunit knockout mice. *Br J Pharmacol*. 2001;132(8):1650-6.
405. García-Montes JR, Boronat-García A, López-Colomé AM, Bargas J, Guerra-Crespo M, Drucker-Colín R. Is nicotine protective against Parkinson's disease? An experimental analysis. *CNS & neurological disorders drug targets*. 2012;11(7):897-906.
406. Abin-Carriquiry JA, McGregor-Armas R, Costa G, Urbanavicius J, Dajas F. Presynaptic involvement in the nicotine prevention of the dopamine loss provoked by 6-OHDA administration in the substantia nigra. *Neurotox Res*. 2002;4(2):133-9.
407. Quik M, Chen L, Parameswaran N, Xie X, Langston JW, McCallum SE. Chronic oral nicotine normalizes dopaminergic function and synaptic plasticity in 1-methyl-4-phenyl-1,2,3,6-tetrahydropyridine-lesioned primates. *The Journal of neuroscience: the official journal of the Society for Neuroscience*. 2006;26(17):4681-9.
408. Iarkov A, Barreto GE, Grizzell JA, Echeverria V. Strategies for the Treatment of Parkinson's Disease: Beyond Dopamine. *Front Aging Neurosci*. 2020;12:4.
409. Henderson BJ, Lester HA. Inside-out neuropharmacology of nicotinic drugs. *Neuropharmacology*. 2015;96(Pt B):178-93.
410. Srinivasan R, Henley BM, Henderson BJ, Indersmitten T, Cohen BN, Kim CH, et al. Smoking-Relevant Nicotine Concentration Attenuates the Unfolded Protein Response in Dopaminergic Neurons. *The Journal of Neuroscience*. 2016;36(1):65.
411. Henderson BJ, Wall T, Henley BM, Kim CH, Nichols WA, Moaddel R, et al. Menthol alone upregulates midbrain nAChRs, alters nAChR subtype stoichiometry, alters dopamine neuron firing frequency, and prevents nicotine reward. *J Neurosci*. 2016;36(10).
412. Henderson BJ, Wall TR, Henley BM, Kim CH, McKinney S, Lester HA. Menthol Enhances Nicotine Reward-Related Behavior by Potentiating Nicotine-Induced Changes in nAChR Function, nAChR Upregulation, and DA Neuron Excitability. *Neuropsychopharmacology : official publication of the American College of Neuropsychopharmacology*. 2017;42(12):2285-91.
413. Cooper SY, Akers AT, Henderson BJ. Flavors Enhance Nicotine Vapor Self-administration in Male Mice. *Nicotine Tob Res*. 2021;23(3):566-72.

414. Silva RM, Ries V, Oo TF, Yarygina O, Jackson-Lewis V, Ryu EJ, et al. CHOP/GADD153 is a mediator of apoptotic death in substantia nigra dopamine neurons in an in vivo neurotoxin model of parkinsonism. *Journal of neurochemistry*. 2005;95(4):974-86.
415. Galehdar Z, Swan P, Fuerth B, Callaghan SM, Park DS, Cregan SP. Neuronal apoptosis induced by endoplasmic reticulum stress is regulated by ATF4-CHOP-mediated induction of the Bcl-2 homology 3-only member PUMA. *The Journal of neuroscience: the official journal of the Society for Neuroscience*. 2010;30(50):16938-48.
416. Mercado G, Valdés P, Hetz C. An ERcentric view of Parkinson's disease. *Trends Mol Med*. 2013;19(3):165-75.
417. Marciniak SJ, Yun CY, Oyadomari S, Novoa I, Zhang Y, Jungreis R, et al. CHOP induces death by promoting protein synthesis and oxidation in the stressed endoplasmic reticulum. *Genes Dev*. 2004;18(24):3066-77.
418. Zinszner H, Kuroda M, Wang X, Batchvarova N, Lightfoot RT, Remotti H, et al. CHOP is implicated in programmed cell death in response to impaired function of the endoplasmic reticulum. *Genes Dev*. 1998;12(7):982-95.
419. Ahmadi FA, Grammatopoulos TN, Poczobutt AM, Jones SM, Snell LD, Das M, et al. Dopamine selectively sensitizes dopaminergic neurons to rotenone-induced apoptosis. *Neurochemical research*. 2008;33(5):886-901.
420. Miyazaki I, Asanuma M. Approaches to prevent dopamine quinone-induced neurotoxicity. *Neurochemical research*. 2009;34(4):698-706.
421. Surmeier DJ, Guzman JN, Sanchez-Padilla J, Schumacker PT. The role of calcium and mitochondrial oxidant stress in the loss of substantia nigra pars compacta dopaminergic neurons in Parkinson's disease. *Neuroscience*. 2011;198:221-31.
422. Hoozemans JJ, van Haastert ES, Eikelenboom P, de Vos RA, Rozemuller JM, Scheper W. Activation of the unfolded protein response in Parkinson's disease. *Biochem Biophys Res Commun*. 2007;354(3):707-11.
423. Srinivasan R, Richards CI, Xiao C, Rhee D, Pantoja R, Dougherty DA, et al. Pharmacological chaperoning of nicotinic acetylcholine receptors reduces the endoplasmic reticulum stress response. *Mol Pharmacol*. 2012;81(6):759-69.
424. Marks MJ, Pauly JR, Gross SD, Deneris ES, Hermans-Borgmeyer I, Heinemann SF, et al. Nicotine binding and nicotinic receptor subunit RNA after chronic nicotine treatment. *Journal of Neuroscience*. 1992;12(7):2765-84.
425. Pauly JR, Marks MJ, Robinson SF, Van De Kamp JL, Collins AC. Chronic nicotine and mecamylamine treatment increase brain nicotinic receptor binding without changing alpha 4 or beta 2 mRNA levels. *Journal of Pharmacology and Experimental Therapeutics*. 1996;278(1):361-9.
426. Govind AP, Walsh H, Green WN. Nicotine-induced upregulation of native neuronal nicotinic receptors is caused by multiple mechanisms. *Journal of Neuroscience*. 2012;32(6):2227-38.
427. Moen JK, Lee AM. Sex Differences in the Nicotinic Acetylcholine Receptor System of Rodents: Impacts on Nicotine and Alcohol Reward Behaviors. *Frontiers in neuroscience*. 2021;15:745783.

428. Cosgrove KP, Esterlis I, McKee SA, Bois F, Seibyl JP, Mazure CM, et al. Sex differences in availability of $\beta 2^*$ -nicotinic acetylcholine receptors in recently abstinent tobacco smokers. *Archives of general psychiatry*. 2012;69(4):418-27.
429. Gozen O, Nesil T, Kanit L, Koylu EO, Pogun S. Nicotinic cholinergic and dopaminergic receptor mRNA expression in male and female rats with high or low preference for nicotine. *The American journal of drug and alcohol abuse*. 2016;42(5):556-66.
430. Lenoir M, Starosciak AK, Ledon J, Booth C, Zakharova E, Wade D, et al. Sex differences in conditioned nicotine reward are age-specific. *Pharmacology Biochemistry and Behavior*. 2015;132:56-62.
431. Correa VL, Flores RJ, Carcoba LM, Arreguin MC, O'Dell LE. Sex differences in cholinergic systems in the interpeduncular nucleus following nicotine exposure and withdrawal. *Neuropharmacology*. 2019;158:107714.
432. Huang LZ, Parameswaran N, Bordia T, Michael McIntosh J, Quik M. Nicotine is neuroprotective when administered before but not after nigrostriatal damage in rats and monkeys. *Journal of neurochemistry*. 2009;109(3):826-37.

APPENDIX A



Office of Research Integrity
Institutional Review Board
One John Marshall Drive
Huntington, WV 25755

FWA 00002704

IRB1 #00002205
IRB2 #00003206

September 11, 2019

Alastair Hoyt, MD
Department of Neurosurgery, MUSOM

RE: IRBNet ID# 1480544-1
At: Marshall University Institutional Review Board #1 (Medical)

Dear Dr. Hoyt:

Protocol Title: [1480544-1] National survey of DBS surgical practices

Site Location: CHH, MU

Submission Type: New Project APPROVED

Review Type: Expedited Review

In accordance with 45CFR46.110(a)(7), the above study was granted Expedited approval today by the Marshall University Institutional Review Board #1 (Medical) Chair. The approval included the Waiver of Informed Consent and the HIPAA Waiver. An annual update will be required on September 11, 2020 for administrative review and approval. The update must include the Annual Update Form and current educational certificates for all investigators involved in the study. All amendments must be submitted for approval by the IRB Chair prior to implementation and a closure request is required upon completion of the study.

This study is for student Arrin Brooks.

If you have any questions, please contact the Marshall University Institutional Review Board #1 (Medical) Coordinator Margaret Hardy at (304) 696-6322 or hardyma@marshall.edu. Please include your study title and reference number in all correspondence with this office.

Sincerely,

A handwritten signature in blue ink that reads 'Bruce F. Day'.

Bruce F. Day, ThD, CIP
Director, Office of Research Integrity

APPENDIX B

Complications Reported in Other Published Works

	No. of patients (electrodes)	Staging	Infection	Hardware Complication	Wound Dehiscence/Erosion	Hemorrhage	Seizures	Loss of Efficacy	Other
Abode-lyamah, et al. (40)	242 (464)	S: 228 N: 17	S 15 (6.6%) N 1 (5.9%)	NR	S: 9 (4.0%) N: 0 (0%)	NR	NR	NR	Postoperative Seroma S: 1 (0.4%) N: 0 (0%)
Chen, et al. (30)	284 (490)	S: 200 N: 84	S: 3 (1.5%) N: 0 (0%)	High impedance S: 1 (0.5%) N: 1 (1.2%)	S: 1 (0.3%) N: 0 (0%)	S: 3 (1.5%) N: 1 (1.2%)	S: 2 (1%) N: 2 (2.4%)	NR	
Fenoy (36)	728 (1333)	Transitioned from N to S, data not segregated	23 (3.2%)	Lead malposition 9 (1.2%) Lead migration 4 (0.5%) High impedance 4 (0.5%) Fracture 10 (1.4%)	4 (0.5%)	Symptomatic 8 (1.1%) Asymptomatic IVH 25 (3.4%) ICH 4 (0.5%)	5 (0.7%)	29 (4%)	IPG flipped, malpositioned or discomfort 8 (1.1%)
Petraglia (23)	713 (1426)	Sim Bilat: 556 Staged Bilat: 157 *IPG placement timing NR	Sim Bilat: 24 (4.3%) Stage d Bilat: 11 (7%)	Sim Bilat: 3 (0.5%) Staged Bilat: 0 (0%)	NR	Sim Bilat: 16 (2.9%) Staged Bilat: 4 (2.5%)	NR	NR	Lead Revision Sim Bilat: 18 (3.2%) Staged Bilat: 20 (12.7%) Generator Revision Sim Bilat: 17 (3.1%) Staged Bilat: 6 (3.8%)

Doshi (35)	153 (298)	All staged	6 (3.9%)	Lead malposition 4 (2.6%) Lead migration 0 (0%) IPG malfunction 2 (1.3%) Fracture 0 (0%)	1 (0.7%)	2 (1.3%)	NR	2 (1.3%)	
Voges, et al. (33)	262 (472) *180 (352) assessed for long-term complications	S: 194 (74.1%) N: 64 (24.4%) *data not segregated	15 (5.7%)	Electrode damage/fracture 4 ((2.2%) Local discomfort 12 (6.7%) Electrode migration 5 (2.8%) Connector displacement 1 (0.6%)	1 (0.6%)	1 (0.4%)	0 (0%)	NR	IPG implantation site hematoma 3 (1.25) Seroma at IPG site 2 (1.1%)
Seijo, et al. (34)	130 (252)	All staged	2 (1.5%)	Lead fracture 1 (0.8%)	NR	9 (6.9%)	13 (10%)	NR	CSF leak 1 (0.8%)
Tolleson, et al. (37)	447 (823)	All staged	26 (5.8%)	Lead migration 2 (0.5%) Lead and IPG malfunction 2 (0.5%)	Infected group 8 (1.8%) Noninfected group 9 (2%)	2 (0.5%)	1 (0.2%)	NR	Pain along apparatus 4 (0.9%)
Kochanski, et al. (41)	178 (270)	Both Staged and Nonstaged procedures include; not segregated	3 (1.7%)	Malpositioned lead 0 (0%)	NR	3 (1.7%)	2 (1.1%)	NR	
Falowski, et al.(38)	432 (606)	S: 326 (475) N: 106 (131)	S: 11 (3.4%)	Lead fractures S 7 (2.1%) N 7 (6.6%)	S: 3 (0.9%) N: NR	S: 12 (3.7%) N: 8 (7.5%)	NR	S: 17 (5.2%)	Extension lead coiling S: 2 (0.6%) N: NR

			N: 4 (3.8%)	High impedance S 5 (1.5%) N NR				N: NR	Seroma S: 1 (0.3%) N: NR
				Lead migration S 1 (0.3%) N NR					
Morishita, et al (39)	132 (138)	All staged	17 (12.9%)	Fracture 7 (5.1%) Lead migration 16 (12.1%)	NR	Symptomatic ICH 5 (3.8%) Asymptomatic ICH 4 (3%)	9 (6.8%)	NR	Air embolus 2 (1.5%)

Total number (% of event by number of patients). S = Staged (IPG implanted in subsequent surgery); N = Non-staged (DBS system including IPG implanted in one operative session); Sim Bilat = Simultaneous Bilateral (DBS leads implanted in each hemisphere in one surgery); Staged Bilat = Staged Bilateral (each hemisphere implanted in staged surgeries); NR = Not Reported; ICH = intracranial hemorrhage; IVH = intraventricular hemorrhage